

Dogfight Search: A Swarm-Based Optimization Algorithm for Complex Engineering Optimization and Mountainous Terrain Path Planning

Yujing Sun^a, Jie Cai^a, Xingguo Xu^{b,*}, Yuansheng Gao^{c,*}, Lei Zhang^b, Kaichen Ouyang^d and Zhanyu Liu^b

^aCollege of Science, Liaoning Technical University, Fuxin, 123000, China

^bSchool of Mathematical Sciences, Dalian University of Technology, Dalian, 116024, China

^cCollege of Computer Science and Technology, Zhejiang University, Hangzhou, 310027, China

^dDepartment of Physics, University of Science and Technology of China, Hefei, 230026, China

ARTICLE INFO

Keywords:

Optimization
Metaheuristic
Dogfight Search
Engineering Optimization
Mountainous Terrain Path Planning

ABSTRACT

Dogfight is a tactical behavior of cooperation between fighters. Inspired by this, this paper proposes a novel metaphor-free metaheuristic algorithm called Dogfight Search (DoS). Unlike traditional algorithms, DoS draws algorithmic framework from the inspiration, but its search mechanism is constructed based on the displacement integration equations in kinematics. Through experimental validation on CEC2017 and CEC2022 benchmark test functions, 10 real-world constrained optimization problems and mountainous terrain path planning tasks, DoS significantly outperforms 7 advanced competitors in overall performance and ranks first in the Friedman ranking. Furthermore, this paper compares the performance of DoS with 3 SOTA algorithms on the CEC2017 and CEC2022 benchmark test functions. The results show that DoS continues to maintain its lead, demonstrating strong competitiveness. The source code of DoS is available at <https://ww2.mathworks.cn/matlabcentral/fileexchange/183519-dogfight-search>.

1. Introduction

Optimization problems are widely present in various real-world domains, including engineering design (Hao et al., 2025), healthcare (Osaba et al., 2019), logistics management (Chu et al., 2021) and financial portfolio optimization (Dye, 2012). The quality of the obtained solutions often directly affects system performance, resource allocation efficiency, and economic benefits. Therefore, designing efficient and robust optimization algorithms to obtain the global optimal solution has become a core research direction in the field of intelligent computing.

Over the years, researchers have proposed a series of traditional optimization algorithms, such as Newton's method (Su et al., 2011) and gradient descent (Hosseinali, 2024), based on the linear characteristics of objective functions. These methods exhibit high computational efficiency and convergence accuracy in solving linear or convex optimization problems. However, their performance is often limited when dealing with complex real-world problems such as non-convexity or non-differentiability (Keivanian and Chiong, 2022; Deb et al., 2002; Myers and Spencer, 2016; Gong et al., 2010). Moreover, traditional algorithms heavily rely on gradient information during iteration. As problem

dimensionality increases, the complexity of gradient computation also rises sharply, further undermining their efficiency in solving high-dimensional engineering problems.

In contrast to the limitations of traditional methods, metaheuristic algorithms have shown greater adaptability and potential in complex optimization tasks due to their simple implementation, low parameter dependency, and strong global search capabilities (Dhiman and Kumar, 2019). For example, Gholizadeh et al. proposed the Newton Metaheuristic Algorithm (NMA) (Gholizadeh et al., 2020) for the seismic design of steel frame structures with discrete performance criteria, effectively overcoming the limitations of traditional methods in nonlinear and discrete design spaces. Houssein et al. developed a hybrid metaheuristic algorithm, BES-GO (Houssein et al., 2025), which demonstrated superior convergence performance and practical applicability in structural design benchmarks. In addition, Lu et al. introduced the Multi-Strategy Beetle Swarm Optimization (MBSO) (Lu et al., 2025) algorithm to optimize air volume in mine ventilation networks, significantly improving the energy efficiency of the system. These studies highlight the broad applicability and significant development potential of metaheuristics in solving nonlinear, high-dimensional, and constrained engineering optimization problems. Representative contributions are summarized in Table 1.

The core idea of metaheuristic algorithms is to build nature-inspired mathematical models and perform global search by simulating biological behaviors, physical phenomena, or natural laws. According to the No Free Lunch Theorem (Wolpert and Macready, 2002), no single algorithm can solve all optimization problems optimally, which highlights

*Corresponding author

✉ 2211060216@stu.lntu.edu.cn (Y. Sun); 2311010201@stu.lntu.edu.cn (J. Cai); xuxingguo@mail.dlut.edu.cn (X. Xu); y.gao@zju.edu.cn (Y. Gao); bhgleizhang@mail.dlut.edu.cn (L. Zhang); oykc@mail.ustc.edu.cn (K. Ouyang); ramirez@mail.dlut.edu.cn (Z. Liu)
ORCID(s): 0009-0008-8286-7367 (X. Xu); 0000-0003-3278-8835 (Y. Gao)

Table 1

Contributions of metaheuristic algorithms to real-world engineering problems.

Algorithm	Engineering Contribution
Dual-Pheromone Crossover Ant Colony Optimization (DPX-ACO) (Wang et al., 2025b)	The proposed method significantly reduces the overall production costs in large-scale cotton blending optimization. Comprehensive experimental analyses further demonstrate its effectiveness, with several benchmark scenarios achieving cost reductions exceeding 30%.
Improved Discrete Particle Swarm Optimization (IDPSO) (Wu et al., 2025)	Provided superior scheduling solutions for automated guided vehicle manufacturing processes by considering dynamic changes, operator skills, and equipment maintenance, leading to a notable reduction in task completion time.
Artificial Rabbits Optimization (ARO) (Kuo et al., 2025)	Optimized control parameters of biped robots, enabling fast adaptation to external disturbances and maintaining balance in complex environments such as disaster response scenarios.
Improved Ant Colony Optimization (IACO) (Wangying and Naiming, 2025)	Applied to helicopter route planning for forest fire prevention, reducing total flight distance by 4.1% and improving emergency response efficiency by 7.3% in dynamic environments.

the importance of structural innovation tailored to specific problem characteristics.

The performance of metaheuristic algorithms largely depends on the balance between exploration and exploitation (Arani et al., 2013). However, most existing algorithms overly rely on the current best solution as a guiding mechanism. For instance, Particle Swarm Optimization (PSO), proposed by Kennedy et al. based on bird foraging behavior (Kennedy and Eberhart, 1995); Grey Wolf Optimizer (GWO), introduced by Mirjalili et al. based on the cooperative hunting strategy of grey wolves (Mirjalili et al., 2014); and Black Winged Kite Algorithm (BKA), proposed by Wang et al. based on the aerial hunting behavior of black-winged kites (Wang et al., 2024). While these algorithms perform well in specific applications, experimental results show that excessive dependence on the current best solution tends to reduce population diversity, leading to premature convergence (Gao et al., 2025b). This brings forth the first research question: How to design more reasonable guidance mechanisms to maintain population diversity and effectively avoid local optima in complex search spaces?

On the other hand, many metaheuristic algorithms adopt only a single search strategy, making it difficult to dynamically balance exploration and exploitation throughout the entire optimization process. For example, both PSO and the PID-based Search Algorithm (PSA) proposed by Gao (Gao, 2023) suffer from this limitation. Although JADE, proposed by Zhang et al. (Zhang and Sanderson, 2009), introduces dynamic parameter adaptation to enhance search diversity, experimental results still show that JADE's population diversity remains limited. This leads to the second research question: How to achieve a more efficient balance between exploration and exploitation through multi-strategy collaboration and adaptive regulation mechanisms?

In recent years, an increasing number of researchers have drawn attention to the phenomenon of over-metaphorization in metaheuristic algorithm design (Sörensen, 2015). These algorithms tend to rely heavily on natural metaphors while

overlooking the underlying mathematical principles. Although such algorithms have achieved success in some engineering applications, their abstract nature and lack of generalizability limit both extensibility and innovation potential (Camacho-Villalón et al., 2023). Therefore, designing metaphor-free metaheuristic algorithms with strong performance and practical value has become a new research trend.

Several studies have made progress in this direction. For example, Logistic Gauss Circle Optimizer, proposed by Wang et al. (Wang et al., 2025a), though inspired by three types of chaotic maps, essentially regulates exploration and exploitation through the cooperative use of Logistic, Gauss, and Circle chaos mechanisms. Similarly, the Delta Plus algorithm developed by Gao et al. completely abandons metaphor-driven design and instead constructs an optimization framework based purely on the general search principles of metaheuristics, offering a new perspective for the development of metaphor-free algorithms.

Based on the above motivations, we propose a metaphor-free metaheuristic algorithm inspired by the dogfight behavior of fighter jets, called Dogfight Search (DoS). Different from traditional algorithms such as Genetic Algorithm (GA) (Holland, 1992) and PSO, DoS introduces a dual formation structure and distinguishes the solutions within the formation as "leader aircraft" and "wing aircraft", where wing aircraft possess the ability to dynamically select search strategies to achieve adaptive adjustment between exploration and exploitation. In the search process, DoS incorporates the displacement integration equations from kinematics (Zohar et al., 2011), coordinating five search strategies through the adjustment of direction vectors, flight speed, and flight time, thereby enhancing the overall algorithm performance. Although the concept of DoS originates from the dogfight behavior of fighter jets, its search mechanism is detached from metaphors and it achieves results superior to SOTA algorithms in CEC2017 and CEC2022 benchmark test functions. The main contributions of this paper are:

- (1) A metaphor-free metaheuristic algorithm, named DoS, is proposed;

- (2) In CEC2017 (30, 50, 100 dimensions) and CEC2022 (10, 20 dimensions) benchmark test functions, DoS demonstrated significantly superior performance compared to seven advanced competitors; Furthermore, DoS achieved the top Friedman ranking when compared against three SOTA algorithms: LSHADE (Tanabe and Fukunaga, 2014), LSHADE-SPACMA (Mohamed et al., 2017) and AL-SHADE (Li et al., 2022), demonstrating strong competitiveness;
- (3) DoS ranks first in overall performance on real-world engineering optimization problems. It remains statistically superior in problems with 91 inequality constraints, confirming its engineering applicability;
- (4) In mountainous terrain path planning tasks with and without no-fly zones, DoS also demonstrates significantly superior performance compared to competitors.

The rest of this paper is organized as follows: Section 2 introduces related research on metaheuristic algorithms; Section 3 describes the design inspiration and mathematical model of DoS; Section 4 evaluates DoS numerically on multidimensional CEC2017 and CEC2022 benchmark test functions; Section 5 verifies the performance of DoS on solving constrained optimization problems through various real-world tasks; Section 6 further validates the advantages of DoS in solving mountainous terrain path planning problems; Section 7 discusses the advantages and limitations of DoS; Section 8 summarizes the work and points out potential future research directions based on DoS.

2. Related studies

The classification of metaheuristic algorithms is mainly reflected in two aspects. As shown in Fig. 1, based on the number of solutions, algorithms can be categorized into two major types: single-solution-based algorithms and multi-solution-based algorithms.

The classification of single-solution-based algorithms lies in their search process relying on a single-solution. A representative example is the Simulated Annealing (SA) proposed by Kirkpatrick et al. in 1983 (Kirkpatrick et al., 1983), which was inspired by the energy changes in the cooling process of solids. Due to the limited global information obtained from a single-solution, SA introduces a probability mechanism for accepting worse solutions to escape local optima and enhance exploration ability. Other representative algorithms include the Tabu Search Algorithm (TSA) (Prajapati et al., 2020), Random Search (RS) (Zabinsky et al., 2009) and Non-monopolize Search (NO) (Abualigah et al., 2024). Although this type of algorithm has advantages in convergence speed, its low information utilization efficiency often makes it difficult to deal with complex high dimensional problems, which in turn has promoted the development of multi-solution-based algorithms.

Multi-solution-based algorithms utilize information from multiple solutions to guide the search, thereby enhancing global search ability. Although the design inspirations of

such methods are diverse, including animal behaviors, natural phenomena, physical laws and mathematical functions, their classification depends on the search mechanisms. Multi-solution-based algorithms can be further categorized into evolution-based algorithms and swarm-based algorithms (Ezugwu et al., 2021).

Evolution-based algorithms are based on Darwin's theory of evolution and stress genetic crossover and mutation operations on decision variables throughout the optimization process. A typical representative is the Genetic Algorithm (GA) proposed by Forrest et al., which continuously optimizes candidate solutions through mechanisms such as selection, crossover and mutation. Other evolutionary approaches include Differential Evolution (DE) (Storn and Price, 1997), Genetic Programming (GP) (Koza, 1994) and Love Evolution Algorithm (LEA) (Gao et al., 2024).

Swarm-based algorithms form the largest subclass, drawing inspiration from biological behaviors, physical processes, and mathematical models. Among them, typical algorithms inspired by biological activities include PSO and Ant Colony Optimization (ACO) (Dorigo, 1991). The latter was proposed by Dorigo in 1991 and simulates the pheromone mechanism of ants for optimization. A representative of physics inspired algorithms is the Gravitational Search Algorithm (GSA) (Rashedi et al., 2009), which simulates gravitational interactions between solutions to achieve global guidance. Mathematics inspired algorithms include the Sine Cosine Algorithm (SCA) (Mirjalili, 2016), which leverages the periodicity of trigonometric functions to enhance search diversity. In addition to the above typical methods, swarm-based algorithms also include: Beaver Behavior Optimizer (BBO) (Ouyang et al., 2025), Philoponella Prominens Optimizer (PPO) (Gao et al., 2025a), Escape Algorithm (ESC) (Ouyang et al., 2024), Traffic Jam Optimizer (TJO) (Wang and Shang, 2025), Multi-Verse Optimizer (MVO) (Mirjalili et al., 2016), Atom Search Optimization (ASO) (Zhao et al., 2019) and Weighted Average Algorithm (WAA) (Cheng and De Waele, 2024).

Although these algorithms perform well in various problems, most swarm-based algorithms share two common shortcomings. First, the guidance information overly depends on the population's best solution and lacks diversified guidance, making the search prone to local optima. Second, the number of search strategies is usually no more than three, resulting in monotonous search behavior. These limitations reduce their search efficiency in complex feasible regions.

To address the above issues, the proposed DoS introduces multiple guiding solutions in its design to enhance diversity. In addition, DoS assigns wing aircrafts a dynamic search strategy selection mechanism to effectively balance exploration and exploitation.

3. Methodology

This section will introduce the design inspiration, mathematical model, pseudocode and theoretical analysis of the computational complexity of DoS.

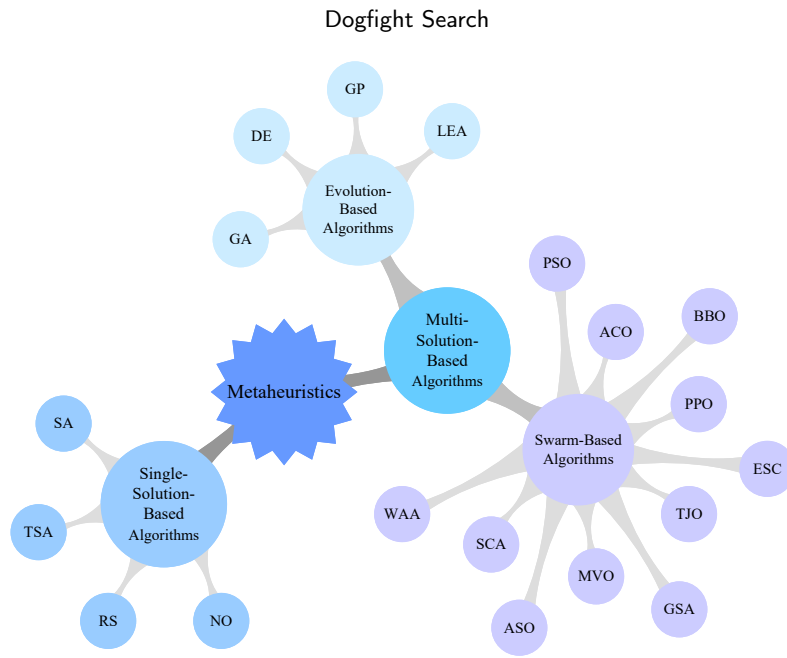


Figure 1: The classification of metaheuristic algorithms.

3.1. Inspiration

Dogfighting (Ashraf et al., 2021) is a highly dynamic air combat behavior, which is typically divided into two phases: attack and evasion. In the attack phase, fighter jets carry out strikes by chasing and locking onto enemy aircraft and launching missiles. In the evasion phase, they rely on irregular and chaotic flight trajectories to escape enemy lock-on and missile tracking (Greenwood, 1992). Two fighter jet formations strive to achieve the best combat readiness through adjustments to their positions and combat strategies, thereby securing victory. This process bears a striking resemblance to the optimization solutions employed in metaheuristic algorithms. This process is highly similar to the optimization solving process in metaheuristic algorithms. Therefore, inspired by this behavior, we designed five types of search strategies for DoS: free flight, maneuver lock-on, missile attack, maneuver evasion and flare evasion. To better explain the algorithm design concept, we abstract the inspirations as follows:

- (1) Solution: the position of a fighter jet. We divide the fighter group into two formations, which are adversarial to each other;
- (2) Feasible domain: the airspace in which the fighter jets conduct their search;
- (3) Function value: the combat state of the fighter jet. For minimization problems, the better the combat state, the smaller the function value;
- (4) Global optimal solution: the location in the airspace with the best combat state.

Fig. 2(a) shows the inspiration source of the free flight strategy in DoS (Olsder and Breakwell, 1974). In this strategy, the leader aircraft and wing aircraft randomly search the airspace based on commands from the command center,

while the wing aircraft continuously cooperates with the leader aircraft, enabling efficient exploration of the airspace. Fig. 2(b) and (c) illustrate the maneuver lock-on and missile attack strategies, respectively. Both strategies focus on enemy aircraft as core targets and exhibit strong convergence and guidance, promoting local exploitation and improving solution accuracy. Fig. 2(d) and (e) illustrate the maneuver evasion and flare evasion strategies. In this phase, fighter jets rapidly disengage from the current airspace and move toward new flight regions to avoid threats. From the perspective of search behavior, this process shows clear global exploration capability. The synergy of these five strategies enables the solutions to continuously move toward better regions, thereby improving overall search efficiency.

It is important to emphasize that although DoS is inspired by dogfighting behavior, its search strategies are mathematically modeled based on the displacement integration equations in kinematics. Specifically, we conduct diversified modeling of key elements such as the direction vector, flight speed and flight duration in DoS, thereby achieving metaphor-free search operations.

3.2. Mathematical model of the search strategy

The workflow of DoS is shown in Fig. 3, which sequentially includes initialization (see Section 3.2.1), the calculation of the number of leader aircrafts and the influencing factors of search strategies (see Sections 3.2.1 and 3.2.2), the search strategies of the two formations (see Sections 3.2.2 to 3.2.4) and the dynamic selection mechanism of wing aircraft (see Section 3.3).

To facilitate understanding of the dual formation design in DoS, Section 3.2.1 first introduces the construction of the dual formation and the method for calculating the number of leader aircrafts in each iteration; Section 3.2.1 also explains the initialization strategy tailored to the dual



Figure 2: The inspiration diagram of DoS search strategies.

formation design of DoS. Considering that the five types of search strategies follow the same fundamental principles, Section 3.2.2 provides a unified explanation of the common principles behind these strategies, including the mathematical meanings of key factors such as direction vector, flight speed and flight duration. Subsequently, Sections 3.2.3 to 3.2.5 respectively present the specific settings of the relevant parameters in the five search strategies.

3.2.1. Initialization of Dual Formations

To meet the requirements of the dual formation structure in DoS, we assume that the total number of formation solutions (N) is an even number. Among them, $N/2$ solutions are defined as the stealth fighter formation (\mathbf{X}) and the

remaining $N/2$ solutions are defined as the regular fighter formation (\mathbf{Y}).

To avoid convergence to local optima caused by relying on a single guiding solution, leader aircrafts serve as the guiding solutions and wing aircrafts adopt search strategies through a dynamic selection mechanism. Furthermore, to broaden the exploration range of the formation, the number of leader aircrafts is randomly selected within a defined interval, as expressed in Equation 1.

$$p = \text{round} \left\{ \left[k_1 + \left(\frac{1}{2} - k_1 \right) - r_1 \right] - \frac{N}{2} \right\} \quad (1)$$

where p denotes the number of leader aircrafts, k_1 is a tunable hyperparameter in DoS and r_1 is a random number uniformly distributed in the interval $[0, 1]$. It can be seen

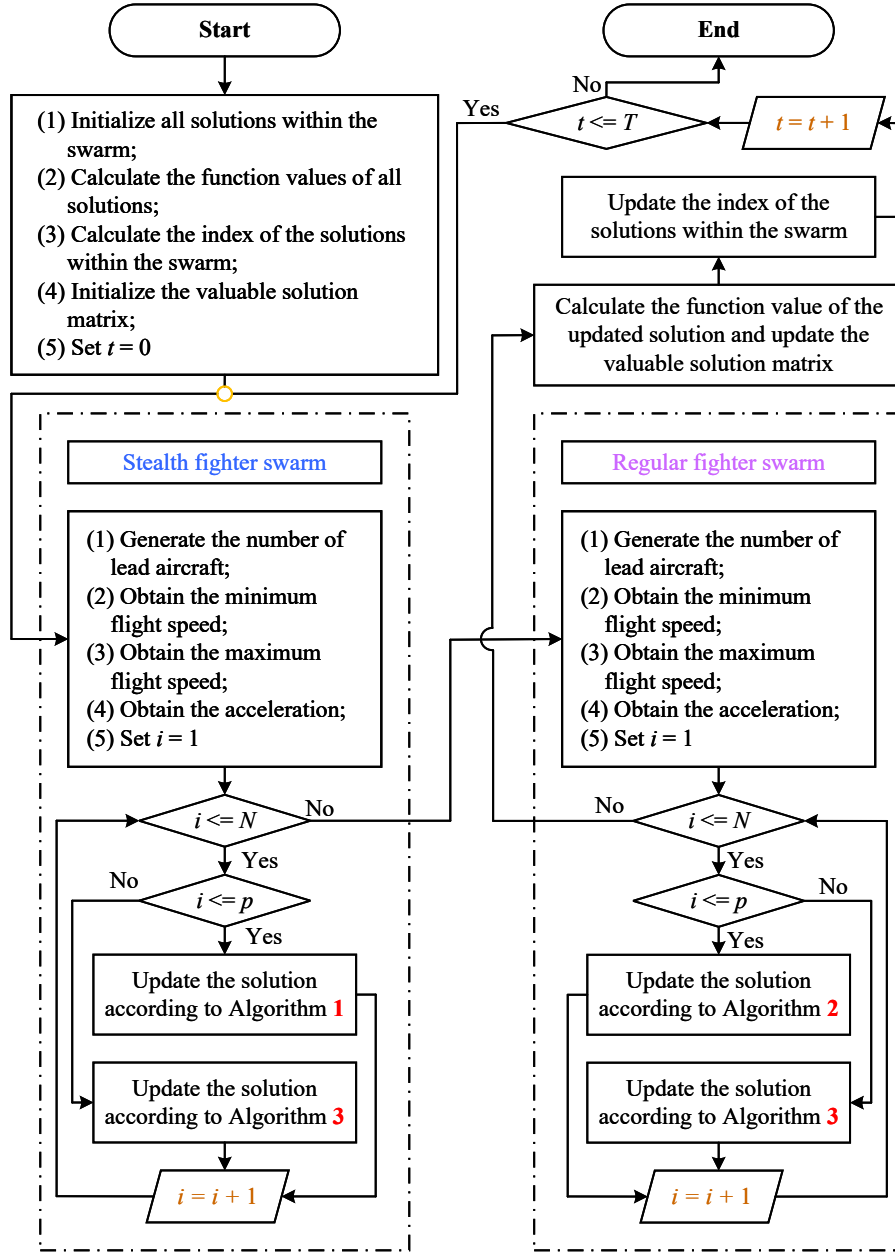


Figure 3: The iterative flowchart of DoS.

that the number of leader aircrafts is constrained within the range $[k_1 N, 0.25 N]$, which not only expands the exploration radius of the formation but also reserves a sufficient proportion of wing aircrafts to better achieve a balance between exploration and exploitation.

Considering that DoS adopts a dual formation structure and integrates multiple search strategies, more dispersed initial formations yield more effective searches. Therefore, this paper proposes an initialization strategy different from

traditional methods, whose form is shown in Equation 2.

$$\begin{aligned} X^{ij} &= L^j + \left(\frac{U^j + L^j}{2} - L^j \right) r_2, \\ Y^{ij} &= \frac{U^j + L^j}{2} + \left(U^j - \frac{U^j + L^j}{2} \right) r_2, \end{aligned} \quad (2)$$

$$i = 1, 2, \dots, N/2, \quad j = 1, 2, \dots, D$$

where \mathbf{X} represents the stealth fighter formation, \mathbf{Y} represents the regular fighter formation, \mathbf{U} and \mathbf{L} are the upper and lower bound vectors of the decision variables, D is the problem dimension and r_2 is a random number uniformly distributed within $[0, 1]$. This initialization strategy divides the feasible domain into two sub intervals, upper and lower

based on the hyperplane formed by the midpoints of each dimension (Winder, 1966), which are then used as the initialization ranges for the stealth fighter formation and the regular fighter formation, respectively.

By placing the two formations in spatially distinct regions based on this domain partitioning, the strategy enhances the spread of solutions in the early search stage. This spatial separation also supports the subsequent attack and evasion strategies, thereby improving the exploration efficiency of DoS.

3.2.2. Common Principles of Search Strategies

Although DoS uses dogfighting behavior as an external expression, the mathematical models of the 5 search strategies are based on the kinematics and displacement integration equations shown in Equation 3.

$$X_{new}^i = X^i + \int_0^{\Delta\xi} \mathbf{u} \cdot v d\xi, \quad i = 1, 2, \dots, N/2 \quad (3)$$

where \mathbf{u} denotes the direction vector, v denotes the flight speed and represents the flight duration. Since DoS sorts the solutions within each formation in ascending order based on their function values at the end of each iteration, solutions with better function values are ranked earlier. The top p solutions are defined as leader aircrafts and the remaining solutions are defined as wing aircrafts. In Sections 3.2.2 to 3.2.4, based on the distinction between leader aircrafts and wing aircrafts, the direction vector \mathbf{u} is further divided into \mathbf{u}_{leader} and \mathbf{u}_{wing} .

As shown in Equation 3, regardless of which search strategy is adopted, the update of a solution depends on three key factors: \mathbf{u} , v and $\Delta\xi$. This paper leverages differentiated definitions of these three factors to implement the effects of the five search strategies.

Decomposition of the direction vector:

In most metaheuristic algorithms, a solution's direction is typically determined by intra-formation information alone. As a result, it is often difficult to escape local optima when solving complex optimization problems. To address this, DoS decomposes \mathbf{u} into two components: pilot guidance (\mathbf{u}^{Pilot}) and command guidance (\mathbf{u}^{Head}). Specifically:

- (1) \mathbf{u}^{Pilot} : the direction vector determined by intra-formation pilot information;
- (2) \mathbf{u}^{Head} : the direction vector determined by informative and high-quality solutions.

Therefore, \mathbf{u}^{Head} helps solutions escape from local optima in a timely manner and explore new potential regions. Since \mathbf{u}^{Pilot} must be designed to meet the exploration and exploitation needs of different strategies, its definition is elaborated in Sections 3.2.2 to 3.2.4. The mathematical form of \mathbf{u}^{Head} is shown in Equation 4.

$$\begin{aligned} R_1 &= \text{round}(NR \cdot r_3), \quad R_2 = \text{round}(NP \cdot r_4), \\ \mathbf{u}^{Head} &= \mathbf{X}^{R_1} - \mathbf{Z}^{R_2} \end{aligned} \quad (4)$$

where R_1 denotes the index of a randomly selected high-quality solution, NR denotes the number of high quality

solutions (fixed at $0.1N$), \mathbf{Z} is the storage matrix of valuable solutions, R_2 denotes the index of a randomly selected valuable solution, NP denotes the number of stored valuable solutions (with a maximum of $2.5N$) and r_3 and r_4 are random numbers uniformly distributed in the range $[0, 1]$.

Minimum speed, maximum speed and acceleration:

In DoS, the motion state of solution updates is modeled as either uniform or uniformly accelerated motion. Therefore, v is determined by three influencing factors: minimum speed (v_{min}), maximum speed (v_{max}) and acceleration (a). As shown in Equation 3, v is closely related to the step size of solution updates. If speed can be appropriately quantified to guide the update of solutions toward positions with lower function values, the search efficiency can be significantly improved. To achieve this, DoS records promising solutions (i.e., those with decreasing function values) at the end of each iteration and uses the velocity and function value information of these promising solutions to update the initial velocity for the next iteration. Details are shown in Equation 5.

$$V_{new} = \frac{\sum_{i \in \Omega} W_i \cdot V_i^2}{\sum_{i \in \Omega} W_i \cdot V_i}, \quad W_i = \frac{df_i}{\sum_{i \in \Omega} df_j} \quad (5)$$

where V_{new} denotes the initial velocity for the next iteration, Ω represents the set of indices of promising solutions, V_i and df_i denote the flight velocity and function value difference of the i -th promising solution, respectively. To enhance solution diversity, DoS adds real-valued random perturbations to the initial velocity, as shown in Equation 6.

$$V = V_{new} + \tan\left[\frac{\pi}{2}(r_5 - 0.5)\right] / 10 \quad (6)$$

where r_5 is a random number uniformly distributed in the range $[0, 1]$ and the velocity V obtained from Equation 6 can be further used to define the minimum speed, maximum speed and acceleration of a solution in the next iteration, as shown in Equation 7.

$$\begin{aligned} v_{min} &= \min\{k_5 V, V\}, \quad v_{max} = \max\{k_5 V, V\}, \\ a &= (v_{max} - v_{min}) / 1.2 \end{aligned} \quad (7)$$

where k_5 is a tunable hyperparameter in DoS and belongs to the interval $[0, 1]$.

Flight duration:

In Equation 3, $\Delta\xi$ is also a key factor shaping the solution's update radius. Since v has already achieved sufficient diversification of the movement radius, this paper $\Delta\xi$ designs as a control factor for diversified search regions, allowing solutions to be updated within a certain range. The specific formulation is shown in Equation 8.

$$\Delta\xi = 0.8 + 0.4r_6 \quad (8)$$

where r_6 is a random number uniformly distributed in the range $[0, 1]$ and thus is a uniformly distributed random value within the interval $[0.8, 1.2]$. This setting allows solutions to perform fine grained exploitation within a small range while also expanding the exploration radius over a larger range, thereby improving overall search efficiency.

3.2.3. Free Flight Strategy

In this subsection and the subsequent descriptions of the mathematical models for search strategies, we focus on the design of the direction vector and flight speed. It is important to note that, to improve the search efficiency of DoS in the early iterations, the two formations differ only in the strategy selection mechanism during the early stage (see Section 3.3), while their mathematical expressions remain identical. Therefore, this paper uses the stealth fighter formation as the unified example for explanation.

In the early stage of iteration, due to the lack of prior knowledge about the solution space of the optimization problem, it is necessary to conduct global exploration of the feasible domain. As information about the solution space accumulates, a gradual balance between exploration and exploitation should be achieved. Based on this, a ‘‘free flight’’ strategy is designed for DoS. Under this strategy, the direction vectors of leader aircrafts and wing aircrafts are defined as follows, as shown in Equation 9.

$$\begin{aligned} \mathbf{u}_{\text{leader}}^{\text{Pilot}} &= \mathbf{X}_{\text{rand}} - \mathbf{X}^i, & \mathbf{u}_{\text{wing}}^{\text{Pilot}} &= \mathbf{X}^H - \mathbf{X}^i, \\ \mathbf{X}_{\text{rand}} &= \mathbf{L} + (\mathbf{U} - \mathbf{L})r_7 \end{aligned} \quad (9)$$

where leader denotes the leader aircraft, wing denotes the wing aircraft, H indicates the index of the leader aircraft followed by the wing aircraft and r_7 is a random number uniformly distributed in the range $[0, 1]$. Under this mechanism, leader aircrafts conduct random exploration within the feasible domain, while wing aircrafts perform local exploitation along the flight path of leader aircrafts, thereby significantly improving the discovery efficiency of high-quality solutions during the early stages of iteration.

Since an excessively large step size may cause the update process to miss some valuable solutions, the motion state under this strategy is modeled as uniform motion with a speed of v_{\min} . By incorporating the flight duration defined in Equation 8 and substituting it into Equation 3, the mathematical model of the free flight strategy is obtained, as shown in Equation 10.

$$\begin{cases} \mathbf{X}_{\text{new}}^i = \mathbf{X}^i + (\mathbf{u}_{\text{leader}}^{\text{Pilot}} + \mathbf{u}^{\text{Head}}) v_{\min} \cdot \Delta\xi, & i \leq p \\ \mathbf{X}_{\text{new}}^i = \mathbf{X}^i + (\mathbf{u}_{\text{wing}}^{\text{Pilot}} + \mathbf{u}^{\text{Head}}) v_{\min} \cdot \Delta\xi, & i > p \end{cases} \quad (10)$$

where $\mathbf{X}_{\text{new}}^i$ denotes the updated position of the i -th leader aircraft or wing aircraft. To intuitively demonstrate the behavioral characteristics of this strategy, it is visualized in a two dimensional plane, as shown in Fig 4.

3.2.4. Offensive Strategy

Although the free flight strategy can achieve a dynamic balance between exploration and exploitation in the early stages of iteration, relying on a single search strategy throughout the entire iteration process will inevitably limit the diversity of search behavior. To address this, two offensive strategies are designed for DoS to enhance its local exploitation ability around valuable solutions. These strategies are inspired by the processes of pursuing and

locking onto enemy aircraft, as well as missile attacks during dogfights and are thus named the maneuver lock-on and missile attack strategies. The mathematical models of these strategies are described below.

Maneuver lock-on strategy:

Most metaheuristic algorithms rely on a single population, which makes them prone to falling into local optima, resulting in many iterations without meaningful improvement. Sudholt (Sudholt, 2019) pointed out that increasing the number of populations can improve search diversity. Based on this, DoS leverages the advantages of its dual formation structure, allowing both offensive strategies to obtain exploitation information from the opposing formation. The computation function for the pilot guided direction vector in the maneuver lock-on strategy is shown in Equation 11.

$$\begin{aligned} \mathbf{u}_1^{\text{Pilot}} &= \mathbf{Y}^h - \mathbf{X}^i, & \mathbf{u}_2^{\text{Pilot}} &= \mathbf{Y}_{\text{pre}}^h - \mathbf{X}^i, \\ \mathbf{u}^{\text{Pilot}} &= r_8 \cdot \mathbf{u}_1^{\text{Pilot}} + (1 - r_8)\mathbf{u}_2^{\text{Pilot}} \end{aligned} \quad (11)$$

where \mathbf{Y} denotes the coordinate matrix of the regular fighter formation, h is the index of the selected regular fighter, $\mathbf{Y}_{\text{pre}}^h$ represents the predicted position and r_8 is a random number uniformly distributed in the range $[0, 1]$. According to the equation, the $\mathbf{u}^{\text{Pilot}}$ under the maneuver lock-on strategy is no longer distinguished between leader aircraft and wing aircraft. Instead, it is determined by two sub vectors:

- (1) $\mathbf{u}_1^{\text{Pilot}}$: determined based on the solution information from the opposing formation;
- (2) $\mathbf{u}_2^{\text{Pilot}}$: determined based on both the opposing formation and the best solution information, with the definition of $\mathbf{Y}_{\text{pre}}^h$ given in Equation 12.

$$\mathbf{Y}_{\text{pre}}^h = \mathbf{Y}^h + (\mathbf{Y}^{\text{best}} - \mathbf{Y}^h) r_9, \quad h \leq p \quad (12)$$

where r_9 is a random number uniformly distributed in the interval $[0, 1]$ and both \mathbf{Y}^h and \mathbf{Y}^{best} are leader aircraft within the regular fighter formation. The linear combination of these two yields $\mathbf{Y}_{\text{pre}}^h$, which possesses high exploitation value. Since $\mathbf{Y}_{\text{pre}}^h$ does not belong to the opposing formation, this design ensures exploitation while also effectively preventing the two formations from converging prematurely.

To enrich the distribution diversity of solutions after executing the maneuver lock-on strategy, the motion state is modeled as uniformly accelerated motion. The corresponding function describing velocity as a function of time is given in Equation 13.

$$v_\xi = v_{\min} + a \cdot \xi \quad (13)$$

By combining Equations 11, 13, 8 and 3, the complete mathematical formulation of the maneuver lock-on strategy can be derived, as shown in Equation 14.

$$\begin{aligned} \mathbf{X}_{\text{new}}^i &= \mathbf{X}^i + \int_0^{\Delta\xi} (\mathbf{u}^{\text{Pilot}} + \mathbf{u}^{\text{Head}}) v_\xi \cdot d\xi \\ &= \mathbf{X}^i + (\mathbf{u}^{\text{Pilot}} + \mathbf{u}^{\text{Head}}) \left(v_{\min} + \frac{1}{2} a \cdot \Delta\xi^2 \right), \\ i &= 1, 2, \dots, \frac{N}{2} \end{aligned} \quad (14)$$

Dogfight Search

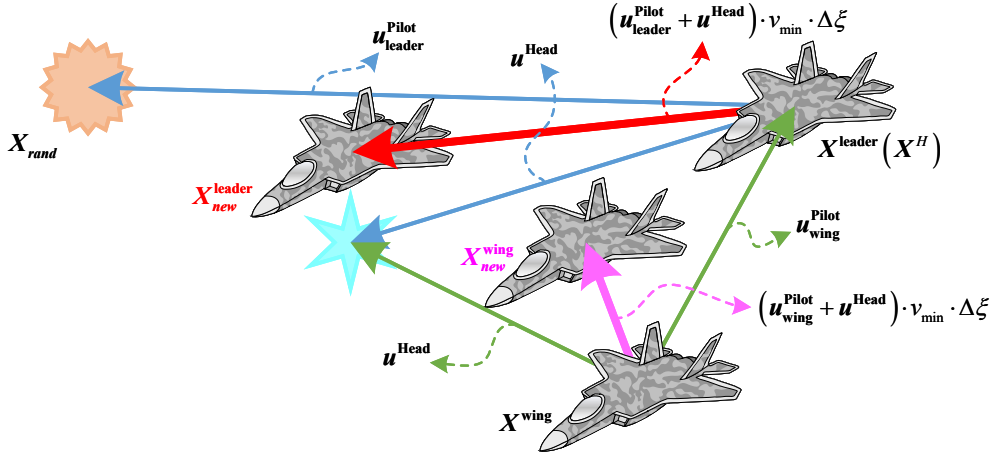


Figure 4: Visualization of the free flight strategy.

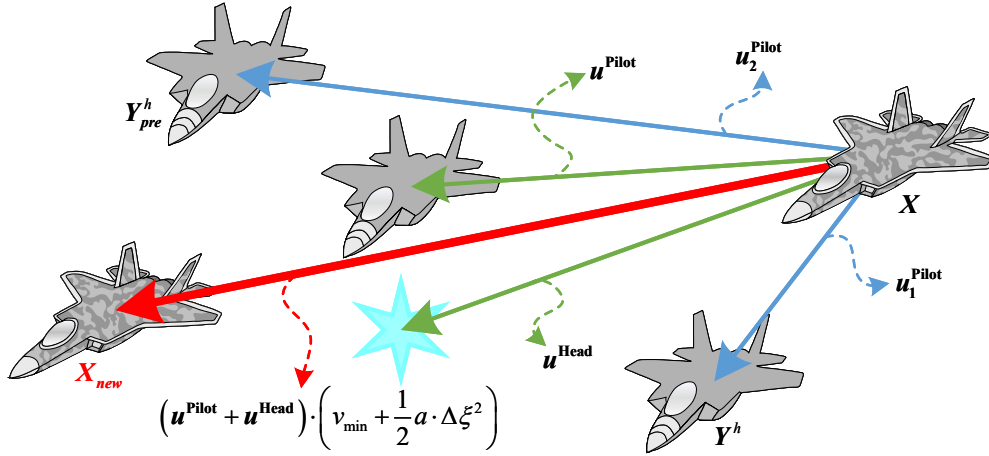


Figure 5: Visualization of the maneuver locking strategy.

To intuitively demonstrate the search behavior of this strategy, the solution update process is visualized in a 2 dimensional space, as shown in Fig. 5.

Missile attack strategy:

Although the maneuver lock-on strategy can prevent the two formations from converging prematurely, the algorithm's reliance on exploitation does not completely eliminate potential risks. When the solution approaches the region containing the global optimal solution, if DoS relies solely on the maneuver lock-on strategy for exploitation, it may be misled by attractive local optima and fail to further explore the global optimal solution region. To address this limitation, a missile attack strategy is proposed in this paper. This strategy relies exclusively on information from the opposing formation. The definition of $\mathbf{u}^{\text{Pilot}}$ under this strategy is provided in Equation 15.

$$\mathbf{u}^{\text{Pilot}} = \mathbf{Y}^h - \mathbf{X}^i, \quad h \leq p \quad (15)$$

Although this setting may cause the two formations to converge prematurely to the same solution region, the execution frequency of this strategy has been appropriately reduced within the iterative process of DoS. As long as

the majority of solutions still adopt the maneuver lock-on strategy, this issue can be effectively avoided.

Since the missile attack strategy requires solutions to move away from their original regions and gradually approach the global optimal, the motion state under this strategy is modeled as uniformly decelerated motion. The corresponding velocity function is given in Equation 16.

$$v_\xi = v_{\max} - a \cdot \xi \quad (16)$$

By combining Equations 15, 16, 8 and 3, the complete mathematical formulation of the missile attack strategy can be derived, as shown in Equation 17.

$$\begin{aligned} \mathbf{X}_{\text{new}}^i &= \mathbf{X}^i + \int_0^{\Delta\xi} (\mathbf{u}^{\text{Pilot}} + \mathbf{u}^{\text{Head}}) v_\xi \cdot d\xi \\ &= \mathbf{X}^i + (\mathbf{u}^{\text{Pilot}} + \mathbf{u}^{\text{Head}}) \left(v_{\max} - \frac{1}{2} a \cdot \Delta\xi^2 \right), \quad (17) \\ i &= 1, 2, \dots, \frac{N}{2} \end{aligned}$$

In summary, the exploitation mechanism of DoS integrates both the maneuver lock-on and missile attack strategies: the former utilizes high quality information beyond

the opposing formation to achieve efficient exploitation and avoid convergence consistency, while the latter ensures deep exploration of the global optimal solution. Their synergy allows DoS to maintain exploitation diversity while improve global performance.

3.2.5. Evasive Strategy

The offensive strategies proposed in Section 3.2.4 have already satisfied the exploitation requirements of DoS; however, exploration is also a critical factor throughout different stages of iteration. If exploration is insufficient in the early stage, the efficiency of gathering information about the solution space will be low; if it is insufficient in the middle and later stages, the algorithm is prone to getting trapped in local optima and may fail to converge to the global optimal solution. To address the exploration needs in the early stage, the free flight strategy has been designed. For the middle and later stages, in order to further enhance the exploration capability of DoS, two evasion strategies are proposed, namely the maneuver evasion and flare evasion strategies. These strategies are inspired by the evasive maneuvers and flare release behaviors of fighter jets during dogfights.

Maneuver evasion strategy:

In the middle and later stages of iteration, the main role of exploration strategies is to help solutions escape local optima. Therefore, $\mathbf{u}^{\text{Pilot}}$ should be decoupled from the current exploitation region and reoriented within the feasible domain. However, if completely random search, as in the free flight strategy, is adopted again, the optimization accuracy may be severely degraded. To avoid this, the mathematical model of $\mathbf{u}^{\text{Pilot}}$ in this paper is based on the set of stored valuable solutions, as defined in Equation 18.

$$\mathbf{u}^{\text{Pilot}} = \sum_{j=1}^n \frac{\mathbf{Z}^j}{n} - \mathbf{X}^i, \quad n = \text{round}(NR \cdot r_4) \quad (18)$$

where $\mathbf{u}^{\text{Pilot}}$ is determined by the centroid of half of the solutions in the valuable solution matrix. This design enables the strategy to depart from the original solution region while effectively suppressing ineffective exploration. To ensure that solutions have a sufficient movement radius and to enrich the diversity of movement ranges, the maneuver evasion strategy is modeled as uniformly accelerated motion. By combining Equations 18, 13, 8 and 3, the complete mathematical formulation is derived, as shown in Equation 19.

$$\begin{aligned} \mathbf{X}_{new}^i &= \mathbf{X}^i + \int_0^{\Delta\xi} (\mathbf{u}^{\text{Pilot}} + \mathbf{u}^{\text{Head}}) v_{\xi} \cdot d\xi \\ &= \mathbf{X}^i + (\mathbf{u}^{\text{Pilot}} + \mathbf{u}^{\text{Head}}) \left(v_{\min} + \frac{1}{2} a \cdot \Delta\xi^2 \right), \quad (19) \\ i &= 1, 2, \dots, \frac{N}{2} \end{aligned}$$

To intuitively demonstrate the search trajectory of the maneuver evasion strategy, a visualization is conducted in a 2-dimensional plane, as shown in Fig. 6.

Flare evasion strategy:

The role of maneuvering evasion strategies is to guide solutions away from local optima and migrate toward other valuable solutions, while the flare evasion strategy is designed from a different perspective. As is well known, the randomness in metaheuristic algorithms usually stems from random numbers embedded in strategies or parameters. However, most algorithms tend to concentrate random searches near the center of the feasible domain, resulting in weaker exploration near the boundaries. When the global optimum is near the boundary, this drawback can markedly degrade performance.

$$\begin{aligned} \mathbf{u}^{\text{Pilot}} &= \mathbf{X}_{rand}^{\text{boundary}} - \mathbf{X}^i, \\ \mathbf{X}_{rand}^{\text{boundary}} &= \mathbf{X}_{rand} \cdot I_1 + I_2 [L \cdot I_2 + U(1 - I_2)] \quad (20) \end{aligned}$$

To tackle this, this paper proposes the flare evasion strategy, which is specifically designed to strengthen the exploration capability in boundary regions. The definition of $\mathbf{u}^{\text{Pilot}}$ for this strategy is given in Equations 20 and 21.

$$I_1 = \begin{cases} 0, & r_{10} < 0.5 \\ 1, & r_{10} \geq 0.5 \end{cases}, \quad I_2 = \begin{cases} 0, & r_{11} < 0.5 \\ 1, & r_{11} \geq 0.5 \end{cases} \quad (21)$$

where $\mathbf{X}_{rand}^{\text{boundary}}$ is a randomly generated boundary point within the feasible domain. The generation principle of \mathbf{X}_{rand} is the same as in Equation 9 and the settings of I_1 and I_2 are defined in Equation 21, where r_{10} and r_{11} are random numbers uniformly distributed within the range $[0, 1]$. Therefore, the exploration information of $\mathbf{u}^{\text{Pilot}}$ originates from randomly selected boundary points. Since boundary search requires a larger movement radius for support, this strategy is modeled as uniform motion with maximum speed. The complete mathematical model is provided in Equation 22.

$$\begin{aligned} \mathbf{X}_{new}^i &= \mathbf{X}^i + \int_0^{\Delta\xi} (\mathbf{u}^{\text{Pilot}} + \mathbf{u}^{\text{Head}}) v_{\max} \cdot d\xi \\ &= \mathbf{X}^i + (\mathbf{u}^{\text{Pilot}} + \mathbf{u}^{\text{Head}}) v_{\max} \cdot \Delta\xi, \quad (22) \\ i &= 1, 2, \dots, \frac{N}{2} \end{aligned}$$

In summary, the exploration capability of DoS is enhanced through two complementary evasion strategies: the maneuver evasion strategy helps solutions effectively escape from local optima and transition to new valuable solutions, while the flare evasion strategy addresses the issue of insufficient exploration in boundary regions. The combination of these two strategies equips DoS with stronger global search ability in the middle and later stages of iteration.

3.3. Dynamic Selection Mechanism

According to Section 3.2, DoS assigns corresponding search strategies to the early, middle and later stages of the iteration process. However, to achieve a dynamic balance between exploration and exploitation, the dynamic strategy selection mechanism is a key factor. This section introduces the mechanism based on the pseudocode of the iterative

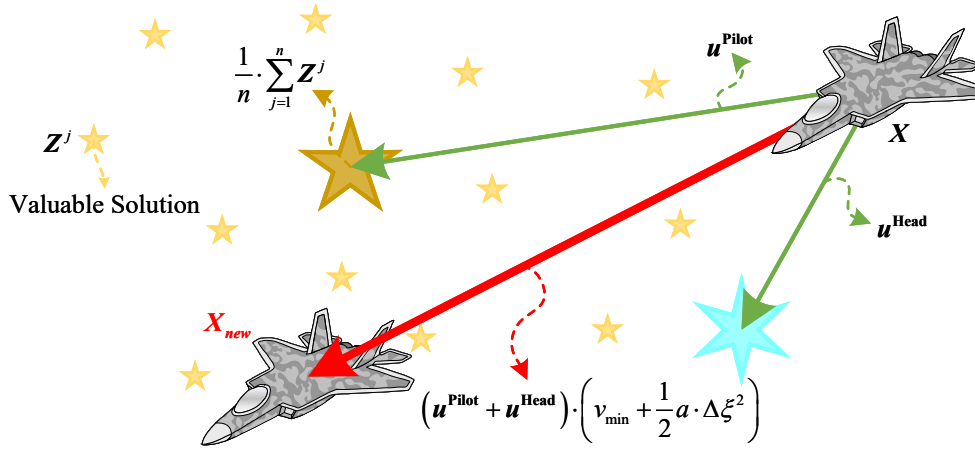


Figure 6: Visualization of the maneuver evasion strategy.

process for four types of solutions. For ease of explanation, the search strategies are represented by numeric identifiers: free flight (1), maneuver lock-on (2), missile attack (3), maneuver evasion (4) and flare evasion (5).

Leader aircraft in the stealth fighter formation:

As guiding solutions within the formation, leader aircraft adopt a more stochastic approach to strategy selection. According to Sections 3.2.3 to 3.2.5, leader aircraft primarily adopt the free flight strategy during the early stage of iteration, gradually shifting toward offensive and evasion strategies in the middle and later stages. To prevent over reliance on free flight, this paper introduces the following constraint for their execution, as shown in Equation 23.

$$b_X^i(i \leq p) = \begin{cases} 1, & r_{12} < K \text{ and } t < k_3 \cdot T \\ \text{Eq. 25,} & r_{12} \geq K \text{ or } t \geq k_3 \cdot T \end{cases} \quad (23)$$

where b_X^i denotes the strategy index selected by the i -th leader aircraft in the stealth fighter formation, k_3 is a tunable hyperparameter in DoS, t and T represent the current and maximum number of iterations, respectively, K is the execution probability of the free flight strategy and r_{12} is a random number uniformly distributed within the range $[0, 1]$. To adapt to the iteration process, K is set as a monotonically decreasing function with respect to the number of iterations, as defined in Equation 24.

$$K = e^{k_2 - \frac{t}{T}} \quad (24)$$

If Equation 23 is not satisfied, the solution will select an offensive or evasion strategy based on a random number. The mathematical form is as follows:

$$b_X^i(i \leq p) = \begin{cases} 2, & r_{13} < P^X \text{ and } r_{14} < 0.5 \\ 3, & r_{13} < P^X \text{ and } r_{14} \geq 0.5 \\ 4, & r_{13} \geq P^X \text{ and } r_{14} < 0.8 \\ 5, & r_{13} \geq P^X \text{ and } r_{14} \geq 0.8 \end{cases} \quad (25)$$

where r_{13} and r_{14} are random numbers uniformly distributed within the range $[0, 1]$ and P^X is the probability coefficient for offensive and evasion strategies, which dynamically changes with the function values of the formation. This coefficient is updated according to the promising-solution selections in each iteration, as defined in Equation 26.

$$P_{new}^X = P^X + 0.05(1 - P^X) \left(\frac{\sum_{i \in \Omega_1} i}{\sum_{j \in \Omega^1} j} - \frac{\sum_{i \in \Omega_2} i}{\sum_{j \in \Omega^2} j} \right) \frac{t}{T} \quad (26)$$

where P_{new}^X denotes the updated probability coefficient, Ω^1 and Ω^2 the sets and represent the indices of solutions that have selected offensive and evasion strategies, respectively. Similarly Ω_1 and Ω_2 denote the indices of promising solutions that have chosen offensive and evasion strategies, respectively. Since solutions with larger indices tend to have worse function values, they are assigned greater weight in influencing strategy selection probabilities. This allows leader aircraft to reasonably regulate the formation's need for exploration or exploitation.

By integrating Equations 23, 25 and 26, the pseudocode for leader aircraft in the stealth fighter formation can be formulated, as shown in Algorithm 1.

Leader aircraft in the regular fighter formation:

According to Section 3.2.3, free flight is crucial for global exploration in the early stages of iteration. To prevent both formations from excessively executing the free flight strategy, which could reduce overall efficiency, this paper sets the leader aircraft in the stealth fighter formation to execute free flight probabilistically, while leader aircraft in the regular fighter formation are restricted to exclusively executing the free flight strategy during the early stage. The corresponding constraint is defined in Equation 27.

$$b_X^i(i \leq p) = \begin{cases} 1, & t < k_4 \cdot T \\ \text{Eq. 25,} & t \geq k_4 \cdot T \end{cases} \quad (27)$$

where k_4 is a tunable parameter in DoS used to control the demand for random search in the early stages of the algorithm. If the iteration count does not satisfy Equation 27,

Algorithm 1 Leader Aircraft of Stealth Fighter Formation.

Require: Updated solution index (i), search strategy selection factors (r_{12}, r_{13}, r_{14}), probability coefficient (P_X).
Ensure: Updated coordinates (X_{t+1}^i), selected search strategy (b_X^i).

- 1: **if** $r_{12} < K$ and $t < k_3 T$ **then**
- 2: $X_{t+1}^i \leftarrow$ Update X_t^i using Equation 10;
- 3: **else**
- 4: **if** $r_{13} < P_X$ **then**
- 5: **if** $r_{14} < 0.5$ **then**
- 6: $X_{t+1}^i \leftarrow$ Update X_t^i using Equation 14;
- 7: **else**
- 8: $X_{t+1}^i \leftarrow$ Update X_t^i using Equation 17;
- 9: **else**
- 10: **if** $r_{14} < 0.8$ **then**
- 11: $X_{t+1}^i \leftarrow$ Update X_t^i using Equation 19;
- 12: **else**
- 13: $X_{t+1}^i \leftarrow$ Update X_t^i using Equation 22;

the leader aircraft of the regular fighter formation selects the offensive or evasive strategy based on Equations 25 and 26. This mechanism avoids the accumulation of ineffective exploration in the early stage and ensures the exploration and exploitation balance between the two formations at different stages. The pseudocode for this mechanism is shown in Algorithm 2.

Algorithm 2 Leader Aircraft of Regular Fighter Formation.

Require: Updated solution index (i), search strategy selection factors (r_{13} and r_{14}), probability coefficients for exploration and exploitation strategies (P_X).
Ensure: Updated coordinates (Y_{t+1}^i), selected search strategy (b_Y^i).

- 1: **if** $t < k_4 T$ **then**
- 2: $Y_{t+1}^i \leftarrow$ update Y_t^i using Equation 10;
- 3: **else**
- 4: **if** $r_{12} < K$ and $t < k_3 T$ **then**
- 5: $Y_{t+1}^i \leftarrow$ update Y_t^i using Equation 10;
- 6: **else**
- 7: **if** $r_{13} < P_X$ **then**
- 8: **if** $r_{14} < 0.5$ **then**
- 9: $Y_{t+1}^i \leftarrow$ update Y_t^i using Equation 14;
- 10: **else**
- 11: $Y_{t+1}^i \leftarrow$ update Y_t^i using Equation 17;
- 12: **else**
- 13: **if** $r_{14} < 0.8$ **then**
- 14: $Y_{t+1}^i \leftarrow$ update Y_t^i using Equation 19;
- 15: **else**
- 16: $Y_{t+1}^i \leftarrow$ update Y_t^i using Equation 22;

Wing aircraft in both formations:

To maintain the balance between exploration and exploitation in DoS, this paper draws inspiration from the leader and wingman formation mechanism and designs a

dynamic selection mechanism for wing aircraft that relies on the decisions of leader aircraft. Since the dynamic selection mechanisms for wing aircraft are identical in both formations, this subsection uses the stealth fighter formation as an example for explanation. The detailed mathematical model is defined in Equation 28.

$$b_X^i(i > p) = \begin{cases} 1, & b_X^H = 1 \\ 2, & (b_X^H = 2 \text{ or } 3) \text{ and } (r_{13} < P^X) \\ 4, & (b_X^H = 2 \text{ or } 3) \text{ and } (r_{13} \geq P^X) \\ 2, & (b_X^H = 4 \text{ or } 5) \text{ and } (r_{14} < 0.5) \\ 3, & (b_X^H = 4 \text{ or } 5) \text{ and } (r_{14} \geq 0.5) \end{cases} \quad (28)$$

According to Equation 28, when the leader aircraft selects the free flight strategy, the wing aircraft also executes free flight to ensure early-stage balance and information sharing. When the leader aircraft adopts an offensive strategy, the wing aircraft can switch between maneuver lock-on and maneuver evasion. If the leader aircraft selects an evasion strategy, the wing aircraft must choose an offensive strategy to enhance exploitation capability. The corresponding pseudocode is presented in Algorithm 3.

Algorithm 3 Wing Aircraft of Stealth Fighter Formation.

Require: Updated solution index (i), search strategy selection factors (r_{13} and r_{14}), probability coefficients for exploration and exploitation strategies (P_X), leader aircraft index (H).
Ensure: Updated coordinates (X_{t+1}^i).

- 1: **if** $b_X^H = 1$ **then**
- 2: $X_{t+1}^i \leftarrow$ update X_t^i using Equation 10;
- 3: **else if** $b_X^H = 2$ or $b_X^H = 3$ **then**
- 4: **if** $r_{13} < P^X$ **then**
- 5: $X_{t+1}^i \leftarrow$ update X_t^i using Equation 14;
- 6: **else**
- 7: $X_{t+1}^i \leftarrow$ update X_t^i using Equation 19;
- 8: **else**
- 9: **if** $r_{14} < 0.5$ **then**
- 10: $X_{t+1}^i \leftarrow$ update X_t^i using Equation 14;
- 11: **else**
- 12: $X_{t+1}^i \leftarrow$ update X_t^i using Equation 17;

In summary, the complete pseudocode and flowchart of DoS are presented in Algorithm 4 and Fig. 3, respectively.

3.4. Theoretical Complexity Analysis

Complexity is one of the key indicators for evaluating an algorithm (Thomas H et al., 2009). In computer simulations, complexity is mainly reflected in terms of time complexity and space complexity. This section provides a theoretical analysis of DoS from both perspectives.

Time Complexity Analysis:

The time complexity of DoS mainly depends on three factors: the total size of the two formations (N), the maximum number of iterations (T) and the dimensionality of the

Algorithm 4 Dogfight Search.

Require: Swarm size (N), maximum number of iterations (T), decision variable dimensions (D), upper and lower bounds of decision variables (U and L) and objective function (f).

Ensure: Optimal solution (Best_Pos), optimal objective value (Best_Score).

- 1: Initialize X and Y using Equation 2;
- 2: Calculate fitness values F for X and G for Y ;
- 3: Assign indices to swarm solutions based on F and G ;
- 4: **while** $t \leq T$ **do**
- 5: Calculate p using Equation 1;
- 6: **for** $i = 1$ to $N/2$ **do**
- 7: **if** $i \leq p$ **then**
- 8: Update X_t^i using Algorithm 1;
- 9: **else**
- 10: Update X_t^i using Algorithm 3;
- 11: **for** $i = 1$ to $N/2$ **do**
- 12: **if** $i \leq p$ **then**
- 13: Update Y_t^i using Algorithm 2;
- 14: **else**
- 15: Update Y_t^i using Algorithm 3;
- 16: Check boundary constraints of X_{t+1} and Y_{t+1} ;
- 17: **for** $i = 1$ to $N/2$ **do**
- 18: Calculate fitness values F_i and G_i ;
- 19: Update valuable solution matrix;
- 20: Collect potential solution information;
- 21: Update probability coefficients P^X , P^Y , and velocity bounds v_{\min} , v_{\max} ;
- 22: Update solution indices based on F and G ;
- 23: $t \leftarrow t + 1$

decision variables (D). In the initialization phase, the algorithm needs to allocate initial positions for the formations, resulting in a time complexity of $O(ND)$. In the iteration phase, although DoS introduces a relatively complex dynamic strategy selection mechanism, each solution executes only one search strategy per iteration, so it does not impose additional computational overhead. The total computational complexity for this phase is $O(NDT)$. Therefore, the overall time complexity of DoS is: $O(ND) + O(NDT) \approx O(NDT)$.

Space Complexity Analysis:

The space complexity of DoS mainly comes from the following four components:

Position matrix: Stores the solution vectors, with complexity $O(ND)$;

Objective value matrix: Stores the function values of the solutions, with complexity $O(N)$;

Strategy index matrix: Records the strategy indices selected by solutions, with complexity $O(N)$;

Valuable solution matrix: Stores information of valuable solutions accumulated during iterations, with a maximum size of $O(2.5ND)$.

By combining the complexities of the four components, the total space complexity of DoS is: $O(ND) + O(N) + O(N) + O(2.5ND) \approx O(ND)$.

In summary, DoS maintains the conventional complexity level of metaheuristic algorithms, with a time complexity of $O(NDT)$ and space complexity of $O(ND)$. The diversity of search strategies and the complexity of the dynamic selection mechanism do not theoretically increase the computational overhead.

4. Experiments and Discussions

This section presents a systematic evaluation of the optimization performance of DoS. The content includes the following aspects: a basic introduction to the benchmark test functions (Section 4.1), performance comparison with advanced competitors (Section 4.2), performance comparison with SOTA algorithms (Section 4.3), analysis of exploration and exploitation capabilities (Section 4.4), convergence analysis (Section 4.5), scalability analysis (Section 4.6), behavior analysis (Section 4.7), and computational time cost analysis (Section 4.8).

4.1. Experimental setup

To evaluate the performance of DoS on single-objective optimization problems, this study selects the CEC2017 (Wu et al., 2017) and CEC2022 (Ahrari et al., 2022) benchmark test functions for comparative experiments. The comparisons involve 7 advanced competitors and 3 SOTA algorithms. The benchmark test functions and competitors are introduced below.

CEC2017 contains 29 classical test functions, covering four categories: unimodal, multimodal, hybrid and composition (see Table 2). Among them, unimodal functions mainly evaluate the exploitation ability of the algorithm; multimodal functions, due to the presence of multiple local minima, rely on the balance between exploration and exploitation; hybrid functions are composed of multiple types of functions, increasing the complexity of the search space; and composition functions place multiple local minima with similar function values in adjacent regions, imposing higher requirements on the algorithm. Therefore, CEC2017 can comprehensively reflect the characteristics of real-world optimization problems and is suitable for verifying algorithmic performance, exploration and exploitation balance and the ability to escape from local optima.

CEC2022 is an enhanced extension of CEC2017. Although the number of functions is reduced to 12, their complexity is significantly increased, with more densely distributed local minima. Therefore, it is more representative for evaluating the performance of algorithms in solving complex single objective problems (see Table 3).

All experiments in this paper are implemented in MATLAB 2024b under a 64-bit Windows 11 operating system. To ensure fairness and comparability of experiments, all competitors employed the hyperparameter settings from their original papers and strictly adhered to the standard testing

Table 2
CEC2017 Benchmark Test Functions.

No.	Type	Function	F^*	
F1	Unimodal	Shifted and Rotated Bent Cigar Function	100	
F3		Shifted and Rotated Zakharov Function	300	
F4	Multimodal	Shifted and Rotated Rosenbrock's Function	400	
F5		Shifted and Rotated Rastrigin's Function	500	
F6		Shifted and Rotated Expanded Scaffer's F6 Function	600	
F7		Shifted and Rotated Lunacek Bi-Rastrigin Function	700	
F8		Non-Continuous Rastrigin's Function	800	
F9		Shifted and Rotated Levy Function	900	
F10		Shifted and Rotated Schwefel's Function	1000	
F11		Hybrid	Hybrid Function 1 (N = 3)	1100
F12			Hybrid Function 2 (N = 3)	1200
F13			Hybrid Function 3 (N = 3)	1300
F14	Hybrid Function 4 (N = 4)		1400	
F15	Hybrid Function 5 (N = 4)		1500	
F16	Hybrid Function 6 (N = 4)		1600	
F17	Hybrid Function 6 (N = 5)		1700	
F18	Hybrid Function 6 (N = 5)		1800	
F19	Hybrid Function 6 (N = 5)		1900	
F20	Hybrid Function 6 (N = 6)		2000	
F21	Composition	Composition Function 1 (N = 3)	2100	
F22		Composition Function 2 (N = 3)	2200	
F23		Composition Function 3 (N = 4)	2300	
F24		Composition Function 4 (N = 4)	2400	
F25		Composition Function 5 (N = 5)	2500	
F26		Composition Function 6 (N = 5)	2600	
F27		Composition Function 7 (N = 6)	2700	
F28		Composition Function 8 (N = 6)	2800	
F29		Composition Function 9 (N = 3)	2900	
F30		Composition Function 10 (N = 3)	3000	

Search Range: $[-100, 100]^D$

Type indicates the category of the test function, Function refers to the name of the test function, and F^* represents the global optimal solution value of the test function.

conditions recommended by the CEC2017 and CEC2022 conferences. Detailed settings are shown in Table 4.

Recent studies have shown that traditional algorithms such as GA, PSO and GWO have gradually become less competitive compared to newly proposed methods. Based on this, this paper selects seven advanced competitors, AOO (Wang et al., 2025c), PSA, FFA (Shayanfar and Gharehchopogh, 2018), AVOA (Abdollahzadeh et al., 2021), ETO (Luan et al., 2024), SGA (Tian et al., 2024) and WAA, as well as three SOTA algorithms that have demonstrated

Table 3
CEC2022 Benchmark Test Functions.

No.	Type	Function	F^*
C1	Unimodal	Shifted and full Rotated Zakharov Function	300
C2	Basic	Shifted and full Rotated Rosenbrock's Function	400
C3		Shifted and full Rotated Expanded Schaffer's F6 Function	600
C4		Shifted and full Rotated Non-Continuous Rastrigin's Function	800
C5		Shifted and full Rotated Levy Function	900
C6		Hybrid Function 1 (N = 3)	1800
C7	Hybrid	Hybrid Function 2 (N = 6)	2000
C8		Hybrid Function 3 (N = 5)	2200
C9	Composition	Composition Function 1 (N = 5)	2300
C10		Composition Function 2 (N = 4)	2400
C11		Composition Function 3 (N = 5)	2600
C12		Composition Function 4 (N = 6)	2700

Search Range: $[-100, 100]^D$

Type indicates the category of the test function, Function refers to the name of the test function and F^* represents the global optimal solution value of the test function.

Table 4
Standard Test Conditions.

	CEC2017	CEC2022
Selected Dimensions (D)	30, 50, 100	10, 20
Number of Evaluations (E)	$D \times 10000$	200000 ($D = 10$), 1000000 ($D = 20$)
Number of Independent Runs	51 times	30 times

Table 5
DoS parameter settings.

Parameters	Value
Population size (N)	50
Leader to follower ratio (k_1)	0.3
Probability factor of free flight strategy (k_2)	-2.5
Time ratio of free flight strategy (k_3)	0.2
Population random search ratio coefficient of regular fighters (k_4)	0.05
Flight speed ratio factor (k_5)	0.5

strong performance in the CEC competitions, LSHADE, LSHADE-SPACMA and AL-SHADE for comparison with DoS. The hyperparameter settings used by DoS in the experiments are listed in Table 5, while all advanced competitors follow the parameter configurations specified in their original literature.

4.2. Comparison with Advanced Competitors

This section provides a systematic analysis of the experimental results of DoS and the advanced competitors mentioned in Section 4.1 on the CEC2017 benchmark test functions (30D, 50D, 100D) and CEC2022 benchmark test functions (10D, 20D). The test results are summarized in Tables 6, 7, 8, 9, 10, 11, 12, 13, 14, 15 and 16. Since the number of functions in CEC2017 is relatively large, the test results for each dimension are divided into three tables according to function types: unimodal and multimodal, hybrid and composition functions, for better presentation.

The statistical indicators used include: mean (Mean), Standard Deviation (Std), Kruskal-Wallis test result (Kruskal) (McKight and Najab, 2010), Wilcoxon signed-rank test result (WSRT) (Wilcoxon, 1992) at the 5% significance level, Friedman test for average rank (FMR) and Final rank (F-Rank). In the tables, the best performing results or those statistically superior to competitors are marked in bold.

Tables 6, 7 and 8 summarize the performance comparison between DoS and advanced competitors on the 30-dimensional CEC2017 benchmark test functions. The results show that DoS achieves the best values in all three indicators, Mean, Std and Kruskal on 25 out of 29 functions, except for F6, F11, F25 and F28, indicating strong stability and overall performance in low dimensional optimization problems.

In terms of the WSRT indicator, DoS demonstrates statistically significant advantages on all functions except F28. The F28 function contains strong local convergence traps, which cause DoS to be more prone to falling into local optima during the search process, leading to slightly inferior performance compared to some competitors.

The FMR result from the Friedman test further shows that DoS ranks first among all compared methods, with a 2.11 point lead over the second-best algorithm, PSA, confirming its remarkable optimization capability on low dimensional benchmark tests.

As shown in the numerical results from Tables 9, 10 and 11, on the 50-dimensional CEC2017 benchmark test functions, DoS achieves the best values in all three indicators, Mean, Std and Kruskal on 21 functions, except for F4, F6, F10, F11, F16, F22, F25 and F28. This demonstrates a clear advantage in terms of performance and stability. In particular, for the unimodal functions F1 and F3, DoS converges to the global optimal solution in all 51 independent runs, reflecting its strong exploitation ability. Moreover, in multimodal, hybrid and composition functions, DoS maintains a significant comparative advantage, indicating its excellent exploration ability as well.

Although in F4, F6, F10, F11, F16, F22 and F25, DoS only outperforms competitors in terms of Mean and is slightly inferior to WAA, FFA and AOO in Std, this actually reflects that its dynamic selection mechanism achieves a better balance between exploration and exploitation. Compared with other algorithms, DoS can more thoroughly explore the feasible domain and avoid getting trapped in local optima. Although this introduces some fluctuations, the overall optimization ability is significantly improved. In

the Kruskal-Wallis test, DoS ranks first on 29 test functions, showing outstanding performance.

In terms of statistical significance, DoS performs significantly better than its competitors on 28 functions and shows comparable performance with AOO and PSA only on F28. The Friedman test results further show that DoS ranks first in average ranking, with a lead of 1.94 over the second-best algorithm, AOO, highlighting its stability and advantage in medium dimensional optimization problems.

Tables 12, 13 and 14 present the experimental results of DoS on the 100-dimensional CEC2017 benchmark test functions. Except for F24 and F26, DoS shows excellent performance in terms of Mean and Kruskal indicators on all other functions, indicating its strong adaptability in high dimensional optimization tasks.

Due to the structural complexity and density of local optima in high dimensional functions, DoS, under the guidance of its dynamic selection mechanism, conducts more extensive global exploration, which leads to slight differences in the exploitation regions across multiple independent runs. As a result, its stability on some functions is slightly lower than that of AOO, WAA, AVOA, FFA and PSA. For example, on F4, F5, F7, F8, F9, F10, F11, F20, F22, F25 and F29 a total of 11 functions, the Std of DoS is slightly worse than those of the competitors. However, this phenomenon is mainly caused by some algorithms getting trapped in local optima early in the search process. Although these algorithms exhibit smaller fluctuations, their Mean values are generally worse than those of DoS, thus their overall performance is not superior.

In the Wilcoxon rank-sum test, DoS performs significantly better than other competitors on 25 functions, except for F13 and F24 F26, further validating its strong robustness and performance advantages in high-dimensional optimization problems. Although DoS performs comparably to FFA on F13 and to AOO on F25 and is slightly inferior to FFA on F24 and F26, the gaps in the Mean indicator between DoS and the best results are small and its overall performance remains within an acceptable range.

The Friedman test results also show that DoS ranks first in average ranking among all methods, with a lead of 1.8 over the second-best algorithm, AOO, fully demonstrating its competitiveness in high-dimensional tasks.

Table 15 summarizes the experimental comparison results between DoS and the advanced competitors on the 10-dimensional CEC2022 benchmark test functions. The results show that DoS achieves the best values in all three indicators, Mean, Std and Kruskal on 7 functions from C1 to C7. For C8, C9 and C10, although the Std of DoS is slightly worse than those of AVOA and AOO, showing slightly higher fluctuations, its Mean is better, indicating that although the competitors are more stable, they are more prone to getting stuck in local optima and lack effective escape mechanisms. In contrast, DoS can still find better solutions through its dynamic selection mechanism and ranks first overall in the Kruskal test, demonstrating its structural advantage in balancing exploration and exploitation.

Table 6

Experimental results of DoS and advanced competitors on 30D CEC2017 benchmark test functions (Unimodal and Multimodal).

No.	Metrics	DoS	AOO	PSA	FFA	AVOA	ETO	SGA	WAA
F1	Mean	100	3573.6777	4778.6883	3929809.8	3879.4607	6.758E+09	2853437.8	1093664.2
	Std	1.33E-14	4520.0466	6066.3438	10582599	5128.8228	3.892E+09	6260055.6	158463.82
	Kruskal	26	125.80392	132.64706	276.4902	126.92157	383	265.13725	300
	WSRT		1.3E-18(+)	1.3E-18(+)	1.3E-18(+)	1.3E-18(+)	1.3E-18(+)	1.3E-18(+)	1.3E-18(+)
F3	Mean	300	300.0103	593.21876	40345.956	308.37	42274.951	4450.1667	308.03883
	Std	8.51E-14	0.0063952	1553.372	8704.7464	22.671363	8942.5492	1807.7862	1.6451758
	Kruskal	26	158.70588	101.98039	354.15686	136.5098	360.84314	279.35294	218.45098
	WSRT		1.6E-18(+)	1.6E-18(+)	1.6E-18(+)	1.6E-18(+)	1.6E-18(+)	1.6E-18(+)	1.6E-18(+)
F4	Mean	410.816	492.25512	466.4252	504.59428	482.80955	1025.4808	513.40804	500.48884
	Std	12.20367	16.339536	32.834153	12.591353	22.705696	504.39798	29.183628	19.213575
	Kruskal	30.80392	198.33333	122.07843	251.03922	157.41176	383	265.47059	227.86275
	WSRT		6.7E-18(+)	1.6E-13(+)	3.3E-18(+)	1.9E-17(+)	3.3E-18(+)	4.4E-18(+)	3.3E-18(+)
F5	Mean	542.901	586.59329	626.82109	667.20595	696.46241	717.85927	736.53624	813.08839
	Std	11.40222	23.889164	33.252734	42.26114	36.453227	26.141061	38.094334	13.085099
	Kruskal	27.98039	86.235294	138.88235	193.82353	238.19608	272.15686	296.66667	382.05882
	WSRT		8.7E-16(+)	3.9E-18(+)	3.3E-18(+)	3.3E-18(+)	3.3E-18(+)	3.3E-18(+)	3.3E-18(+)
F6	Mean	600.1275	610.17691	600.27012	600.18082	635.58839	643.58632	658.70026	667.02719
	Std	0.2042876	5.2376552	0.7649296	0.177903	8.9543386	8.0890007	7.2989513	4.1158917
	Kruskal	65.88235	178.92157	69.333333	96	244.15686	273	334.11765	374.58824
	WSRT		3.3E-18(+)	6.4E-01(\approx)	9.0E-04(+)	3.3E-18(+)	3.3E-18(+)	3.3E-18(+)	3.3E-18(+)
F7	Mean	778.3365	824.48427	892.43764	851.89009	1071.2078	1044.6876	1183.072	1363.2113
	Std	11.92261	27.837361	41.590273	38.815368	75.450567	59.264625	90.371426	30.107359
	Kruskal	29.15686	93.431373	163.13725	125.29412	268.90196	254.45098	320.43137	381.19608
	WSRT		4.4E-15(+)	3.3E-18(+)	2.3E-17(+)	3.3E-18(+)	3.3E-18(+)	3.3E-18(+)	3.3E-18(+)
F8	Mean	840.8458	887.16766	914.57401	981.3438	961.87161	975.10959	979.211	1022.3178
	Std	8.857624	17.347282	30.699509	31.565117	33.562664	25.363266	31.19243	14.818309
	Kruskal	26.07843	89.823529	135.56863	272.88235	224.88235	254.52941	265.4902	366.7451
	WSRT		4.2E-18(+)	3.3E-18(+)	3.3E-18(+)	3.3E-18(+)	3.3E-18(+)	3.3E-18(+)	3.3E-18(+)
F9	Mean	906.4729	1324.4667	3463.5826	940.27927	5082.4391	5877.3694	5398.8897	6498.7964
	Std	6.175741	513.12248	1382.6671	23.046509	921.53943	1702.7937	1047.4418	630.87715
	Kruskal	28.21569	127.27451	201.11765	77.647059	265.76471	304.05882	283.94118	347.98039
	WSRT		3.5E-18(+)	3.3E-18(+)	1.8E-15(+)	3.3E-18(+)	3.3E-18(+)	3.3E-18(+)	3.3E-18(+)
F10	Mean	2995.011	4086.0552	4409.5398	7968.3505	4994.6571	6386.2307	6004.4391	5942.2188
	Std	258.6889	611.91558	650.89795	288.77962	733.4811	626.35825	756.63324	716.13103
	Kruskal	30.05882	103.2549	129.54902	382.03922	176.96078	294.27451	261.7451	258.11765
	WSRT		9.2E-15(+)	1.4E-16(+)	3.3E-18(+)	3.3E-18(+)	3.3E-18(+)	3.3E-18(+)	3.3E-18(+)

The Wilcoxon rank-sum test results further show that DoS significantly outperforms other methods on all test functions except C11 and C12. Although it does not exhibit a statistically significant advantage on C11 and C12, its Mean values are close to those of the best performing algorithms AOO and FFA, indicating a small performance gap and demonstrating good robustness of DoS on complex low dimensional functions. The Friedman test further shows that DoS ranks first in average ranking, confirming its superior overall optimization performance over the competitors.

Table 16 presents the numerical results of DoS on the 20-dimensional CEC2022 benchmark test functions. The results show that DoS achieves the best values for both Mean and Std on 9 functions (F1, F3 F8, F11 and F12), indicating

strong performance and stability in solving complex optimization problems. Although DoS is slightly less stable than FFA, AOO and PSA on F2, F9 and F10, its search mechanism yields the best Mean on 12 functions and tops the Kruskal-Wallis test on all functions except F5, highlighting its overall performance advantage.

Notably, although DoS ranks slightly lower than AOO in the Kruskal-Wallis test on F5, it still outperforms all competitors in terms of Mean and Std on this function, suggesting its performance remains unaffected. According to WSRT results, DoS is significantly better than all competitors on 10 out of 12 functions, except F3 and F5, where its performance is comparable to PSA and AOO. It's worth noting that DoS demonstrates stronger stability on these two

Table 7

Experimental results of DoS and advanced competitors on 30D CEC2017 benchmark test functions (Hybrid).

No.	Metrics	DoS	AOO	PSA	FFA	AVOA	ETO	SGA	WAA
F11	Mean	1183.613	1219.0968	1253.0216	1185.991	1229.6233	2225.483	1290.5779	1188.8889
	Std	36.046174	42.029705	47.928244	26.45045	48.440969	1019.3045	52.346656	60.84981
	Kruskal	109.21569	183.86275	244.66667	116.52941	202.82353	381.21569	292.52941	105.1569
	WSRT		1.8E-05(+)	2.2E-11(+)	4.5E-01(\approx)	9.3E-07(+)	3.5E-18(+)	8.2E-16(+)	3.7E-01(\approx)
F12	Mean	8085.755	2137054.1	53285.144	1571978.5	1294660.8	185093497	9254480.1	1990462.5
	Std	6121.55	1627807.7	34066.696	1114836	1098320.4	197397007	6337323.7	1011953
	Kruskal	26.70588	221.94118	77.352941	201.17647	182.4902	382.98039	313.80392	229.54902
	WSRT		3.3E-18(+)	2.7E-17(+)	3.3E-18(+)	3.3E-18(+)	3.3E-18(+)	3.3E-18(+)	3.3E-18(+)
F13	Mean	1705.753	101324.66	15056.948	134904.41	46358.217	104372665	120952.93	125780.91
	Std	497.7931	64318.328	16046.347	281717.73	21055.857	433967685	84997.261	66578.534
	Kruskal	30.62745	246.2549	95.372549	176.70588	174.17647	382.96078	254.17647	275.72549
	WSRT		3.3E-18(+)	2.3E-13(+)	2.0E-17(+)	3.3E-18(+)	3.3E-18(+)	3.3E-18(+)	3.3E-18(+)
F14	Mean	1559.072	6002.4604	13361.966	21320.115	20496.278	186725.27	35215.013	21934.693
	Std	69.58593	4263.1723	9362.4427	12927.257	15735.06	254904.26	24687.251	16509.427
	Kruskal	26.13725	108.60784	184.29412	235.41176	221.58824	351.4902	280.17647	228.29412
	WSRT		5.0E-18(+)	3.3E-18(+)	3.3E-18(+)	3.3E-18(+)	3.3E-18(+)	3.3E-18(+)	3.3E-18(+)
F15	Mean	1687.1	43916.293	8934.6881	14464.558	13178.516	1123306.2	59591.664	35090.024
	Std	127.3315	26040.927	10148.567	23001.181	10220.328	4813338	50597.464	27299.846
	Kruskal	35.58824	273.98039	120.11765	140.60784	163.90196	368.80392	290.03922	242.96078
	WSRT		3.3E-18(+)	1.6E-10(+)	1.0E-14(+)	3.3E-18(+)	3.3E-18(+)	3.3E-18(+)	3.3E-18(+)
F16	Mean	2023.233	2283.0587	2664.5465	3079.7483	2822.4906	2915.0385	3165.9144	3339.4033
	Std	138.6301	244.09129	268.0909	212.1503	279.6546	304.00652	463.13849	439.43968
	Kruskal	37	85.45098	167.88235	286.43137	213.35294	235.82353	287.58824	322.47059
	WSRT		2.0E-08(+)	6.7E-17(+)	3.3E-18(+)	1.7E-17(+)	7.5E-18(+)	4.7E-18(+)	3.3E-18(+)
F17	Mean	1798.463	1937.46	2295.2608	1997.9355	2358.3617	2221.7716	2318.1095	2896.4661
	Std	59.48037	141.94374	202.57959	142.11471	214.28736	188.66926	236.98423	312.40785
	Kruskal	37.03922	103.45098	249.27451	131.66667	269.23529	222.47059	253.31373	369.54902
	WSRT		2.9E-11(+)	8.9E-18(+)	1.6E-13(+)	4.7E-18(+)	1.1E-17(+)	8.4E-18(+)	3.3E-18(+)
F18	Mean	2087.501	163447.15	118019.86	1071703.4	177884.02	866851.31	740017.84	329967.79
	Std	307.3159	116770.49	91983.392	571179.64	153927.97	674802.4	595229.88	268771.98
	Kruskal	26	155.82353	126.54902	338.72549	159.39216	308.58824	297.84314	223.07843
	WSRT		3.3E-18(+)	3.3E-18(+)	3.3E-18(+)	3.3E-18(+)	3.3E-18(+)	3.3E-18(+)	3.3E-18(+)
F19	Mean	1996.864	112804.49	9359.0025	9898.8753	10322.404	1081434.4	79372.589	51036.061
	Std	67.47545	103314.23	11486.387	19160.847	11641.369	4333856.1	82373.244	17341.289
	Kruskal	32.52941	288.39216	131.27451	124.47059	151.11765	367.45098	268.86275	271.90196
	WSRT		3.3E-18(+)	6.7E-15(+)	1.6E-13(+)	3.3E-18(+)	3.3E-18(+)	3.3E-18(+)	3.3E-18(+)
F20	Mean	2124.574	2330.1334	2501.5145	2395.3068	2560.2715	2561.5864	2640.4097	2946.624
	Std	61.49456	135.36806	180.90689	131.35557	203.7329	159.6346	194.32465	240.49813
	Kruskal	32.09804	123.76471	212.19608	158.76471	235.94118	242.01961	273.29412	357.92157
	WSRT		7.7E-14(+)	1.1E-17(+)	1.0E-15(+)	4.7E-18(+)	3.3E-18(+)	3.3E-18(+)	3.3E-18(+)

functions and consistently approximates the global optimal solution along with the best performing competitors.

The Friedman test further confirms that DoS ranks first in average performance, with a significant lead over the second-best algorithm, AOO, validating its comprehensive optimization capabilities.

4.3. Comparison with SOTA Algorithms

To further highlight DoS's performance, this section compares it with the three SOTA algorithms described

in Section 4.1 on the 50-dimensional CEC2017 and 20-dimensional CEC2022 benchmark test functions. The relevant results are summarized in Tables 17, 18, 19 and 20. Beyond conventional statistical metrics like Mean, Std, Kruskal and WSRT, the tables also report the best function value (Best) achieved by each algorithm within the standard number of trials, enabling a more comprehensive evaluation of their optimization performance.

The results in Tables 17, 18 and 19 show that DoS achieves the best values in Mean, Best, Std and Kruskal indicators simultaneously on 7 test functions: F3, F4, F6,

Table 8

Experimental results of DoS and advanced competitors on 30D CEC2017 benchmark test functions (Composition).

No.	Metrics	DoS	AOO	PSA	FFA	AVOA	ETO	SGA	WAA
F21	Mean	2338.601	2386.2256	2428.9095	2457.4887	2488.7295	2501.4059	2531.6737	2662.2154
	Std	8.448033	26.486128	36.15707	43.151154	43.680388	31.96612	51.749341	53.280363
	Kruskal	28.76471	88.078431	146.98039	193.92157	239.66667	263.54902	294.90196	380.13725
	WSRT		5.6E-16(+)	3.3E-18(+)	6.3E-17(+)	3.3E-18(+)	3.3E-18(+)	3.3E-18(+)	3.3E-18(+)
F22	Mean	2401.722	4562.4384	4530.3552	2469.8868	5455.501	7084.6276	5545.7902	7440.9618
	Std	505.0165	1694.7972	1942.0851	927.84542	2223.7592	1818.7774	2648.7982	1131.3822
	Kruskal	39.43137	172.03922	165.84314	146.84314	216.88235	318.56863	254.07843	322.31373
	WSRT		1.3E-14(+)	3.7E-14(+)	7.1E-16(+)	3.9E-15(+)	2.2E-18(+)	8.3E-18(+)	8.4E-19(+)
F23	Mean	2690.025	2748.2516	2789.0488	2738.5936	2911.6209	2932.7588	3059.6711	3485.6388
	Std	8.240597	27.929707	40.345631	28.711814	64.157107	53.812124	110.0099	165.41296
	Kruskal	28.01961	117.86275	164.80392	103.4902	253.15686	266.19608	319.86275	382.60784
	WSRT		2.4E-17(+)	3.3E-18(+)	1.7E-16(+)	3.3E-18(+)	3.3E-18(+)	3.3E-18(+)	3.3E-18(+)
F24	Mean	2859.896	2908.1356	2961.2945	3012.096	3097.911	3139.7113	3219.6786	3699.6527
	Std	9.739557	23.439242	38.465654	18.404057	90.272064	38.537506	111.12692	139.87083
	Kruskal	26.31373	82.627451	131.2549	182.60784	245.29412	277.37255	307.60784	382.92157
	WSRT		8.4E-18(+)	3.3E-18(+)	3.3E-18(+)	3.3E-18(+)	3.3E-18(+)	3.3E-18(+)	3.3E-18(+)
F25	Mean	2882.181	2893.1476	2900.3333	2893.0253	2900.5516	3109.0003	2932.5518	2890.0572
	Std	9.8631592	16.718655	19.311325	5.208034	19.265772	114.26641	24.838985	3.10024
	Kruskal	51.62745	120.80392	192.66667	205.43137	196.54902	382.68627	305.29412	180.94118
	WSRT		1.6E-09(+)	7.3E-14(+)	4.2E-14(+)	1.1E-12(+)	3.3E-18(+)	9.4E-17(+)	3.4E-12(+)
F26	Mean	3596.484	4337.8935	5073.1215	4202.0084	6046.612	6237.3857	6979.9428	9333.7044
	Std	313.5879	609.72323	1173.543	448.27555	1388.0012	627.55266	1985.8611	1898.0906
	Kruskal	58.60784	135.11765	181.09804	119.47059	244.54902	258.21569	279.29412	359.64706
	WSRT		7.2E-12(+)	2.7E-09(+)	3.5E-12(+)	4.9E-11(+)	5.6E-18(+)	1.6E-11(+)	7.3E-16(+)
F27	Mean	3200.006	3223.6832	3241.4742	3211.1006	3259.5374	3372.2234	3377.074	3918.8171
	Std	0.000133	14.518918	15.621088	6.1220123	20.14633	57.440145	129.96702	378.51176
	Kruskal	32	128.54902	184.05882	84.27451	221.86275	309.68627	295.82353	379.7451
	WSRT		1.6E-14(+)	3.3E-18(+)	1.6E-14(+)	3.3E-18(+)	3.3E-18(+)	3.3E-18(+)	3.3E-18(+)
F28	Mean	3298.2369	3188.0497	3184.5793	3236.2144	3181.2	3662.6274	3264.5353	3174.048
	Std	3.675618	54.330403	55.584821	18.859915	49.388376	321.8931	22.284333	43.92663
	Kruskal	328.84314	124.78431	120.43137	211.94118	107.19608	383	267.21569	92.58824
	WSRT		6.3E-17(-)	3.3E-18(-)	3.3E-18(-)	3.3E-18(-)	3.3E-18(+)	1.7E-15(-)	3.3E-18(-)
F29	Mean	3363.415	3660.6339	3788.7912	3945.0394	4027.1821	4160.0736	4736.6651	4790.3267
	Std	92.8501	145.09637	195.65842	220.42833	256.26873	264.16975	367.91525	377.80745
	Kruskal	28.4902	107.45098	144.09804	192.72549	214.39216	248.66667	346.7451	353.43137
	WSRT		9.9E-17(+)	4.0E-17(+)	8.4E-18(+)	5.3E-18(+)	3.5E-18(+)	3.3E-18(+)	3.3E-18(+)
F30	Mean	3617.183	524929.73	9139.082	25318.13	36223.583	6339751.5	1349562.6	333842.02
	Std	1677.274	367260.51	2875.3313	50698.576	15216.399	4605588.5	1402574.4	200689.48
	Kruskal	28.4902	275.76471	87.254902	123.33333	172.82353	379.90196	312.11765	256.31373
	WSRT		3.3E-18(+)	2.9E-16(+)	5.6E-17(+)	3.3E-18(+)	3.3E-18(+)	3.3E-18(+)	3.3E-18(+)
FMR		1.392833	3.4178499	3.4016227	4.2237999	4.4861393	6.6396214	6.1575389	6.280595
F-Rank		1	3	2	4	5	8	6	7

FMR and F-Rank are the statistical results over all CEC2017 benchmark test functions (30D).

F11, F27, F29 and F30. This fully demonstrates its comprehensive advantage in terms of performance, stability and statistical significance. It can be seen that even when compared with representative SOTA algorithms, DoS still maintains a leading position on multiple functions in the CEC2017 benchmark tests. This is especially true for functions like

F27, F29 and F30, which feature complex problem structures and irregular search spaces, further confirming DoS's strength in solving highly complex problems.

Although DoS only achieves the best results in Mean, Std and Kruskal on F14, F15, F19, F23 and F26 and its Std is slightly worse than some SOTA algorithms, this also reflects

Table 9

Experimental results of DoS and advanced competitors on 50D CEC2017 benchmark test functions (Unimodal and Multimodal).

No.	Metrics	DoS	AOO	PSA	FFA	AVOA	ETO	SGA	WAA
F1	Mean	100	7458.7766	4205.0167	80718.056	5228.0557	2.015E+10	26034150	4965931
	Std	8.27E-10	7197.5812	6252.8935	377927.33	4731.6526	6.059E+09	26262110	568339.28
	Kruskal	26	155.92157	121.31373	195.60784	141.15686	383	329.88235	283.11765
	WSRT		3.3E-18(+)	3.3E-18(+)	3.3E-18(+)	3.3E-18(+)	3.3E-18(+)	3.3E-18(+)	3.3E-18(+)
F3	Mean	300	300.01759	9531.6933	155854.74	891.77674	96977.11	23051.704	471.10537
	Std	2.36E-13	0.0086403	22769.732	15777.301	827.11499	16078.457	4098.5324	102.90146
	Kruskal	26	78.176471	181.33333	382.7451	192.29412	330.70588	274.13725	170.60784
	WSRT		3.0E-18(+)	3.0E-18(+)	3.0E-18(+)	3.0E-18(+)	3.0E-18(+)	3.0E-18(+)	3.0E-18(+)
F4	Mean	422.0392	519.03187	494.35771	561.1983	515.74742	3238.7534	616.6472	557.38907
	Std	35.920017	46.454784	49.673021	35.511733	58.226563	1243.9116	61.231415	33.76841
	Kruskal	37.33333	164.92157	129.05882	236.84314	165.17647	383	294.35294	225.31373
	WSRT		1.2E-15(+)	2.0E-12(+)	2.1E-17(+)	8.3E-15(+)	3.3E-18(+)	5.9E-18(+)	4.0E-17(+)
F5	Mean	616.226	692.26334	758.30356	900.97302	841.94139	929.5862	877.1667	912.60771
	Std	20.86876	35.061109	51.575974	55.761143	29.85556	37.124135	46.495572	25.857135
	Kruskal	28.21569	83.137255	127.05882	297.41176	202.33333	335.62745	254.56863	307.64706
	WSRT		1.6E-15(+)	4.2E-18(+)	3.3E-18(+)	3.3E-18(+)	3.3E-18(+)	3.3E-18(+)	3.3E-18(+)
F6	Mean	600.0709	621.36133	600.8858	600.27842	637.36958	659.05157	668.75256	671.05589
	Std	0.2564354	7.7845019	0.9587414	0.166567	6.2372134	7.840533	6.2154284	2.0258048
	Kruskal	32.35294	182.58824	111.11765	87.529412	227.21569	293.01961	342.31373	359.86275
	WSRT		3.0E-18(+)	3.2E-15(+)	1.7E-13(+)	3.0E-18(+)	3.0E-18(+)	3.0E-18(+)	3.0E-18(+)
F7	Mean	881.0636	973.3422	1125.4193	1058.854	1478.6609	1407.5583	1647.9132	1836.9871
	Std	24.8489	56.212727	69.638523	73.321046	102.85529	69.617662	118.27748	43.187892
	Kruskal	29.03922	85.921569	162.92157	132.15686	274.05882	246.39216	325.35294	380.15686
	WSRT		7.0E-15(+)	3.3E-18(+)	9.5E-18(+)	3.3E-18(+)	3.3E-18(+)	3.3E-18(+)	3.3E-18(+)
F8	Mean	907.918	995.45201	1057.0124	1200.8858	1135.5209	1241.0952	1195.0693	1210.3759
	Std	19.88024	45.695405	56.869752	54.479444	37.656796	36.671633	46.647196	34.183085
	Kruskal	27.60784	86.254902	129.45098	290.31373	192.98039	342.33333	271.23529	295.82353
	WSRT		2.7E-16(+)	4.4E-18(+)	3.3E-18(+)	3.3E-18(+)	3.3E-18(+)	3.3E-18(+)	3.3E-18(+)
F9	Mean	1257.971	5367.3213	12360.52	1548.6009	12925.665	25590.045	14749.781	20020.578
	Std	367.3211	2039.6856	3083.1816	375.04432	1840.4879	5048.4321	2004.6052	1804.9739
	Kruskal	39.05882	129.27451	214.52941	64.196078	220.13725	374.84314	258.45098	335.5098
	WSRT		4.2E-18(+)	3.3E-18(+)	2.0E-05(+)	3.3E-18(+)	3.3E-18(+)	3.3E-18(+)	3.3E-18(+)
F10	Mean	4782.937	6306.9044	6871.0237	14173.124	8326.4449	11666.121	9463.8427	8720.207
	Std	386.18247	767.74351	725.74363	358.3042	906.39592	914.61567	1408.5348	910.50144
	Kruskal	28.03922	94.294118	122.07843	382.64706	204.01961	326.47059	253.72549	224.72549
	WSRT		9.6E-16(+)	3.3E-18(+)	3.3E-18(+)	4.2E-18(+)	3.3E-18(+)	3.3E-18(+)	3.3E-18(+)

the effectiveness of its dynamic selection mechanism. Compared to SOTA algorithms, DoS is better able to maintain a reasonable balance between exploration and exploitation in the later stages, thus achieving more thorough searches in the feasible domain. Although this may lead to slightly increased variability in solutions, the overall performance remains excellent.

In terms of performance significance analysis, the results of the Wilcoxon rank-sum test show that DoS exhibits significant advantages on F3, F4, F6, F11, F15, F19, F23, F25, F26, F27, F29 and F30 and performs comparably to SOTA algorithms on F1, F9, F12, F13, F14, F16, F17, F18, F20 and F22. This fully demonstrates that DoS has clear performance advantages on most test functions or at least performs on par with SOTA algorithms. Although DoS

performs significantly worse than SOTA algorithms on F5, F7, F8, F10, F21, F24 and F28, its performance on these functions remains within an acceptable range in terms of Mean and Best indicators, showing no obvious failure. The FMR obtained from the Friedman test further shows that DoS ranks first among all compared algorithms, verifying its potential and adaptability in optimization problems.

According to Table 20's results, DoS exhibits a clear performance advantage in terms of both the Mean and Best indicators. For example, on 8 functions except for C4, C6, C7 and C10, DoS achieves the best values in both Mean and Best, indicating that even when facing the more structurally complex CEC2022 benchmark test functions, DoS still shows strong optimization capability and search efficiency compared to SOTA methods.

Table 10

Experimental results of DoS and advanced competitors on 50D CEC2017 benchmark test functions (Hybrid).

No.	Metrics	DoS	AOO	PSA	FFA	AVOA	ETO	SGA	WAA
F11	Mean	1279.913	1314.3262	1372.6352	1336.712	1307.114	6080.2766	1458.8419	1366.6447
	Std	47.390331	50.612961	80.017588	66.267192	50.907215	2354.975	91.302341	32.06185
	Kruskal	86.37255	135.2549	215.33333	169.23529	124.19608	383	299.05882	223.54902
	WSRT		2.3E-03(+)	8.4E-10(+)	3.2E-05(+)	1.4E-02(+)	3.3E-18(+)	1.2E-16(+)	6.3E-14(+)
F12	Mean	6940.079	9491633.5	531961.24	7188695.6	4039899.8	4.889E+09	45078699	10512110
	Std	3988.266	4551846.5	390543.95	3675557.8	2179042.5	4.201E+09	28315049	5898223.7
	Kruskal	26	231.78431	78.176471	202.52941	150.17647	383	327.90196	236.43137
	WSRT		3.3E-18(+)	3.3E-18(+)	3.3E-18(+)	3.3E-18(+)	3.3E-18(+)	3.3E-18(+)	3.3E-18(+)
F13	Mean	3664.402	153373.79	6819.5476	87632.24	61687.305	388392019	146683.6	288113.36
	Std	3178.467	90205.977	7114.717	184106.75	24297.225	1.244E+09	87685.879	141981.07
	Kruskal	51.72549	250.7451	77.196078	137.17647	179.17647	383	245.11765	311.86275
	WSRT		3.3E-18(+)	9.5E-04(+)	1.0E-07(+)	3.5E-18(+)	3.3E-18(+)	3.3E-18(+)	3.3E-18(+)
F14	Mean	1705.921	44096.741	29450.302	246333.45	70966.003	931345.3	164414.59	69433.339
	Std	115.1329	34268.23	22095.405	169392.84	65332.351	914056.12	105648.79	41790.379
	Kruskal	26	151	121.29412	306.80392	188.52941	364.84314	279.37255	198.15686
	WSRT		3.3E-18(+)	3.3E-18(+)	3.3E-18(+)	3.3E-18(+)	3.3E-18(+)	3.3E-18(+)	3.3E-18(+)
F15	Mean	1835.009	45955.61	8805.2286	12452.34	27609.218	26655984	64201.776	47242.202
	Std	170.3198	22360.863	5349.426	12662.092	10802.562	62129681	48340.016	33885.092
	Kruskal	31.23529	264.88235	103.17647	113.84314	200.4902	383	285.76471	253.60784
	WSRT		3.3E-18(+)	1.1E-17(+)	1.8E-12(+)	3.3E-18(+)	3.3E-18(+)	3.3E-18(+)	3.3E-18(+)
F16	Mean	2547.262	2915.2508	3561.9158	4683.2115	3844.888	4034.6808	4105.5049	4278.5403
	Std	253.96026	378.20303	415.43788	251.6003	425.10843	350.97201	510.68634	519.25189
	Kruskal	39.60784	76.686275	164.23529	354.88235	213.17647	245.41176	256.62745	285.37255
	WSRT		2.2E-06(+)	5.3E-16(+)	3.3E-18(+)	5.0E-18(+)	3.3E-18(+)	3.9E-18(+)	3.7E-18(+)
F17	Mean	2418.729	2719.7053	3185.1532	3568.7941	3503.938	3271.9265	3775.8722	3724.1766
	Std	173.8556	273.46237	423.69382	279.89768	425.66708	317.99089	416.59638	272.84868
	Kruskal	38.78431	86.901961	179.09804	272.4902	255.4902	194.27451	303.72549	305.23529
	WSRT		3.2E-08(+)	4.1E-15(+)	3.7E-18(+)	4.4E-18(+)	4.2E-17(+)	3.3E-18(+)	3.3E-18(+)
F18	Mean	2889.954	252038.96	149527.74	5100801.1	382040.7	7963272.3	2078889.8	551327.19
	Std	837.5434	136017.17	67683.289	2225158.8	193530.5	11746533	1518737.6	179796.68
	Kruskal	26	134.2549	95.607843	356.41176	176.78431	335.37255	289.88235	221.68627
	WSRT		3.3E-18(+)	3.3E-18(+)	3.3E-18(+)	3.3E-18(+)	3.3E-18(+)	3.3E-18(+)	3.3E-18(+)
F19	Mean	2056.599	117421.65	17545.893	17701.825	23796.405	6311633.6	591776.92	152148.13
	Std	60.36797	76454.106	10820.538	10792.076	12846.567	7026606.7	1079727.3	134463.91
	Kruskal	29.03922	254.39216	122.29412	120.62745	146.4902	381.84314	317.09804	264.21569
	WSRT		3.3E-18(+)	3.3E-18(+)	1.8E-14(+)	3.3E-18(+)	3.3E-18(+)	3.3E-18(+)	3.3E-18(+)
F20	Mean	2437.44	2839.3975	3111.7539	3688.2487	3346.1449	3358.2875	3459.6085	3839.1618
	Std	131.8813	243.2789	320.4854	145.48906	318.27883	232.07294	310.20894	210.51489
	Kruskal	30.68627	98.294118	158.03922	317.76471	217.11765	216.35294	248.17647	349.56863
	WSRT		1.4E-13(+)	2.3E-17(+)	3.3E-18(+)	4.7E-18(+)	3.5E-18(+)	4.2E-18(+)	3.3E-18(+)

However, due to the higher complexity of the CEC2022 benchmark test functions, the stability of DoS is somewhat affected. Except for C3, C5 and C12, DoS does not outperform the three SOTA algorithms in Std on the remaining 9 functions, suggesting relatively larger result variability on some functions.

Based on the statistical results of the Wilcoxon rank-sum test, DoS performs significantly better than the SOTA algorithms on C1, C2, C3, C9, C10 and C12. On C5, C6, C7 and C8, DoS performs comparably to the three SOTA algorithms, indicating that DoS possesses strong or

equivalent optimization ability on most problems in the CEC2022 benchmark test functions. Although DoS shows slightly inferior performance on C4 and C11 compared to SOTA algorithms, its Mean and Best values are close to the best and the overall impact on performance is minimal, remaining within an acceptable range. Finally, the average ranking obtained from the Friedman test shows that DoS once again ranks first among all algorithms, with a greater statistically significant gap compared to the second ranked AL-SHADE, further verifying its strong competitiveness and robustness in solving complex optimization problems.

Table 11

Experimental results of DoS and advanced competitors on 50D CEC2017 benchmark test functions (Composition).

No.	Metrics	DoS	AOO	PSA	FFA	AVOA	ETO	SGA	WAA
F21	Mean	2404.251	2478.1009	2560.141	2666.5647	2740.9989	2766.9726	2809.8841	3106.3958
	Std	14.8067	40.419561	41.070358	74.808223	83.488362	52.063935	102.38993	112.45899
	Kruskal	27.13725	81.411765	131.2549	197.96078	251.56863	274.35294	291	381.31373
	WSRT		9.4E-17(+)	3.3E-18(+)	3.3E-18(+)	3.3E-18(+)	3.3E-18(+)	3.3E-18(+)	3.3E-18(+)
F22	Mean	6284.981	8371.8925	8733.8068	13007.794	10401.36	13942.92	11350.239	10992.011
	Std	892.27191	731.5659	1341.8168	4826.0349	1014.7198	1235.6665	1299.1237	961.13311
	Kruskal	37.80392	111.23529	134.96078	298.62745	214.41176	338.96078	256.4902	243.5098
	WSRT		3.5E-18(+)	1.1E-16(+)	3.8E-07(+)	3.3E-18(+)	3.3E-18(+)	3.3E-18(+)	3.3E-18(+)
F23	Mean	2790.402	2929.2471	3076.9321	2955.7869	3357.475	3364.0782	3669.0811	4391.0206
	Std	21.30589	45.640249	83.79211	87.38988	107.30542	70.132346	174.23964	234.55009
	Kruskal	26.05882	101.4902	169.31373	114.47059	257.31373	257.70588	326.90196	382.7451
	WSRT		3.5E-18(+)	3.3E-18(+)	3.7E-18(+)	3.3E-18(+)	3.3E-18(+)	3.3E-18(+)	3.3E-18(+)
F24	Mean	3009.852	3093.9456	3231.4075	3296.9562	3591.9587	3608.9625	3824.4668	4377.3548
	Std	24.03879	57.327666	107.91972	19.957172	141.02818	76.246627	211.80716	149.1794
	Kruskal	28.70588	79.784314	135.7451	168.17647	260.96078	267.15686	313.19608	382.27451
	WSRT		6.0E-15(+)	4.2E-18(+)	3.3E-18(+)	3.3E-18(+)	3.3E-18(+)	3.3E-18(+)	3.3E-18(+)
F25	Mean	2968.833	3025.8936	3047.7998	3064.4626	3061.4041	4638.9591	3120.553	3073.2565
	Std	33.590393	33.362062	39.059624	24.501291	33.164013	528.44852	28.235566	24.39106
	Kruskal	39.01961	116.33333	164.15686	198.84314	192.2549	383	318.90196	223.4902
	WSRT		1.8E-12(+)	3.5E-13(+)	1.1E-16(+)	1.6E-15(+)	3.3E-18(+)	3.9E-18(+)	2.0E-17(+)
F26	Mean	4028.313	5094.9033	6989.2165	5616.083	8868.7991	10155.383	12019.176	12566.885
	Std	383.5196	1459.1209	1636.9614	647.12254	2852.5	766.31556	1863.6407	550.71848
	Kruskal	54.5098	104.68627	171.7451	121.21569	220.03922	262.90196	338.72549	362.17647
	WSRT		6.3E-05(+)	2.1E-12(+)	3.0E-17(+)	2.8E-09(+)	3.3E-18(+)	6.7E-17(+)	3.3E-18(+)
F27	Mean	3200.011	3351.9457	3522.0545	3329.3773	3744.9983	4161.0991	3942.265	5902.2563
	Std	0.00014	64.593004	133.82913	43.778659	241.73346	188.93897	245.07028	829.66284
	Kruskal	26	113.7451	182.5098	101.98039	235.82353	317	276.2549	382.68627
	WSRT		3.3E-18(+)	3.3E-18(+)	3.3E-18(+)	3.3E-18(+)	3.3E-18(+)	3.3E-18(+)	3.3E-18(+)
F28	Mean	3299.2651	3288.217	3301.0225	3338.9459	3302.6131	5045.0724	3333.3892	3302.2879
	Std	3.595295	21.439867	30.503813	26.12062	20.981256	460.34286	22.544042	20.48227
	Kruskal	111.3922	111.58824	130.43137	287.29412	153	383	283.23529	176.05882
	WSRT		9.1E-01(\approx)	9.4E-02(\approx)	8.7E-16(+)	3.4E-02(+)	3.3E-18(+)	9.6E-16(+)	9.2E-04(+)
F29	Mean	3442.742	4121.89	4299.3474	4180.1437	4761.6165	5815.6851	6649.5095	5960.7296
	Std	127.5843	276.50494	300.36578	442.53767	420.72607	418.83022	762.90399	607.44898
	Kruskal	28.41176	122.01961	150.5098	131.96078	211.96078	310.47059	361.98039	318.68627
	WSRT		1.8E-17(+)	3.7E-18(+)	6.2E-16(+)	3.3E-18(+)	3.3E-18(+)	3.3E-18(+)	3.3E-18(+)
F30	Mean	3545.922	7145878.4	999690.62	871792.39	1643392.5	185894209	39191527	11067002
	Std	391.276	1760462.2	178439.45	166130.3	412704.26	269064073	12085920	2988111.9
	Kruskal	26	236.62745	116.11765	93.411765	174.47059	383	331.88235	274.4902
	WSRT		3.3E-18(+)	3.3E-18(+)	3.3E-18(+)	3.3E-18(+)	3.3E-18(+)	3.3E-18(+)	3.3E-18(+)
FMR		1.207573	3.1406356	3.2792427	4.643002	4.4347532	6.8891143	6.2623394	6.1433401
F-Rank		1	2	3	5	4	8	7	6

FMR and F-Rank are the statistical results over all CEC2017 benchmark test functions (50D).

4.4. Exploration and Exploitation Analysis

To qualitatively analyze the dynamic characteristics of exploration and exploitation during the search process of DoS, this section adopts the dimension-wise diversity measurement method (Hussain et al., 2019) to analyze the exploration rate and exploitation rate of DoS. The number of

evaluations is set to one-tenth of the standard evaluation count for the experiment and the resulting variation curves of the exploration rate and exploitation rate are shown in Fig. 7.

As shown in Fig. 7, for F18 in 30-dimensions and F14 in 100-dimensions, the exploration rate and exploitation rate curves of DoS exhibit a trend of focusing on exploration in

Table 12

Experimental results of DoS and advanced competitors on 100D CEC2017 benchmark test functions (Unimodal and Multimodal).

No.	Metrics	DoS	AOO	PSA	FFA	AVOA	ETO	SGA	WAA
F1	Mean	100	11434.827	9153.6919	2544239.6	15030.121	8.79E+10	553528597	28429335
	Std	1.79E-09	12022.747	10985.079	1057815.3	26942.256	1.178E+10	478815373	2733487.8
	Kruskal	26	132.80392	123.88235	230	127.31373	383	332	281
	WSRT		3.3E-18(+)	3.3E-18(+)	3.3E-18(+)	3.3E-18(+)	3.3E-18(+)	3.3E-18(+)	3.3E-18(+)
F3	Mean	300.0001	316.54711	60838.978	489769.43	16618.625	247187.64	125616.3	15583.486
	Std	0.000108	13.01766	63938.281	35277.33	4668.4778	19100.352	14829.806	3253.5886
	Kruskal	26	77	215.64706	383	168.98039	330.82353	274.47059	160.07843
	WSRT		3.3E-18(+)	3.3E-18(+)	3.3E-18(+)	3.3E-18(+)	3.3E-18(+)	3.3E-18(+)	3.3E-18(+)
F4	Mean	499.4334	643.94986	636.87283	771.30545	638.51502	11434.472	1061.8479	667.13172
	Std	64.788848	25.95666	49.47919	46.836753	40.477182	2834.7527	107.44049	43.502178
	Kruskal	30.66667	148.86275	137.96078	276.84314	143.17647	383	331.94118	183.54902
	WSRT		2.1E-17(+)	1.1E-15(+)	3.3E-18(+)	2.2E-16(+)	3.3E-18(+)	3.3E-18(+)	2.0E-17(+)
F5	Mean	904.6199	980.36006	1238.994	1516.454	1314.5973	1660.0572	1393.9979	1408.4371
	Std	46.84234	69.67801	98.469226	132.64523	76.511927	51.396168	67.294038	33.53873
	Kruskal	35.90196	67.666667	152.15686	308.11765	188.92157	376.84314	245.33333	261.05882
	WSRT		1.0E-07(+)	3.3E-18(+)	3.3E-18(+)	3.3E-18(+)	3.3E-18(+)	3.3E-18(+)	3.3E-18(+)
F6	Mean	600	636.02547	601.81291	602.87896	643.78282	675.19617	672.02774	671.22654
	Std	1.79E-07	5.4579063	1.330067	0.9751589	4.5218746	5.4426438	3.5616361	2.0948545
	Kruskal	26	185.4902	88.254902	116.7451	223.5098	357.07843	326.62745	312.29412
	WSRT		3.2E-18(+)	3.2E-18(+)	3.2E-18(+)	3.2E-18(+)	3.2E-18(+)	3.2E-18(+)	3.2E-18(+)
F7	Mean	1299.162	1438.8492	2075.9228	1637.8928	2826.4009	2805.5654	3212.2258	3491.3025
	Std	70.832237	103.97397	191.46112	148.07439	159.68196	136.39185	158.30975	68.38764
	Kruskal	33	78.215686	177.45098	121.64706	259.45098	255.05882	329.76471	381.41176
	WSRT		2.3E-11(+)	3.3E-18(+)	8.4E-17(+)	3.3E-18(+)	3.3E-18(+)	3.3E-18(+)	3.3E-18(+)
F8	Mean	1196.997	1301.1995	1580.1334	1778.4256	1711.509	1999.2754	1829.3321	1892.6368
	Std	44.761791	85.12443	103.00011	166.94534	63.089571	72.90298	66.657071	31.49254
	Kruskal	32.41176	73.137255	141.84314	247.37255	191.07843	372.90196	263.56863	313.68627
	WSRT		5.2E-11(+)	3.3E-18(+)	5.3E-18(+)	3.3E-18(+)	3.3E-18(+)	3.3E-18(+)	3.3E-18(+)
F9	Mean	9842.292	17371.124	26628.345	25952.071	22605.19	67107.475	27707.789	43774.083
	Std	2121.9743	4064.3951	3857.9097	8646.918	1051.23	6576.3486	2179.1687	3166.527
	Kruskal	28.52941	93.568627	215.72549	192.88235	152.03922	382.90196	240.7451	329.60784
	WSRT		8.7E-16(+)	3.3E-18(+)	2.0E-17(+)	3.3E-18(+)	3.3E-18(+)	3.3E-18(+)	3.3E-18(+)
F10	Mean	11269.18	13069.852	14570.173	30959.545	16523.415	27990.615	20080.44	17274.403
	Std	622.0695	1295.7596	1332.2332	461.1482	1602.8631	1348.1399	2956.8032	972.66823
	Kruskal	31.45098	85.117647	128.72549	382.60784	190.86275	331.2549	266.52941	219.45098
	WSRT		1.7E-12(+)	2.1E-17(+)	3.3E-18(+)	3.3E-18(+)	3.3E-18(+)	3.3E-18(+)	3.3E-18(+)

the early stages and on exploitation in the later stages, with frequent fluctuations. This indicates that even in the later stages of iteration, DoS can still maintain global exploration in order to pursue the globally optimal solution.

According to existing research, many metaheuristic algorithms increase the execution probability of exploitation strategies in the later stages in order to ensure good convergence. Therefore, the exploration and exploitation rate curves of these algorithms usually show that the exploration rate is higher than the exploitation rate in the early stage, while the exploration rate approaches zero in the later stage. However, as shown in Fig. 7, DoS exhibits a different trend in F17 and F29 (50-dimensions), F30 (100-dimensions), C7 (10-dimensions) and C8 and C12 (20-dimensions), where the exploration rate remains higher than the exploitation rate

even in the later stages of iteration and the dynamic changes in exploration and exploitation rates are very significant. Although the search behavior on these functions differs greatly from that of most metaheuristic algorithms, the experimental results in Tables 6, 7, 8, 9, 10, 11, 12, 13, 14, 15 and 16 show that DoS performs significantly better than advanced competitors on these functions, further confirming the performance advantage brought by the unique structural design of DoS.

In summary, DoS exhibits different optimization behaviors on different problems. Some of these behaviors diverge significantly from traditional patterns, further highlighting DoS's adaptability to diverse scenarios.

Table 13

Experimental results of DoS and advanced competitors on 100D CEC2017 benchmark test functions (Hybrid).

No.	Metrics	DoS	AOO	PSA	FFA	AVOA	ETO	SGA	WAA
F11	Mean	2093.826	2336.136	2499.4601	45253.726	2364.2269	63454.389	5624.7345	2666.6838
	Std	260.32616	223.32864	365.46358	6151.0608	203.67499	11307.545	1001.9915	185.3469
	Kruskal	60.82353	112.07843	150.45098	335.92157	119.47059	379.07843	281	197.17647
	WSRT		1.2E-05(+)	6.1E-08(+)	3.3E-18(+)	1.1E-06(+)	3.3E-18(+)	3.3E-18(+)	1.6E-16(+)
F12	Mean	70696.23	27497571	1321869	26204306	10543347	2.452E+10	378055056	46529684
	Std	46332.36	12742127	689098.2	9472511.5	4533071.7	1.194E+10	159585023	6876212.1
	Kruskal	26	205.33333	77.156863	203.39216	134.80392	383	332	274.31373
	WSRT		3.3E-18(+)	3.3E-18(+)	3.3E-18(+)	3.3E-18(+)	3.3E-18(+)	3.3E-18(+)	3.3E-18(+)
F13	Mean	4454.267	85648.223	8132.8355	15356.532	47599.804	2.789E+09	104445.51	599208.66
	Std	2231.859	36140.043	7294.2077	51117.923	15756.806	2.655E+09	116417.53	66059.953
	Kruskal	70	247.45098	95.803922	73.745098	188.7451	383	246.80392	330.45098
	WSRT		3.3E-18(+)	1.6E-03(+)	4.4E-01(\approx)	3.3E-18(+)	3.3E-18(+)	3.3E-18(+)	3.3E-18(+)
F14	Mean	2176.241	215634.62	102155.61	8802351.6	162433.31	6010552.4	1463966.9	299704.97
	Std	223.8973	123978.52	50784.534	3015230.9	61713.227	2961045.6	801206.11	72743.323
	Kruskal	26	162.23529	97.862745	369.82353	140.5098	342.88235	281.84314	214.84314
	WSRT		3.3E-18(+)	3.3E-18(+)	3.3E-18(+)	3.3E-18(+)	3.3E-18(+)	3.3E-18(+)	3.3E-18(+)
F15	Mean	2391.339	69900.429	5518.5835	21516.984	31328.556	361516597	119079.57	153572
	Std	1418.561	30682.356	4783.5966	58341.072	10585.893	608735919	302248.11	30003.227
	Kruskal	44.07843	245.4902	97.843137	107.84314	178.62745	383	255.03922	324.07843
	WSRT		3.3E-18(+)	9.7E-11(+)	1.9E-06(+)	3.5E-18(+)	3.3E-18(+)	3.3E-18(+)	3.3E-18(+)
F16	Mean	4322.565	4951.892	5795.6355	10163.523	6349.6419	9710.3545	7750.8686	7414.9598
	Std	405.9632	651.60008	609.45896	357.30588	682.62745	1258.1596	1060.2266	577.5631
	Kruskal	36.88235	79.490196	136.4902	364.17647	174.52941	342.92157	258	243.5098
	WSRT		1.1E-07(+)	3.2E-17(+)	3.3E-18(+)	5.9E-18(+)	3.3E-18(+)	3.3E-18(+)	3.3E-18(+)
F17	Mean	3932.694	4477.6843	5437.6177	6831.2505	5955.2657	8248.3973	6919.1373	5988.4034
	Std	327.2295	536.4395	641.08481	493.61691	686.81887	3852.3467	946.52654	690.73377
	Kruskal	36.82353	79.078431	160.31373	310.47059	211.88235	320.64706	301.52941	215.2549
	WSRT		9.6E-08(+)	1.1E-17(+)	3.3E-18(+)	1.7E-17(+)	3.3E-18(+)	3.3E-18(+)	3.3E-18(+)
F18	Mean	4298.386	416232.2	280470.84	17342725	284063.12	6321902.1	2416922.2	885691.47
	Std	1602.503	165783.79	163227.62	3925354	99000.537	2860777.4	882296.51	394334.48
	Kruskal	26	158.7451	110.78431	382.31373	120.09804	328.72549	281.58824	227.7451
	WSRT		3.3E-18(+)	3.3E-18(+)	3.3E-18(+)	3.3E-18(+)	3.3E-18(+)	3.3E-18(+)	3.3E-18(+)
F19	Mean	3710.711	290837.38	5722.7038	12303.77	16963.956	514617222	5425954.7	1585898.6
	Std	2211.767	135120.16	4728.225	24051.218	7892.9895	616405725	3141094.9	548486.25
	Kruskal	60.86275	230.09804	92.019608	90.333333	166.78431	383	326.76471	286.13725
	WSRT		3.3E-18(+)	3.4E-04(+)	2.9E-02(+)	3.2E-17(+)	3.3E-18(+)	3.3E-18(+)	3.3E-18(+)
F20	Mean	4022.997	4587.5177	5355.894	7095.0004	5735.6564	6100.8094	6071.921	6237.9918
	Std	269.95347	460.41147	596.22632	198.7064	633.39178	605.70915	590.19839	556.8732
	Kruskal	35.09804	84.686275	162.33333	371.62745	208.76471	249.96078	250.92157	272.60784
	WSRT		3.7E-10(+)	7.3E-16(+)	3.3E-18(+)	4.4E-18(+)	3.3E-18(+)	3.3E-18(+)	3.3E-18(+)

4.5. Convergence Analysis

Convergence is also one of the key indicators for evaluating the performance of metaheuristic algorithms. To comprehensively assess the convergence ability of DoS, this paper conducts a visual analysis of the function value trends of DoS and 7 advanced competitors on CEC2017 and CEC2022 benchmark test functions with different dimensions. The results are shown in Fig. 8.

As shown in Fig. 8, DoS is able to identify high quality exploitation regions earlier than its competitors on multiple

test functions, achieving more efficient convergence. Although AOO reaches final function values close to those of DoS on certain test functions, its search speed is significantly slower and often relies on occasional late-stage exploration strategies to escape local optima. Overall, its convergence performance is still inferior to DoS.

On functions such as F10 (30-dimensions), F22 (50-dimensions), F20 (100-dimensions) and C4 (20-dimensions), DoS avoids the problem of falling into local optima in the early stages compared to competitors such as WAA, SGA, ETO, AVOA, FFA and PSA. This demonstrates DoS's

Table 14

Experimental results of DoS and advanced competitors on 100D CEC2017 benchmark test functions (Composition).

No.	Metrics	DoS	AOO	PSA	FFA	AVOA	ETO	SGA	WAA
F21	Mean	2687.31	2817.1405	3089.7996	3195.7371	3549.1034	3773.2339	3891.7374	4531.5168
	Std	42.61848	85.264587	104.49185	176.04385	192.28252	111.68982	239.68755	165.59949
	Kruskal	30.2549	75.627451	142.72549	166	240.68627	289.29412	309.23529	382.17647
	WSRT		2.8E-13(+)	3.3E-18(+)	5.3E-18(+)	3.3E-18(+)	3.3E-18(+)	3.3E-18(+)	3.3E-18(+)
F22	Mean	13378.01	15909.747	17807.914	33116.244	19590.348	30978.01	23117.352	20489.071
	Std	1682.1851	1481.4432	1560.3427	539.5097	1692.7854	1388.0878	2169.571	1328.2754
	Kruskal	30.86275	85.745098	134.98039	379.60784	187.19608	335.23529	268.58824	213.78431
	WSRT		1.9E-12(+)	3.3E-18(+)	3.3E-18(+)	3.3E-18(+)	3.3E-18(+)	3.3E-18(+)	3.3E-18(+)
F23	Mean	3032.522	3328.5723	3389.6055	3083.5447	3783.339	4518.4414	5043.2614	6436.9036
	Std	27.67774	73.602701	117.78652	34.219696	153.71478	124.79537	311.09346	768.66897
	Kruskal	32.33333	145.82353	162.09804	70.72549	229.01961	283.58824	330.82353	381.58824
	WSRT		3.3E-18(+)	3.3E-18(+)	6.2E-11(+)	3.3E-18(+)	3.3E-18(+)	3.3E-18(+)	3.3E-18(+)
F24	Mean	3674.1432	3820.2856	4128.3965	3598.212	4737.9563	5745.9319	6339.9629	8580.0161
	Std	74.67906	97.07425	152.63608	94.014668	253.97023	265.1987	514.51641	1548.2708
	Kruskal	73.11765	121.2549	177.64706	38.509804	229.82353	288.90196	329.60784	377.13725
	WSRT		2.3E-11(+)	3.3E-18(+)	8.3E-08(-)	3.3E-18(+)	3.3E-18(+)	3.3E-18(+)	3.3E-18(+)
F25	Mean	3232.027	3256.0455	3303.9447	3489.7101	3310.6253	8665.1744	3550.1983	3317.1892
	Std	67.830152	57.747201	73.760736	55.87312	64.481479	1336.0849	84.615751	50.813122
	Kruskal	76.37255	95.705882	151.54902	294.01961	156.35294	383	316.05882	162.94118
	WSRT		5.5E-02(\approx)	2.7E-06(+)	3.3E-18(+)	1.8E-07(+)	3.3E-18(+)	3.7E-18(+)	7.1E-09(+)
F26	Mean	10554.709	10894.301	16019.937	9331.776	22504.056	25063.478	29891.053	26260.802
	Std	1059.3182	2333.5268	3108.4928	837.6775	2440.5727	1434.2431	5081.4525	1221.4587
	Kruskal	88.098039	107.47059	181.41176	39.58824	243.70588	290.35294	362.41176	322.96078
	WSRT		2.9E-03(+)	9.4E-17(+)	2.2E-10(-)	3.3E-18(+)	3.3E-18(+)	4.4E-18(+)	3.3E-18(+)
F27	Mean	3200.022	3473.0578	3694.7876	3550.3028	3957.9768	5138.5934	4704.5723	6511.3032
	Std	0.000198	59.393888	96.870455	80.498393	190.86168	292.03137	474.18335	1414.1513
	Kruskal	26	87.647059	178.31373	124.4902	226.52941	328.76471	294.05882	370.19608
	WSRT		3.3E-18(+)	3.3E-18(+)	3.3E-18(+)	3.3E-18(+)	3.3E-18(+)	3.3E-18(+)	3.3E-18(+)
F28	Mean	3300.022	3374.6808	3382.7937	3605.4397	3347.5405	10628.347	3706.4048	3371.1428
	Std	0.000224	33.73612	34.239748	38.34197	31.215903	1686.0586	73.021728	28.121203
	Kruskal	29	161.39216	177.62745	286.37255	112	383	326.62745	159.98039
	WSRT		3.3E-18(+)	3.3E-18(+)	3.3E-18(+)	1.6E-14(+)	3.3E-18(+)	3.3E-18(+)	3.3E-18(+)
F29	Mean	5214.179	6684.1913	7013.0317	6765.6676	7872.0657	10892.841	12699.242	9128.366
	Std	506.21232	496.21594	490.2713	1069.4739	667.77233	807.73563	1620.2471	591.11213
	Kruskal	31.62745	120.64706	150.88235	129.2549	213.35294	337.66667	374.29412	278.27451
	WSRT		8.4E-17(+)	3.0E-17(+)	1.0E-13(+)	4.2E-18(+)	3.3E-18(+)	3.3E-18(+)	3.3E-18(+)
F30	Mean	6430.107	3246799.4	12398.871	104714.3	207840.52	2.088E+09	82562715	5713969.6
	Std	3366.11	1206638	5176.9533	149532.06	96848.202	1.584E+09	42286195	1376174.1
	Kruskal	34.01961	232.60784	72.352941	133.29412	170.37255	383	332	278.35294
	WSRT		3.3E-18(+)	1.1E-09(+)	1.0E-17(+)	3.3E-18(+)	3.3E-18(+)	3.3E-18(+)	3.3E-18(+)
FMR		1.266396	3.0682894	3.2535497	4.8999324	4.0594997	7.2393509	6.3461799	5.8668019
F-Rank		1	2	3	5	4	8	7	6

FMR and F-Rank are the statistical results over all CEC2017 benchmark test functions (100D).

unique ability to comprehensively explore the feasible region, resulting in superior optimization performance. Although AOO also shows a second round of convergence on these functions, its final function values remain significantly worse than those of DoS.

In summary, when solving simple optimization problems, DoS can quickly locate the optimal solution domain through a well balanced exploration and exploitation mechanism. When facing complex optimization problems, it can effectively avoid falling into local optima. This feature not only enables the algorithm to perform broad exploration but

Table 15

Experimental results of DoS and advanced competitors on 10D CEC2022 benchmark test functions.

No.	Metrics	DoS	AOO	PSA	FFA	AVOA	ETO	SGA	WAA
C1	Mean	300	300	300	300.33526	300	2591.1845	300.02927	300.0381
	Std	0	5.047E-08	6.922E-14	0.5229235	1.301E-13	2181.0563	0.0450559	0.0115081
	Kruskal	17	105.5	55.066667	186.33333	64.433333	225.5	145.4	164.76667
	WSRT		1.2E-12(+)	1.1E-11(+)	1.2E-12(+)	3.2E-12(+)	1.2E-12(+)	1.2E-12(+)	1.2E-12(+)
C2	Mean	403.1328	405.99319	403.92253	407.34966	413.59611	428.71844	418.64804	409.12183
	Std	1.030256	3.5072486	3.7235414	3.2614581	23.134137	37.315088	28.497419	17.201281
	Kruskal	74	124.3	81.516667	162.86667	109.65	139.36667	149.6	122.7
	WSRT		3.4E-05(+)	1.2E-01(≈)	8.1E-05(+)	1.3E-02(+)	7.0E-02(≈)	5.1E-06(+)	3.8E-02(+)
C3	Mean	600	600.20325	600	600.00979	604.69499	613.61211	618.84397	644.14483
	Std	0	0.380026	9.244E-11	0.022072	5.5438782	8.7362625	11.301923	10.096949
	Kruskal	16	107	45.766667	78	138.33333	172.23333	183	223.66667
	WSRT		1.2E-12(+)	2.5E-12(+)	1.2E-12(+)	1.2E-12(+)	1.2E-12(+)	1.2E-12(+)	1.2E-12(+)
C4	Mean	804.4445	813.67136	821.25901	822.62518	830.45045	826.55429	825.40461	839.14213
	Std	1.376077	6.8207061	7.4752319	4.3039578	11.565046	10.617232	9.34342	7.4060587
	Kruskal	16.8	66.566667	109.85	121.4	162.91667	139.83333	139.36667	207.26667
	WSRT		8.9E-10(+)	3.0E-11(+)	3.0E-11(+)	4.5E-11(+)	3.0E-11(+)	3.0E-11(+)	3.0E-11(+)
C5	Mean	900	900.04842	943.63206	900.26687	1046.4564	1049.5779	1015.1158	1474.1793
	Std	0	0.1385791	76.258644	0.2804191	186.69996	179.76697	86.994952	144.26707
	Kruskal	15.5	48.3	125.96667	73.833333	158.13333	158.6	161.93333	221.73333
	WSRT		1.2E-12(+)	1.2E-12(+)	1.2E-12(+)	1.2E-12(+)	1.2E-12(+)	1.2E-12(+)	1.2E-12(+)
C6	Mean	1803.835	4933.8797	3566.9497	3928.8872	4606.0945	15995.753	5120.3224	2122.3238
	Std	5.362242	2222.2208	1611.3283	2317.9508	2216.0887	11247.6	2303.1726	387.10921
	Kruskal	15.5	147.1	113.36667	116.53333	137.06667	212.26667	154.5	67.666667
	WSRT		3.0E-11(+)	3.0E-11(+)	3.0E-11(+)	3.0E-11(+)	3.0E-11(+)	3.0E-11(+)	3.0E-11(+)
C7	Mean	2000.963	2022.206	2018.0725	2008.8364	2022.8608	2040.6097	2036.89	2099.5237
	Std	3.658985	8.479453	5.9034516	8.3959996	7.1027243	19.087814	12.816271	42.872582
	Kruskal	18.93333	117.76667	75.266667	60.266667	125.56667	175.3	172.63333	218.26667
	WSRT		6.7E-11(+)	3.5E-10(+)	1.0E-08(+)	4.5E-11(+)	3.3E-11(+)	4.1E-11(+)	3.0E-11(+)
C8	Mean	2202.504	2217.2387	2219.2726	2215.2868	2221.534	2226.9403	2228.0515	2302.7774
	Std	3.9505512	8.5367334	5.1832188	8.610161	3.73739	5.7251247	5.6842061	97.110312
	Kruskal	21.16667	97.166667	77.8	88.7	113.03333	178.86667	177.56667	209.7
	WSRT		2.4E-09(+)	1.6E-08(+)	2.7E-09(+)	5.5E-11(+)	4.1E-11(+)	3.3E-11(+)	3.0E-11(+)
C9	Mean	2486.87	2529.2847	2529.2844	2529.5164	2529.2844	2559.0567	2534.1822	2529.2847
	Std	2.0089098	0.0005269	9.956E-13	0.6135013	1.46E-13	31.561907	26.825978	0.0001537
	Kruskal	15.5	140.26667	69.9	192.86667	51.1	223.63333	116.26667	154.46667
	WSRT		3.0E-11(+)	2.2E-11(+)	3.0E-11(+)	3.2E-12(+)	3.0E-11(+)	3.0E-11(+)	3.0E-11(+)
C10	Mean	2500.415	2503.9091	2535.1462	2503.9086	2549.386	2525.027	2522.8988	2762.5456
	Std	26.952171	19.9886	53.781311	19.486939	61.10995	38.639138	50.952252	368.31004
	Kruskal	35.6	43.733333	159.5	75.933333	157.93333	149.13333	142.56667	199.6
	WSRT		3.8E-01(≈)	2.4E-10(+)	1.6E-07(+)	1.8E-10(+)	6.1E-10(+)	8.1E-10(+)	1.2E-10(+)
C11	Mean	2850	2697.484	2937.1769	2716.5658	2740.9847	2995.6384	2757.8508	2852.2844
	Std	113.71471	153.11814	184.48101	70.76167	137.21471	160.22422	128.9277	114.28792
	Kruskal	98.833333	76.13333	151.36667	80	82.6	204.36667	108.36667	162.33333
	WSRT		2.5E-01(≈)	7.3E-10(+)	1.3E-04(-)	7.1E-01(≈)	8.0E-08(+)	2.5E-01(≈)	6.3E-07(+)
C12	Mean	2889.772	2863.2723	2865.526	2861.705	2864.8995	2880.6942	2865.1139	2963.9553
	Std	20.821272	1.251124	2.182712	1.3734052	2.42454	19.067232	1.9165205	70.583671
	Kruskal	158.7	64.733333	116.53333	34.56667	100.66667	162.26667	106	220.53333
	WSRT		6.8E-05(-)	6.8E-05(-)	6.8E-05(-)	6.8E-05(-)	2.7E-02(-)	6.8E-05(-)	1.7E-07(+)
FMR	1.883333	3.6555556	3.7527778	4.0263889	4.3541667	6.4444444	5.3555556	6.5277778	
F-Rank	1	2	3	4	5	7	6	8	

FMR and F-Rank are the statistical results over all CEC2022 benchmark test functions (10D).

Table 16

Experimental results of DoS and advanced competitors on 20D CEC2022 benchmark test functions.

No.	Metrics	DoS	AOO	PSA	FFA	AVOA	ETO	SGA	WAA
C1	Mean	300	300	300	306.03495	300	11803.089	307.16622	300.39313
	Std	3.66E-14	8.449E-09	1.84E-12	6.8698472	1.855E-13	4703.1851	8.1940942	0.1019005
	Kruskal	15.5	105.5	68.983333	179.23333	52.016667	225.5	177.26667	140
	WSRT		1.3E-11(+)	1.3E-11(+)	1.3E-11(+)	1.2E-11(+)	1.3E-11(+)	1.3E-11(+)	1.3E-11(+)
C2	Mean	409.2096	441.76036	436.91201	453.40179	431.14145	530.20493	452.20248	451.34328
	Std	9.3737047	16.365079	22.07657	5.766707	24.286936	60.651785	22.946428	12.37996
	Kruskal	29.5	91.633333	83.75	171.46667	66.016667	223.93333	151.83333	145.86667
	WSRT		7.9E-09(+)	1.1E-06(+)	2.8E-11(+)	2.5E-05(+)	2.8E-11(+)	7.9E-09(+)	1.2E-10(+)
C3	Mean	600.0003	601.24916	600.07275	600.09485	612.29284	626.58495	650.12214	663.4934
	Std	0.00065	1.8702363	0.3068289	0.1426903	7.6594782	8.3308069	12.017137	8.5810271
	Kruskal	28.96667	103.13333	35.766667	75.266667	137.3	164.73333	198.56667	220.26667
	WSRT		2.5E-11(+)	3.9E-01(≈)	8.3E-11(+)	2.5E-11(+)	2.5E-11(+)	2.5E-11(+)	2.5E-11(+)
C4	Mean	817.9441	846.99617	868.48742	890.94447	888.23454	893.1711	886.87962	902.38775
	Std	4.891897	15.185806	18.540806	7.4258835	21.749882	21.052151	22.494013	19.847342
	Kruskal	16.03333	55.966667	96.4	161.56667	146.66667	161.03333	142.96667	183.36667
	WSRT		1.5E-10(+)	3.0E-11(+)	3.0E-11(+)	3.0E-11(+)	3.0E-11(+)	3.0E-11(+)	3.0E-11(+)
C5	Mean	900.509	901.10872	2061.4428	906.11336	2174.7726	2073.8973	2187.695	2677.0431
	Std	0.584541	3.4361638	750.80819	4.8491158	332.38818	479.77182	331.46565	361.48852
	Kruskal	33.566667	30	144.4	72.933333	161.2	151.26667	162.66667	207.96667
	WSRT		2.6E-01(≈)	2.9E-11(+)	1.3E-10(+)	2.9E-11(+)	2.9E-11(+)	2.9E-11(+)	2.9E-11(+)
C6	Mean	1877.902	7981.3414	4112.4339	30373.841	6556.6909	956476.69	8621.9567	7154.3353
	Std	49.59876	6589.327	2747.5297	64926.322	5325.4433	1256758.3	6967.6583	3372.3559
	Kruskal	18.23333	125.43333	84.066667	138.96667	111.86667	225.26667	125.6	134.56667
	WSRT		3.0E-11(+)	1.0E-08(+)	3.3E-11(+)	6.7E-11(+)	3.0E-11(+)	9.0E-11(+)	3.0E-11(+)
C7	Mean	2016.568	2032.7279	2067.6759	2032.7674	2083.7473	2112.3879	2111.8595	2258.9069
	Std	6.996966	10.666281	47.067405	7.6841236	41.035303	42.169606	37.101645	98.870378
	Kruskal	17.53333	67.1	116.73333	68.733333	138.4	167.06667	168.4	220.03333
	WSRT		2.4E-10(+)	3.0E-11(+)	2.2E-10(+)	2.2E-10(+)	3.0E-11(+)	3.0E-11(+)	3.0E-11(+)
C8	Mean	2219.708	2224.1792	2246.8719	2229.7121	2228.1167	2246.0707	2275.6722	2419.4856
	Std	2.672545	3.8690004	44.58114	3.5858018	7.9241616	32.321295	54.96744	150.3355
	Kruskal	16.8	80.7	103.76667	126.86667	100.3	151.16667	180.2	204.2
	WSRT		5.6E-10(+)	7.4E-11(+)	3.0E-11(+)	3.0E-11(+)	3.0E-11(+)	3.0E-11(+)	3.0E-11(+)
C9	Mean	2466.983	2480.7852	2480.7813	2481.2435	2480.7813	2504.1376	2480.8885	2480.7874
	Std	0.47377	0.0031774	7.83E-12	0.4450729	3.055E-09	18.595197	0.0656501	0.0031057
	Kruskal	15.5	116.7	45.5	184.3	75.5	225.36667	170.06667	131.06667
	WSRT		3.0E-11(+)	3.0E-11(+)	3.0E-11(+)	3.0E-11(+)	3.0E-11(+)	3.0E-11(+)	3.0E-11(+)
C10	Mean	2432.837	2587.7035	2653.6576	2500.5107	2664.7057	2895.1071	3104.8031	4836.6844
	Std	45.606809	196.87289	202.64586	0.087707	210.60401	576.96241	1085.0082	966.51639
	Kruskal	24.93333	72.766667	142.86667	74.066667	128.8	160.2	146.53333	213.83333
	WSRT		8.1E-05(+)	9.9E-11(+)	7.1E-09(+)	4.2E-10(+)	3.0E-11(+)	4.1E-11(+)	3.0E-11(+)
C11	Mean	2900	2920.0002	2900	2986.0277	2930	3811.5196	2950.103	2951.9492
	Std	3.04E-13	40.68374	2.508E-12	69.291934	46.60916	522.16053	77.538283	44.121338
	Kruskal	15.5	110.5	48.466667	167.43333	98.033333	225.26667	143.43333	155.36667
	WSRT		1.4E-11(+)	1.3E-11(+)	1.4E-11(+)	1.4E-11(+)	1.4E-11(+)	1.4E-11(+)	1.4E-11(+)
C12	Mean	2900.004	2944.5165	2969.2382	2940.0136	2972.7629	3031.0166	3005.7321	3648.542
	Std	0.000117	6.0104328	23.658208	4.0042601	23.791441	53.230748	48.757913	296.09399
	Kruskal	15.5	72.966667	126.16667	55.033333	131.46667	178.86667	158.86667	225.13333
	WSRT		3.0E-11(+)	3.0E-11(+)	3.0E-11(+)	3.0E-11(+)	3.0E-11(+)	3.0E-11(+)	3.0E-11(+)
FMR		1.172222	3.3694444	3.4736111	4.6027778	4.2541667	6.75	5.8277778	6.55
F-Rank		1	2	3	5	4	8	6	7

FMR and F-Rank are the statistical results over all CEC2022 benchmark test functions (20D).

Table 17

Experimental results of DoS and SOTA algorithms on 50D CEC2017 benchmark test functions (Unimodal and Multimodal).

No.	Metrics	Mean	Best	Std	Kruskal	WSRT
F1	DoS	100	100	8.266E-10	86.676471	
	LSHADE	100	100	1.591E-07	163.98039	2.4E-14(+)
	LSHADE-SPACMA	100	100	2.57E-14	27.84314	4.4E-16(-)
	AL-SHADE	100	100	1.164E-09	131.5	5.0E-09(+)
F3	DoS	300	300	2.36E-13	46.16667	
	LSHADE	40946.98	300	79720.112	153.36275	1.8E-17(+)
	LSHADE-SPACMA	60631.926	300	95842.571	95.088235	1.8E-04(+)
	AL-SHADE	300	300	4.175E-12	115.38235	2.4E-12(+)
F4	DoS	422.0392	400	35.92002	77.55882	
	LSHADE	463.70769	400.00212	46.551156	137.7549	1.3E-08(+)
	LSHADE-SPACMA	437.48371	400	46.064835	89.529412	8.4E-01(\approx)
	AL-SHADE	434.38821	400	42.792302	105.15686	2.4E-03(+)
F5	DoS	616.22595	576.65356	20.868763	178.03922	
	LSHADE	558.3527	533.82927	11.07337	62.76471	4.7E-18(-)
	LSHADE-SPACMA	565.86406	540.79397	10.94323	92.490196	1.5E-17(-)
	AL-SHADE	561.68739	532.8336	13.281825	76.705882	8.9E-18(-)
F6	DoS	600.0709	600	0.256435	31.80392	
	LSHADE	600.80875	600.00991	0.7665073	106.03922	5.2E-15(+)
	LSHADE-SPACMA	601.9224	600.39045	1.1694028	161.13725	2.4E-17(+)
	AL-SHADE	600.84039	600.09291	0.6344647	111.01961	3.8E-15(+)
F7	DoS	881.06362	826.21983	24.848898	159.01961	
	LSHADE	849.79627	811.16742	21.96977	94.588235	2.3E-09(-)
	LSHADE-SPACMA	836.3118	783.4292	22.297265	66.84314	1.8E-13(-)
	AL-SHADE	847.31205	798.11222	24.275304	89.54902	2.8E-09(-)
F8	DoS	907.91801	873.65473	19.880242	175.58824	
	LSHADE	856.9283	837.8107	13.75822	58.70588	3.6E-17(-)
	LSHADE-SPACMA	865.23972	840.79385	12.38462	91.176471	1.4E-16(-)
	AL-SHADE	864.5357	844.77313	13.853883	84.529412	1.6E-16(-)
F9	DoS	1257.9707	900	367.32114	104.52941	
	LSHADE	1212.3163	924.17463	273.78712	105.58824	9.7E-01(\approx)
	LSHADE-SPACMA	1294.1224	956.75563	325.51319	124.7451	2.3E-01(\approx)
	AL-SHADE	1090.38	918.80654	164.7694	75.13725	5.2E-02(\approx)
F10	DoS	4782.9366	3899.8102	386.18247	137.54902	
	LSHADE	4625.0048	3830.4219	327.6693	118.11765	4.3E-02(-)
	LSHADE-SPACMA	4226.487	3569.296	333.14474	59.15686	2.5E-10(-)
	AL-SHADE	4492.4279	3717.5407	388.03587	95.176471	3.2E-04(-)

also allows it to continue exploitation operations. In terms of both convergence speed and convergence quality, DoS demonstrates significant advantages.

4.6. Scalability Analysis

Dimensionality is one of the key factors affecting the complexity of optimization problems and has a direct impact on algorithm performance. Therefore, this section analyzes the scalability of DoS based on the Mean rankings and Friedman rankings of CEC2017 and CEC2022 benchmark test functions under different dimensions, as presented in Section 4.3. The visualizations of the Mean rankings and Friedman rankings of DoS compared with other competitors are shown in Fig. 9, 10, 11 and 12.

Fig. 9 shows the Mean ranking of DoS and its competitors on the 30D, 50D and 100D CEC2017 benchmark test functions. According to the results, except for slightly inferior performance on F28 in 30D, DoS performs excellently on all other functions. As the dimensionality increases, its performance on F28 gradually improves ranking second in 50D (slightly lower than AOO) and rising to first place in 100D. This indicates that the extra evaluations from higher dimensionality give DoS more exploration time, thus improving its performance on this function.

For functions F24 and F26, DoS ranks first in terms of the Mean metric in both 30D and 50D, but is surpassed by FFA in 100D, dropping to second place. Nevertheless, in terms of numerical values, the Mean difference between DoS

Table 18

Experimental results of DoS and SOTA algorithms on 50D CEC2017 benchmark test functions (Hybrid).

No.	Metrics	Mean	Best	Std	Kruskal	WSRT
F11	DoS	1279.913	1167.419	47.39033	77.84314	
	LSHADE	1335.352	1237.6025	70.316482	127.86275	2.4E-05(+)
	LSHADE-SPACMA	1317.3168	1216.7653	56.918422	112.60784	2.0E-03(+)
	AL-SHADE	1294.5099	1190.8966	59.899022	91.686275	2.7E-01(\approx)
F12	DoS	6940.079	2276.173	3988.2658	95.784314	
	LSHADE	14013.363	4292.871	10769.826	146.66667	8.7E-07(+)
	LSHADE-SPACMA	3675.482	2688.0149	515.1498	33.31373	5.4E-11(-)
	AL-SHADE	10385.516	3735.6708	5425.2378	134.23529	8.5E-05(+)
F13	DoS	3664.4024	1430.8619	3178.4674	100	
	LSHADE	3325.9359	1610.5161	3474.2883	93.215686	7.5E-01(\approx)
	LSHADE-SPACMA	4252.6011	2380.6939	1034.2212	155.56863	2.0E-05(+)
	AL-SHADE	2126.275	1399.92	607.4895	61.21569	2.0E-03(-)
F14	DoS	1705.921	1480.839	115.13288	97.07843	
	LSHADE	1720.2395	1548.4749	70.12658	111.27451	2.3E-01(\approx)
	LSHADE-SPACMA	1718.6654	1560.3522	95.8092	103.98039	5.9E-01(\approx)
	AL-SHADE	1706.6258	1557.2875	85.717375	97.666667	9.1E-01(\approx)
F15	DoS	1835.009	1529.352	170.31982	79.82353	
	LSHADE	1913.0865	1622.0463	162.68382	102.31373	4.3E-02(+)
	LSHADE-SPACMA	2059.2344	1759.3827	212.34541	141.92157	3.9E-07(+)
	AL-SHADE	1857.6854	1595.5396	156.3706	85.941176	5.3E-01(\approx)
F16	DoS	2547.2624	1988.9621	253.96026	113.88235	
	LSHADE	2509.1228	1950.1857	215.3516	105.84314	4.1E-01(\approx)
	LSHADE-SPACMA	2475.4606	1854.779	287.9017	95.960784	1.3E-01(\approx)
	AL-SHADE	2469.641	1859.0595	305.04425	94.31373	1.3E-01(\approx)
F17	DoS	2418.7292	1989.9291	173.8556	111.92157	
	LSHADE	2443.6957	2063.042	167.98872	120.47059	4.5E-01(\approx)
	LSHADE-SPACMA	2339.293	2032.8425	175.44524	80.70588	8.4E-03(-)
	AL-SHADE	2381.2666	1938.228	187.2952	96.901961	1.9E-01(\approx)
F18	DoS	2889.9539	1915.6841	837.54343	122.76471	
	LSHADE	3246.1577	1904.0504	1233.8132	134.66667	2.1E-01(\approx)
	LSHADE-SPACMA	2086.042	1875.893	132.3506	50.07843	1.9E-10(-)
	AL-SHADE	2723.3786	1902.0375	1007.4075	102.4902	7.1E-02(\approx)
F19	DoS	2056.599	1929.094	60.367966	84.66667	
	LSHADE	2077.7849	1990.4833	57.37541	94.784314	4.0E-01(\approx)
	LSHADE-SPACMA	2160.8638	1988.825	148.15809	145.76471	1.9E-07(+)
	AL-SHADE	2063.9512	1993.6955	43.008306	84.784314	9.8E-01(\approx)
F20	DoS	2437.4399	2152.9213	131.8813	103.80392	
	LSHADE	2504.5134	2172.6279	155.73278	126.47059	5.2E-02(\approx)
	LSHADE-SPACMA	2421.9738	2090.7928	149.82474	98.862745	6.8E-01(\approx)
	AL-SHADE	2370.908	2037.509	187.92547	80.86275	4.9E-02(-)

and FFA is small and both are significantly better than the other competitors.

Fig. 10 presents the Friedman average rankings of DoS and its competitors on the CEC2017 test functions. It can be observed that the Friedman rankings of DoS remain relatively stable across the three dimensions, maintaining first place with a significant lead, which demonstrates good scalability. Meanwhile, AOO, PSA, AVOA and WAA show slight improvements in their Friedman rankings as the dimensionality increases, also indicating relatively strong scalability. In contrast, the average rankings of FFA, ETO and SGA decline

noticeably, especially for FFA and ETO, whose performance drops significantly, suggesting weaker adaptability to higher dimensions and poorer scalability.

Fig. 11 illustrates the radar chart of the Mean rankings of DoS and advanced competitors on the 10D and 20D CEC2022 benchmark test functions. The results show that DoS consistently ranks first on ten out of the twelve functions, except for C11 and C12. In 10D, DoS performs relatively poorly on C11 and C12, but in 20D, its performance improves significantly, surpassing all competitors. This discrepancy is mainly due to the fewer evaluation times

Table 19

Experimental results of DoS and SOTA algorithms on 50D CEC2017 benchmark test functions (Composition).

No.	Metrics	Mean	Best	Std	Kruskal	WSRT
F21	DoS	2404.2514	2372.333	14.806696	177.70588	
	LSHADE	2355.131	2334.8268	11.24392	68.76471	5.3E-18(-)
	LSHADE-SPACMA	2360.6729	2339.5417	11.606271	88.72549	1.0E-17(-)
	AL-SHADE	2356.7652	2331.429	14.092693	74.803922	3.2E-17(-)
F22	DoS	6284.9812	2300	892.27191	109.5098	
	LSHADE	6459.7616	2301.4107	685.0383	124	1.9E-01(≈)
	LSHADE-SPACMA	5376.747	2300	1760.7421	78.86275	7.3E-03(-)
	AL-SHADE	6037.6519	2300	1309.1275	97.627451	3.1E-01(≈)
F23	DoS	2790.402	2746.397	21.305894	77.66667	
	LSHADE	2796.1118	2767.7534	17.03535	92.509804	1.3E-01(≈)
	LSHADE-SPACMA	2814.1393	2772.3922	22.115573	139.33333	1.2E-06(+)
	AL-SHADE	2799.3236	2763.9507	20.440585	100.4902	3.6E-02(+)
F24	DoS	3009.852	2956.0793	24.03879	159.31373	
	LSHADE	2963.059	2934.013	16.60232	59.17647	5.7E-15(-)
	LSHADE-SPACMA	2984.5581	2947.5657	24.460412	109.56863	3.3E-07(-)
	AL-SHADE	2972.8762	2934.116	24.034438	81.941176	1.0E-10(-)
F25	DoS	2968.833	2931.2689	33.59039	46.70588	
	LSHADE	3029.4396	2960.1618	44.04549	115.92157	3.2E-09(+)
	LSHADE-SPACMA	3034.0004	2958.1133	43.409329	124.37255	7.1E-11(+)
	AL-SHADE	3033.648	2928.82	42.165142	123	4.3E-11(+)
F26	DoS	4028.313	2900	383.51956	40.17647	
	LSHADE	4542.3483	4124.9167	205.398	102.52941	9.5E-12(+)
	LSHADE-SPACMA	4727.5656	4216.3413	261.95951	135.98039	3.3E-13(+)
	AL-SHADE	4691.8314	4158.2567	226.44455	131.31373	7.6E-13(+)
F27	DoS	3200.011	3200.01	0.00014	26	
	LSHADE	3354.315	3236.7039	70.682236	120.58824	3.3E-18(+)
	LSHADE-SPACMA	3406.4369	3289.8923	75.060222	150.31373	3.3E-18(+)
	AL-SHADE	3340.8421	3221.6297	72.071441	113.09804	3.3E-18(+)
F28	DoS	3299.2651	3279.8089	3.595295	121.23529	
	LSHADE	3293.2885	3258.8487	26.909047	103.62745	2.5E-02(-)
	LSHADE-SPACMA	3287.072	3253.352	30.787893	87.48039	6.9E-04(-)
	AL-SHADE	3292.1996	3253.352	32.123185	97.656863	4.5E-01(≈)
F29	DoS	3442.742	3217.06	127.5843	83.43137	
	LSHADE	3568.0981	3245.5777	184.68755	122.62745	6.3E-04(+)
	LSHADE-SPACMA	3534.3358	3257.1179	161.01547	114.31373	5.6E-03(+)
	AL-SHADE	3484.103	3223.4824	219.0791	89.627451	7.6E-01(≈)
F30	DoS	3545.922	3270.068	391.276	26	
	LSHADE	743861.5	582496.75	135523.45	125.90196	3.3E-18(+)
	LSHADE-SPACMA	775423.83	582420.14	140828.88	137.84314	3.3E-18(+)
	AL-SHADE	719364.27	582412.59	105318.04	120.2549	3.3E-18(+)

FMR: DoS (**2.416836**), LSHADE (2.6585531), LSHADE-SPACMA (2.4989858), AL-SHADE(2.4256254).F-Rank: DoS (**1**), LSHADE (4), LSHADE-SPACMA (3), AL-SHADE(2).

FMR and F-Rank are the statistical results over all CEC2017 benchmark test functions (50D).

in the 10D tests, which limit the full effectiveness of DoS's search mechanisms on these two functions.

Fig. 12 shows the bar chart of the Friedman average rankings of each algorithm on the CEC2022 benchmark test functions. Combining Fig. 11 and 12, it can be seen that DoS maintains strong overall performance in both 10D and 20D settings and its Friedman ranking continuously improves as

the dimensionality increases, reflecting excellent scalability. Similarly, AOO, PSA and AVOA also exhibit a certain degree of scalability, as their rankings improve with increasing dimensions. In contrast, WAA performs relatively poorly in both dimensions, with little change in ranking, indicating limited scalability. FFA, ETO and SGA show a declining

Table 20

Experimental results of DoS and SOTA algorithms on 20D CEC2022 benchmark test functions.

No.	Metrics	Mean	Best	Std	Kruskal	WSRT
C1	DoS	300	300	3.657E-14	54.3	
	LSHADE	1321.9344	300	4227.5481	84.25	3.1E-05(+)
	LSHADE-SPACMA	3754.3535	300	6223.297	54.6	8.4E-01(≈)
	AL-SHADE	300	300	3.17E-14	48.85	4.3E-01(≈)
C2	DoS	409.2096	400	9.3737047	18.25	
	LSHADE	448.80521	444.89547	1.062786	81.216667	4.7E-12(+)
	LSHADE-SPACMA	443.89676	400	14.919996	72.216667	2.1E-08(+)
	AL-SHADE	448.10704	444.89547	1.802041	70.316667	6.9E-12(+)
C3	DoS	600.0001	600	0.000143	29.08333	
	LSHADE	600.00088	600	0.0027695	69.95	1.0E-05(+)
	LSHADE-SPACMA	600.01526	600	0.0536951	86.416667	2.8E-08(+)
	AL-SHADE	600.00684	600	0.0343109	56.55	2.5E-05(+)
C4	DoS	817.94414	810.94481	4.8918965	94.466667	
	LSHADE	811.67419	806.96472	2.920516	54.8	3.3E-07(-)
	LSHADE-SPACMA	812.10533	804.9748	4.571311	55.383333	1.7E-05(-)
	AL-SHADE	810.2149	804.9748	4.0219236	37.35	1.7E-08(-)
C5	DoS	900.509	900	0.584541	59.633333	
	LSHADE	900.89887	900	1.0320978	74.533333	8.9E-02(≈)
	LSHADE-SPACMA	900.63022	900	1.126228	58.066667	8.5E-01(≈)
	AL-SHADE	900.78316	900	2.0991567	49.76667	2.6E-01(≈)
C6	DoS	1877.9024	1804.273	49.598764	71.833333	
	LSHADE	1860.7911	1806.505	38.895073	59.933333	2.0E-01(≈)
	LSHADE-SPACMA	1854.8243	1819.314	30.68686	56.933333	7.0E-02(≈)
	AL-SHADE	1853.532	1805.4535	38.973975	53.3	5.7E-02(≈)
C7	DoS	2016.568	2004.9575	6.9969661	59.433333	
	LSHADE	2017.7427	2004.6305	6.768248	63.2	5.4E-01(≈)
	LSHADE-SPACMA	2017.9714	2001.357	7.6158463	65.266667	5.0E-01(≈)
	AL-SHADE	2017.4489	2002.3021	7.1361371	54.1	4.1E-01(≈)
C8	DoS	2219.708	2207.679	2.6725453	62.033333	
	LSHADE	2220.579	2218.0775	0.773127	64.666667	9.4E-01(≈)
	LSHADE-SPACMA	2220.5105	2216.5918	0.9010526	68.2	3.9E-01(≈)
	AL-SHADE	2220.213	2217.3343	0.756027	47.1	1.0E-01(≈)
C9	DoS	2466.967	2465.609	0.4475143	15.5	
	LSHADE	2480.7813	2480.7813	4.222E-13	73.5	5.1E-12(+)
	LSHADE-SPACMA	2480.7813	2480.7813	3.16E-13	87	1.4E-11(+)
	AL-SHADE	2480.7813	2480.7813	0	66	1.2E-12(+)
C10	DoS	2432.837	2400.0312	45.606809	31.73333	
	LSHADE	2494.3365	2400	38.508124	71.683333	7.7E-05(+)
	LSHADE-SPACMA	2493.7898	2400.0312	25.26385	64.733333	3.2E-05(+)
	AL-SHADE	2512.911	2400	46.224733	73.85	3.8E-06(+)
C11	DoS	2900	2900	3.045E-13	57	
	LSHADE	2900	2900	2.801E-13	53	6.1E-01(≈)
	LSHADE-SPACMA	2900	2900	2.67E-13	51	4.3E-01(≈)
	AL-SHADE	2900	2900	4.222E-13	81	1.5E-03(-)
C12	DoS	2900.004	2900.004	0.00012	15.5	
	LSHADE	2938.0431	2931.0617	4.291119	60.283333	3.0E-11(+)
	LSHADE-SPACMA	2946.4365	2935.419	9.2818255	90.333333	3.0E-11(+)
	AL-SHADE	2941.9602	2932.4577	7.0578608	75.883333	3.0E-11(+)

FMR: DoS (**2.072222**), LSHADE (2.7125), LSHADE-SPACMA (2.7597222), AL-SHADE(2.4555556).

F-Rank: DoS (1), LSHADE (3), LSHADE-SPACMA (4), AL-SHADE(2).

FMR and F-Rank are the statistical results over all CEC2022 benchmark test functions (20D).

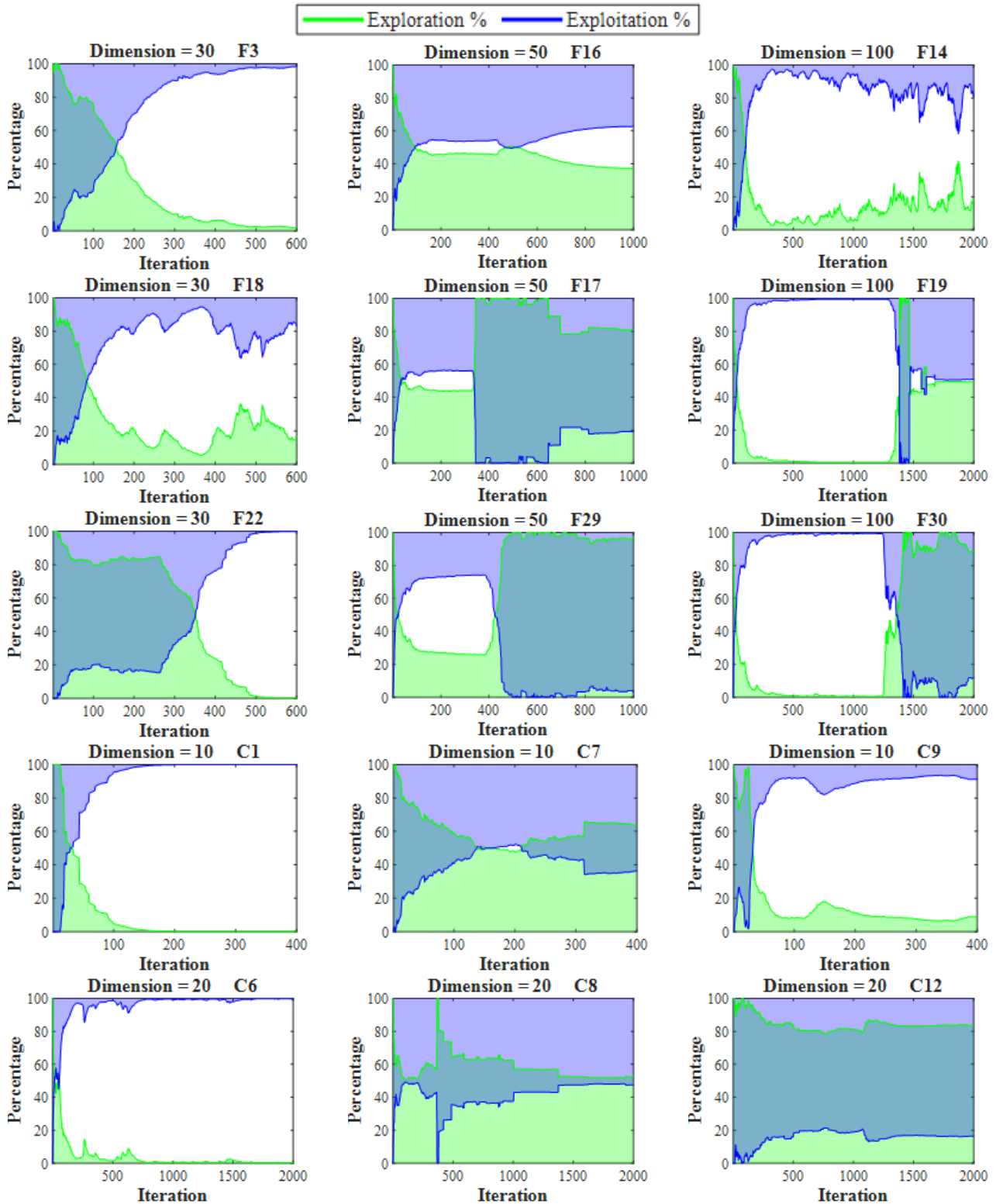


Figure 7: Convergence curves of objective function values.

trend in their Friedman rankings across both dimensions, suggesting poor scalability on this benchmark.

In summary, DoS maintains stable and improving performance on the CEC2022 benchmark test functions as

dimensionality increases. The continuous improvement in its Friedman ranking further confirms its strong scalability. Although AOO, PSA and AVOA do not outperform DoS in overall performance, their improvements with increasing

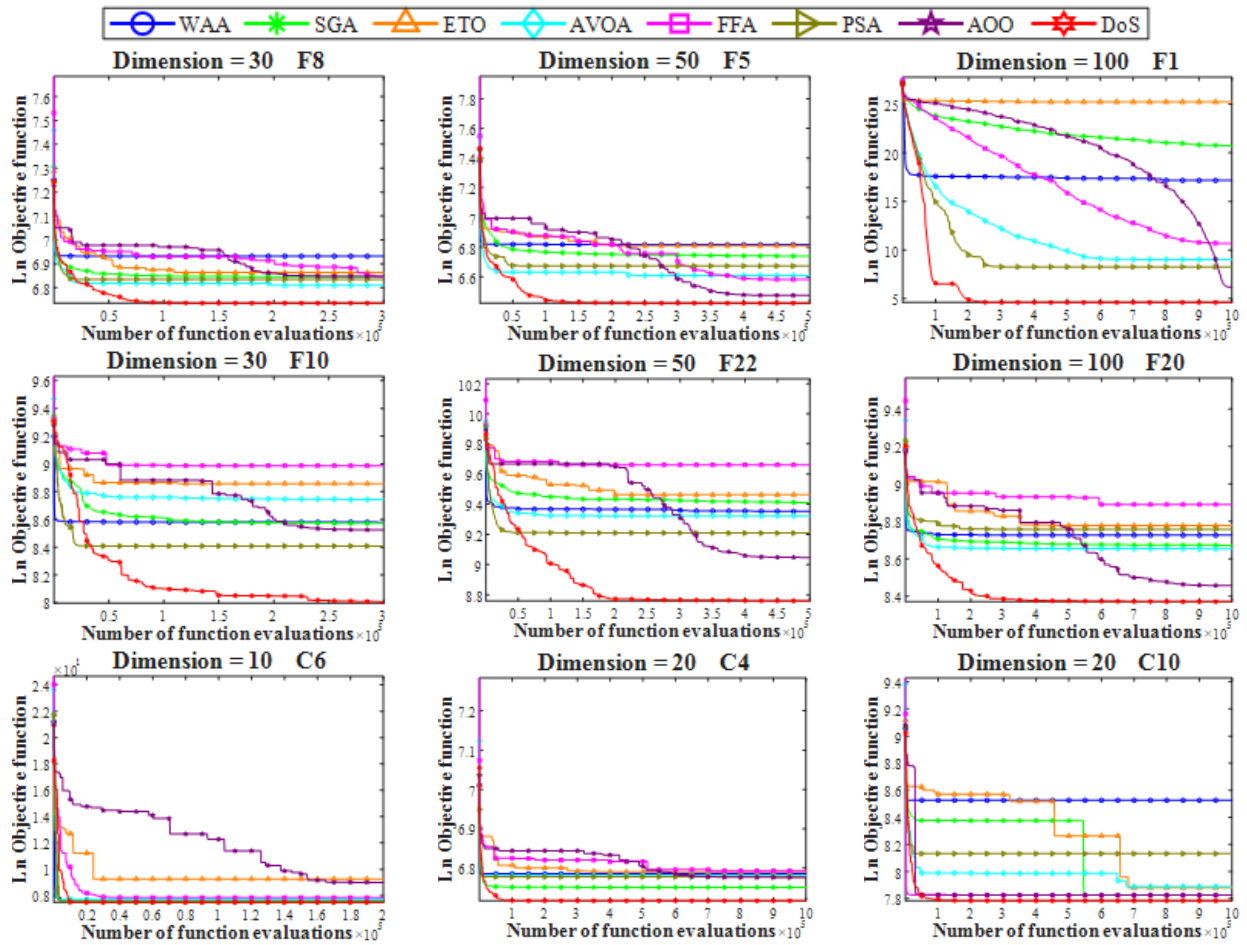


Figure 8: Convergence curves of objective function values.

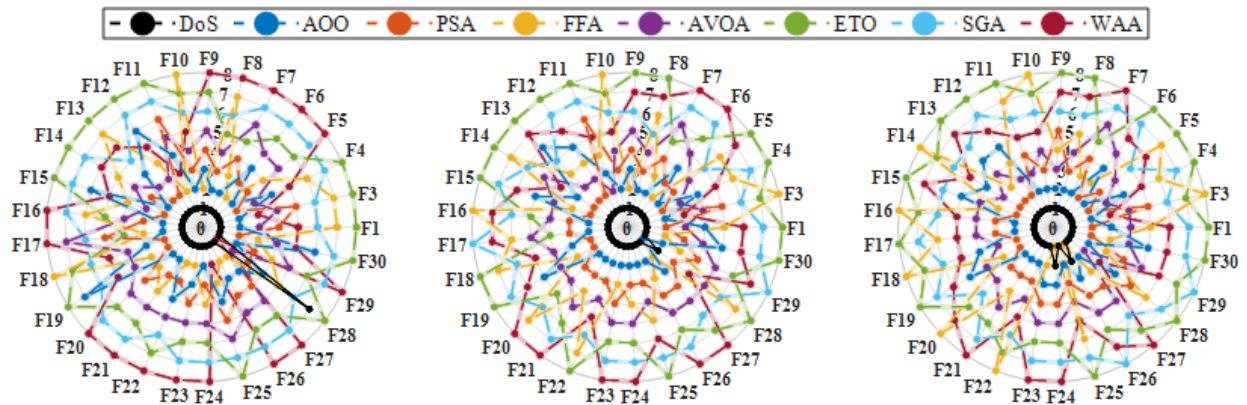


Figure 9: Radar chart of Mean rankings on CEC2017 benchmark test functions.

dimensionality indicate they are also suitable for higher-dimensional optimization tasks. By comparison, FFA, ETO and SGA show decreasing performance as dimensionality increases, highlighting their insufficient scalability.

4.7. Behavior Analysis

Behavior analysis is an important method for gaining an in depth understanding of the search process of meta-heuristic algorithms, as it intuitively reveals the evolutionary characteristics of algorithm strategies during iterations. To further analyze the search mechanism of DoS, this paper conducts a visual analysis of selected 2-dimensional CEC2017 and CEC2022 benchmark test functions in Fig. 13.

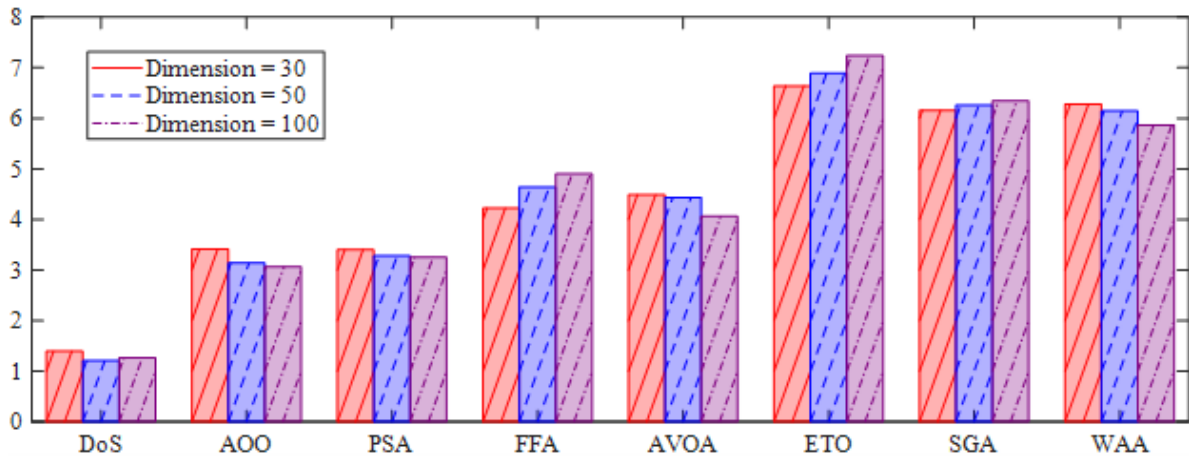


Figure 10: Bar chart of Friedman rankings on CEC2017 benchmark test functions.

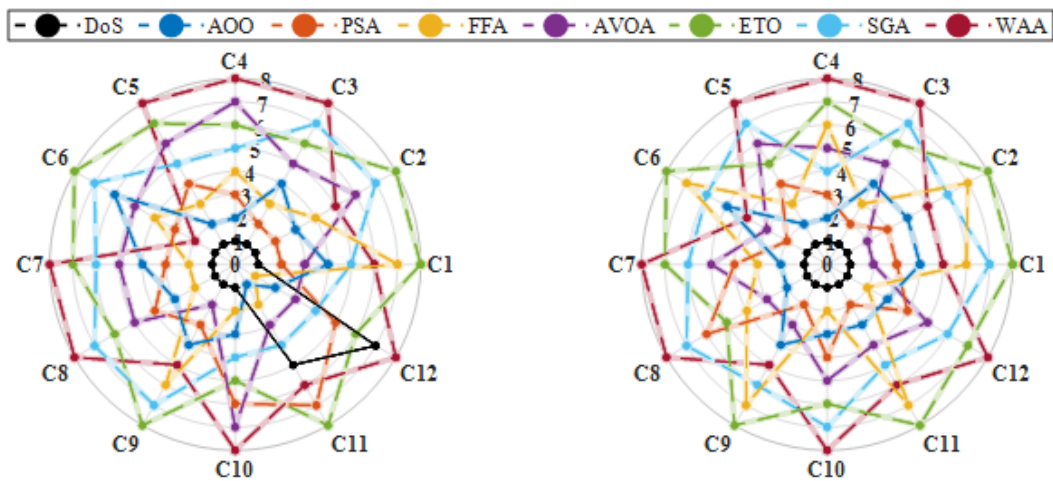


Figure 11: Radar chart of Mean rankings on CEC2022 benchmark test functions.

The analysis includes: historical search trajectories, the variation curves of the centroids of the formations on the first dimension coordinate and the evolutionary trends of the expected function values.

As shown in the search trajectories in Fig. 13, combined with the 3D structural plots of each function, DoS successfully converges to the global optimal solution (indicated by the red hexagram) on all 6 test functions. It forms dense exploitation paths near the best solutions, particularly evident in functions like F10 and C10, where local optima are densely distributed. For functions with relatively easy to locate global optimal solution, such as F1 and C2, DoS exhibits a faster convergence rate. From the variation trends of the centroid on the first dimension, it can be observed that DoS typically locks onto the global optimal solution within the first 1/16 of the total iterations and then rapidly transitions into a deep exploitation phase under the guidance of the dynamic selection mechanism. Even in functions such as F25 and F28, which are intentionally designed with many local optima traps, DoS is able to accurately locate the global

optimal solution through effective early-stage exploration and simultaneously achieve efficient exploitation.

Analysis of the search trajectories for F1, F25 and F28 reveals that the DoS search paths exhibit distinct linear characteristics on these functions. The center-of-mass curve for the first-dimensional coordinate fluctuates significantly during iterations, reflecting how DoS enhances the accuracy of the global optimal solution by dynamically switching between different guide solutions using offensive strategies during multiple approaches to the global optimal solution. Particularly in F28, DoS formed two primary search trajectories, ultimately converging at the intersection point to develop the solution domain for the global optimal solution. This phenomenon demonstrates that under balanced control of exploration and exploitation strategies, DoS can switch between multiple high-potential regions, thereby breaking through local optima constraints.

Furthermore, the jamming avoidance strategy proposed in Section 3.2.5 is especially evident in function C2. Since the global optimal solution of this function lies near the boundary of the feasible region and is connected to the

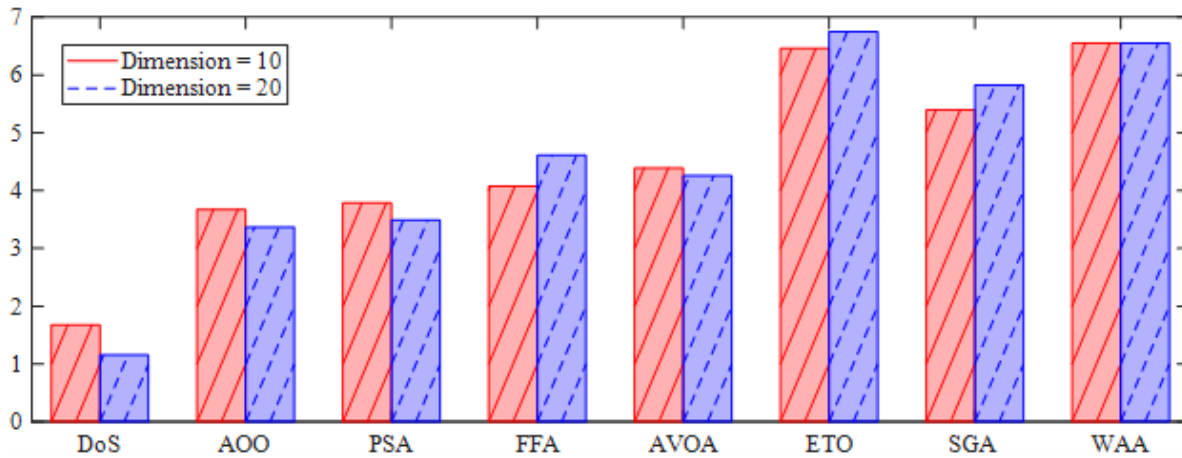


Figure 12: Bar chart of Friedman rankings on CEC2022 benchmark test functions.

upper and lower bound vertices, DoS utilizes the jamming avoidance strategy to effectively search the boundary region. As shown in the figure, DoS adaptively guides the search from the boundary toward the interior and finally converges to the global optimal solution.

In conclusion, the behavioral analysis on CEC2017 and CEC2022 benchmark test functions demonstrates that DoS exhibits strong exploratory and exploitative capabilities. With the exploration and exploitation balance achieved by the dynamic selection mechanism, DoS not only escapes local optima effectively but also locates the global optimal solution in a short time and efficiently exploits the surrounding region, thereby showcasing excellent optimization performance and search efficiency.

4.8. Computational Time Cost Analysis

In the evaluation of metaheuristic algorithms, performance and computational time cost are two critical metrics. Although most SOTA algorithms demonstrate excellent optimization performance, they are often accompanied by high computational overhead due to the increased complexity of their internal structural designs. Therefore, assessing the computational efficiency of DoS is of significant importance for evaluating its practical applicability.

This section evaluates the computational time cost of DoS based on the 30-dimensional CEC2017 benchmark test functions. To ensure fairness, the population size of all algorithms is uniformly set to 50. Four influencing factors are introduced in the experiment:

T_0 : the time required to execute Equation (30) one million times under the initial condition $x = 0.55$;

T_1 : the time consumed to perform 200,000 function evaluations of F18 with a fixed random solution;

T_2 : the total time required to run the complete algorithm for 200,000 evaluations of F18 with a fixed initial solution;

T_2^{mean} : the average value of T_2 obtained from five independent experiments.

$$\begin{aligned} x &= x + x; & x &= \frac{x}{2}; & x &= x \times x; & x &= \sqrt{x}; \\ x &= \ln(x); & x &= e^x; & x &= \frac{x}{x+2} \end{aligned} \quad (29)$$

Table 21 summarizes the computational time costs of DoS and the seven advanced competing algorithms. The metric $(T_2^{mean} - T_1)/T_0$ effects the computational time cost variable of the algorithm, the smaller the value, the lower the computational time cost. It can be observed that the computational cost of DoS is lower than that of AOO, FFA, ETO and WAA, indicating its certain advantage in balancing performance and efficiency. Combined with the structural analysis in Section 3, DoS introduces multiple search strategies and a dynamic selection mechanism, making its overall design slightly more complex compared to PSA (which adopts a single strategy), as well as the structurally simpler AVOA and SGA. As a result, its computational cost is slightly higher than these three algorithms. However, as demonstrated in Sections 4.2 and 4.3, this added complexity brings significant improvements in optimization performance, leading DoS to outperform PSA, AVOA and SGA across benchmark test functions.

In conclusion, DoS maintains high performance while keeping computational time costs within a reasonable range, achieving a sound balance between efficiency and optimization capability and demonstrating strong practical value.

5. Engineering Problems

The original intention behind the design of metaheuristic algorithms is to address the efficiency bottlenecks encountered by traditional methods when solving highly nonlinear, non-differentiable problems with multiple local optima. Compared with traditional optimization methods, metaheuristic algorithms demonstrate stronger adaptability and problem-solving capabilities for such complex problems. However, real-world engineering optimization problems are

Dogfight Search

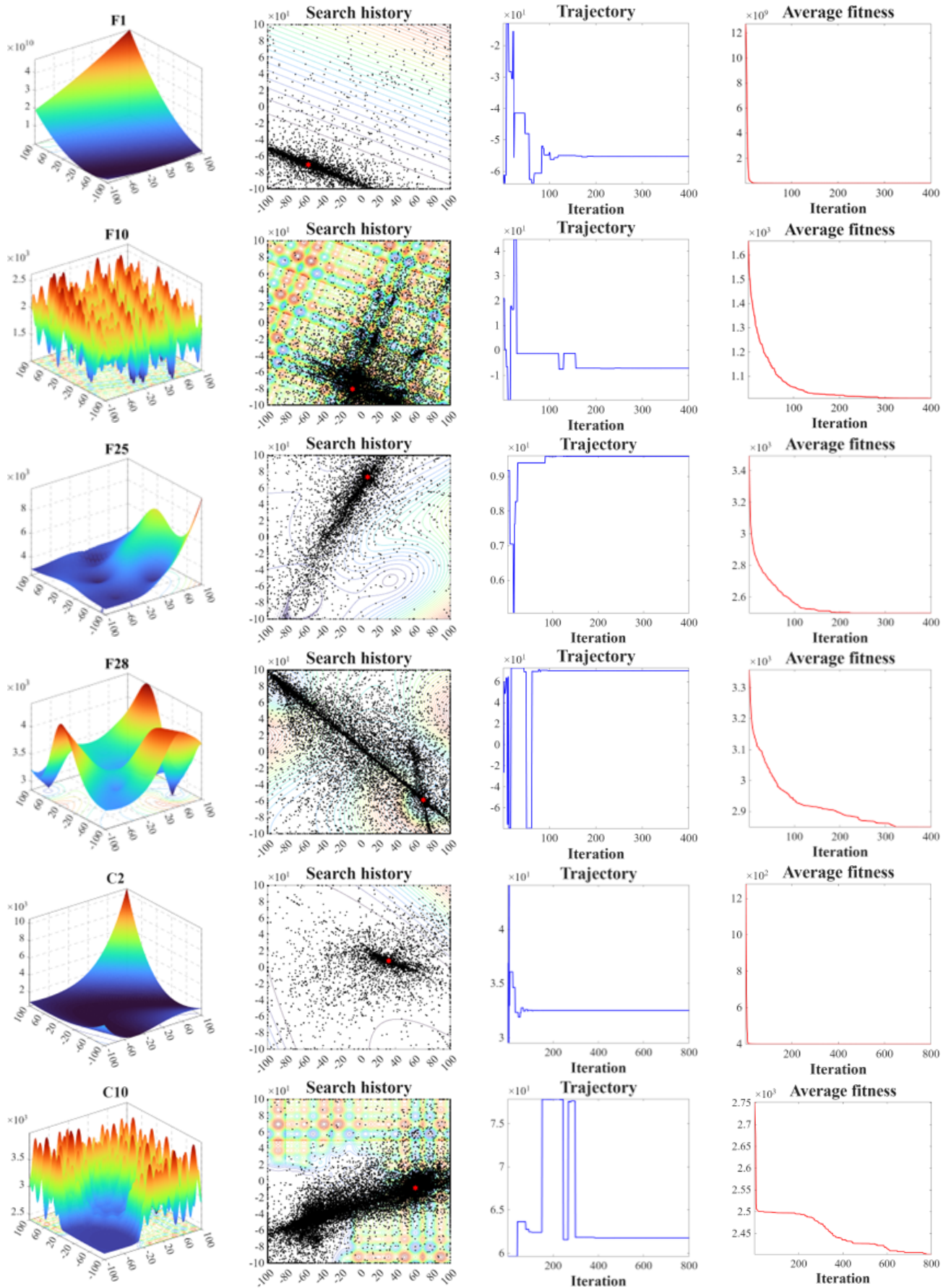


Figure 13: Search History, Trajectory and Average Fitness of DoS on Some CEC2017 Benchmark Test Functions (2D).

Table 21

Results of computational time cost.

	DoS	AOO	PSA	FFA	AVOA	ETO	SGA	WAA
T_0	0.0073590	0.0075530	0.0076597	0.0075053	0.0068882	0.0074479	0.0071382	0.0070808
T_1	0.3870446	0.4021236	0.3944610	0.4043148	0.3995194	0.387512	0.3841997	0.3897004
T_2^{mean}	1.1057091	1.3215604	0.8729215	1.5493374	0.9475669	1.9344475	0.6012483	4.7229055
$(T_2^{mean} - T_1)/T_0$	97.657899	121.73134	62.464655	152.56187	79.563241	207.70089	30.406635	611.96547

Table 22

Basic information of constrained optimization problems.

No.	Type	Name	D	g	h
R1	Industrial Chemical Processes	Optimal operation of alkylation unit	7	14	0
R2	Process Synthesis and Design	Process flow sheeting	3	3	0
R3	Mechanical Engineering	Welded beam design	4	7	0
R4	Mechanical Engineering	Pressure vessel design	4	4	0
R5	Mechanical Engineering	Side impact design of automobiles	11	10	0
R6	Mechanical Engineering	Optimal design of industrial refrigeration system	14	15	0
R7	Mechanical Engineering	Step-cone pulley	5	8	3
R8	Mechanical Engineering	Hydro-static thrust bearing design	4	7	0
R9	Mechanical Engineering	Four-stage gear box	22	86	0
R10	Power System	Wind farm layout	30	91	0

not only influenced by dimensionality (D), but also involve complex inequality constraints (g) and equality constraints (h), further increasing the difficulty of solution and posing challenges to algorithm generalization.

To verify the performance of DoS on constrained optimization problems, this paper selects 10 real-world engineering optimization problems from CEC2020, covering four major categories: Industrial Chemical Processes, Process Synthesis and Design, Mechanical Engineering and Power Systems. Detailed information on the specific problems is provided in Table 22.

For the above 10 problems, this paper adopts the standard experimental settings for CEC2020 engineering problems proposed by Kumar et al. (Kumar et al., 2020) and performs 25 independent runs. To enhance the distinguishability of performance differences among algorithms, This paper halves the standard evaluation count specified in the original text, with the specific setting for the maximum evaluation count shown in Equation 30.

$$E = \begin{cases} 5 \times 10^4, & D \leq 10 \\ 1 \times 10^5, & 10 < D \leq 30 \\ 2 \times 10^5, & 30 < D \leq 50 \\ 4 \times 10^5, & 50 < D \leq 150 \\ 5 \times 10^5, & D > 150 \end{cases} \quad (30)$$

The statistical content of the experimental results includes: the best value (Best), mean value (Mean), standard deviation (Std), feasible solution rate (Success), Wilcoxon rank-sum test results (WSRT) at a 5% significance level, Friedman ranking (FMR) and overall ranking (F-Rank). All results in Tables 23, 24, 25, 26, 27, 28, 29, 30, 31,

32, 33, 34, 35, 36, 37, 38, 39, 40, 41 and 42 represent valid results satisfying the constraints; solutions failing to meet constraints are denoted as NaN. The best values for each indicator are shown in bold.

5.1. Optimal Operation of Alkylation Unit

The Optimal Operation of Alkylation Unit problem aims to maximize the economic benefit or product yield of the alkylation reaction system while satisfying 14 inequality constraints. Its decision variables involve several key process parameters, such as feed flow rate, reaction temperature and reflux ratio of the distillation column, denoted as $\mathbf{x} = (x_1, x_2, \dots, x_7)$. The mathematical model of this problem is formulated as follows:

Minimize:

$$f(\mathbf{x}) = 0.035x_1 \cdot x_6 + 1.715x_1 + 10.0x_2 + 4.0565x_3 - 0.063x_3 \cdot x_5 \quad (31)$$

Subject to:

$$g_1(\mathbf{x}) = 0.0059553571x_6^2 \cdot x_1 + 0.88392857x_3 - 0.1175625x_6 \cdot x_1 - x_1 \leq 0$$

$$g_2(\mathbf{x}) = 1.1088x_1 + 0.1303533x_1 \cdot x_6 - 0.0066033x_1 \cdot x_6^2 - x_3 \leq 0$$

$$g_3(\mathbf{x}) = 6.66173269x_6^2 - 56.596669x_4 + 172.39878x_5 - 191.20592x_6 - 10000 \leq 0$$

$$g_4(\mathbf{x}) = 1.08702x_6 - 0.03762x_6^2 + 0.32175x_4 + 56.85075 - x_5 \leq 0$$

Table 23

The best results for the Optimal operation of alkylation unit.

	DoS	AOO	PSA	FFA	AVOA	ETO	SGA	WAA
x_1	2000	1999.96884	1292.95679	1999.99371	2000	1994.89058	NaN	1195.04863
x_2	0	0	59.1542907	0	0	0	NaN	43.9829715
x_3	2576.38006	2498.27354	2158.35587	3162.21346	2403.38284	3223.05907	NaN	2116.12799
x_4	0	0	85.5187486	0	0	0	NaN	82.1842824
x_5	58.1606111	57.8291168	92.1783142	60.8575728	57.4311232	61.8920633	NaN	91.0010561
x_6	1.25994095	0.92996449	13.4113046	4.33703641	0.5441601	5.18089297	NaN	11.3993706
x_7	41.5998808	40.6421005	143.515131	49.794398	39.4993316	52.4282639	NaN	141.400686
Best	-4529.12	-4527.4937	362.83445	-4437.0876	-4521.5882	-4289.9606	NaN	581.693178

Table 24

Statistical results for the Optimal operation of alkylation unit.

	DoS	AOO	PSA	FFA	AVOA	ETO	SGA	WAA
Mean	-4481.477	-3649.8628	620.373012	-2583.1734	-4200.1079	-4034.2287	NaN	726.378768
Std	238.213415	634.096046	165.068727	2075.36504	373.127814	332.001258	NaN	0
Success	1	1	0.48	0.6	1	0.28	0	0.04
WSRT		8.3E-09(+)	1.0E-09(+)	3.2E-09(+)	2.6E-08(+)	1.2E-08(+)	NaN	9.7E-11(+)
FMR	1.12	3.64	6	4.56	2.64	3.2	NaN	6.84
F-Rank	1	4	6	5	2	3	8	7

$$g_5(\mathbf{x}) = 0.006198x_7 \cdot x_4 \cdot x_3 + 2462.3121x_2 - 25.125634x_2 \cdot x_4 - x_3 \cdot x_4 \leq 0$$

$$g_6(\mathbf{x}) = 161.18996x_3 \cdot x_4 + 5000x_2 \cdot x_4 - 489510x_2 - x_3 \cdot x_4 \cdot x_7 \leq 0$$

$$g_7(\mathbf{x}) = 0.33x_7 + 44.333333 - x_5 \leq 0$$

$$g_8(\mathbf{x}) = 0.22556x_5 - 1 - 0.007595x_7 \leq 0$$

$$g_9(\mathbf{x}) = 0.00061x_3 - 1 - 0.0005x_1 \leq 0$$

$$g_{10}(\mathbf{x}) = 0.819672x_1 - x_3 + 0.819672 \leq 0$$

$$g_{11}(\mathbf{x}) = 24500x_2 - 250x_2 \cdot x_4 - x_3 \cdot x_4 \leq 0$$

$$g_{12}(\mathbf{x}) = 1020.1082x_4 \cdot x_2 + 1.2244898x_3 \cdot x_4 - 100000x_2 \leq 0$$

$$g_{13}(\mathbf{x}) = 6.25x_1 \cdot x_6 + 6.25x_1 - 7.625x_3 - 100000 \leq 0$$

$$g_{14}(\mathbf{x}) = 1.22x_3 - x_6 \cdot x_1 - x_1 + 1 \leq 0$$

With bounds:

$$1000 \leq x_1 \leq 2000, \quad 0 \leq x_2, x_4, x_5 \leq 100,$$

$$2000 \leq x_3 \leq 4000, \quad 0 \leq x_6 \leq 20,$$

$$0 \leq x_7 \leq 200$$

Tables 23 and 24 respectively present the best results and statistical results of DoS and the competing algorithms on this problem. The results indicate that this problem imposes high requirements on constraint handling capabilities, as many algorithms performed poorly in terms of feasibility. SGA failed to obtain any feasible solution in all 25 independent runs, while PSA, FFA, ETO and WAA also exhibited

low success rates, revealing significant limitations in their search strategies for this problem.

In contrast, DoS, AOO and AVOA successfully converged to feasible solutions in all runs, demonstrating stronger adaptability and constraint-handling stability. Among them, DoS not only achieved a 100% success rate but also obtained the best values in both Best and Mean performance metrics, significantly outperforming the second ranked AVOA, clearly indicating its advantages in global search capability and solution efficiency.

Although DoS ranked second in the Std metric, it is worth noting that WAA only obtained one feasible solution, making its stability results less meaningful for reference. Therefore, DoS exhibits not only high optimization performance but also good stability.

In terms of statistical significance, the WSRT results show that DoS holds a significant advantage over all other algorithms. Finally, DoS ranks first in the Friedman ranking, further validating its strong adaptability and comprehensive optimization capability when addressing such complex industrial problems.

5.2. Process Flow Sheeting

Process flow sheeting is a classical optimization problem in process systems engineering, aiming to minimize the operating cost or maximize the product profit of a process system, under the constraints of mass balance, energy balance and operational limits. This problem involves three decision variables, representing the operating conditions of key equipment and the distribution ratio of material flows, denoted as $\mathbf{x} = (x_1, x_2, x_3)$. The specific mathematical formulation is presented in Equation 32.

Table 25

The best results for the Process flow sheeting.

	DoS	AOO	PSA	FFA	AVOA	ETO	SGA	WAA
x_1	0.94193734	0.94193735	0.94193734	0.94193759	0.94193734	0.94212928	0.94193738	0.94201652
x_2	-2.1	-2.1	-2.1	-2.1000003	-2.1	-2.1002767	-2.1000001	-2.1001605
x_3	0.75209273	1.31123275	0.95099277	1.1686118	1.48992977	1.00614078	1.26073299	1.1339543
Best	1.0765431	1.07654309	1.07654308	1.07654415	1.07654308	1.07739151	1.07654326	1.07689302

Table 26

Statistical results for the Process flow sheeting.

	DoS	AOO	PSA	FFA	AVOA	ETO	SGA	WAA
Mean	1.0765431	1.07654364	1.1320493	1.08980276	1.18061723	1.0804378	1.19451316	1.12838518
Std	4.532E-16	1.3065E-06	0.08258201	0.02321725	0.08672846	0.00176624	0.08255323	0.07745561
Success	1	1	1	1	1	0.6	1	1
WSRT		9.7E-11(+)	2.4E-03(+)	9.7E-11(+)	4.9E-11(+)	8.0E-11(+)	3.6E-11(+)	9.1E-11(+)
FMR	1.34	3.2	3.4	5.04	5.44	5.44	6.26	5.88
F-Rank	1	2	3	4	5	6	8	7

Minimize:

$$f(\mathbf{x}) = -0.7x_3 + 0.8 + 5(0.5 - x_1)^2 \quad (32)$$

Subject to:

$$g_1(\mathbf{x}) = -\exp(x_1 - 0.2) - x_2 \leq 0$$

$$g_2(\mathbf{x}) = x_2 + 1.1x_3 + 1 \leq 0$$

$$g_3(\mathbf{x}) = x_1 - x_3 - 0.2 \leq 0$$

With bounds:

$$0.2 \leq x_1 \leq 1, \quad -2.22554 \leq x_2 \leq -1, \quad x_3 \in \{0, 1\}$$

Tables 25 and 26 present the best results and statistical indicators of each algorithm on this problem. The results show that DoS achieves the best performance in terms of Best, Mean and Std, fully demonstrating its excellent convergence capability and stability. Although most algorithms achieve values close to DoS in the Best metric, DoS shows significantly better performance in Mean and Std, with a standard deviation as low as 4.532E-16, revealing strong robustness and consistency.

In terms of statistical significance, the WSRT show that DoS exhibits significant superiority over all competitors. The Friedman ranking further confirms this conclusion, with DoS ranking first on this problem, demonstrating its outstanding adaptability and overall performance in Process Synthesis and Design engineering optimization problems.

5.3. Welded Beam Design

The welded beam design problem seeks to minimize manufacturing cost and structural weight while satisfying strength, geometric, and manufacturability constraints. This problem involves four decision variables, representing the weld seam height, top flange width, beam height and beam length, denoted as: $\mathbf{x} = (x_1, x_2, x_3, x_4)$. The constraints

include seven inequality constraints, covering aspects such as maximum stress, shear stress, deflection and geometric boundaries. The complete mathematical model is provided in Equation 33.

Minimize:

$$f(\mathbf{x}) = 1.1047x_1^2 \cdot x_2 + 0.04811x_3 \cdot x_4(14 + x_2) \quad (33)$$

Subject to:

$$g_1(\mathbf{x}) = \tau(\mathbf{x}) - 13600 \leq 0$$

$$g_2(\mathbf{x}) = \sigma(\mathbf{x}) - 30000 \leq 0$$

$$g_3(\mathbf{x}) = \delta(\mathbf{x}) - 0.25 \leq 0$$

$$g_4(\mathbf{x}) = x_1 - x_4 \leq 0$$

$$g_5(\mathbf{x}) = 6000 - P_c(\mathbf{x}) \leq 0$$

$$g_6(\mathbf{x}) = 0.125 - x_1 \leq 0$$

$$g_7(\mathbf{x}) = 1.1047x_1 + 0.04811x_3 \cdot x_4(14 + x_2) - 5 \leq 0$$

Where:

$$\tau(\mathbf{x}) = \sqrt{(\tau')^2 + (\tau'')^2 + \frac{x_2 \cdot \tau' \cdot \tau''}{\sqrt{0.25 [x_2^2 + (x_1 + x_3)^2]}}}$$

$$\tau' = \frac{6000}{\sqrt{2}x_1 \cdot x_2}$$

$$\tau'' = \frac{6000(14 + 0.5x_2)\sqrt{0.25 [x_2^2 + (x_1 + x_3)^2]}}{2 \times 0.707x_1 \cdot x_2 \left[\frac{x_2^2}{12} + 0.25(x_1 + x_3)^2 \right]}$$

$$\sigma(\mathbf{x}) = \frac{504000}{x_3^2 x_4}$$

$$\delta(\mathbf{x}) = \frac{65856000}{30 \times 10^6 x_4 \cdot x_3^3}$$

Table 27

The best results for the Welded beam design.

	DoS	AOO	PSA	FFA	AVOA	ETO	SGA	WAA
x_1	0.20572964	0.20460826	0.20572964	0.20572963	0.20565992	0.20379636	0.20385754	0.20151701
x_2	3.25312004	3.2733965	3.25312004	3.25312028	3.25436302	3.28201771	3.28630361	3.34964561
x_3	9.03662391	9.03605126	9.0366239	9.03662391	9.03662131	9.07355424	9.0385155	9.08696903
x_4	0.20572964	0.20575609	0.20572964	0.20572964	0.20572976	0.20554814	0.20572023	0.20557583
Best	1.6952472	1.69644556	1.69524717	1.6952472	1.69531381	1.70126017	1.69723581	1.70952413

Table 28

Statistical results for the Welded beam design.

	DoS	AOO	PSA	FFA	AVOA	ETO	SGA	WAA
Mean	1.6952472	1.7033707	1.76975031	1.73309548	1.71426008	1.70811517	1.71747601	1.82058308
Std	2.266E-16	0.01235605	0.1188277	0.04718389	0.01906936	0.00371913	0.024741	0.16032823
Success	1	1	1	0.08	1	1	1	1
WSRT		9.7E-11(+)	9.7E-11(+)	6.7E-12(+)	9.7E-11(+)	9.7E-11(+)	9.7E-11(+)	9.7E-11(+)
FMR	1	3.44	4.72	6.44	4.4	4.32	4.68	7
F-Rank	1	2	6	7	4	3	5	8

$$P_c(\mathbf{x}) = 64746.022 (1 - 0.0282346x_3) x_3 \cdot x_4^3$$

With bounds:

$$0.1 \leq x_1, x_4 \leq 2, \quad 0.1 \leq x_2, x_3 \leq 10$$

Tables 27 and 28 present the comparative experimental results of DoS against several advanced competing algorithms on this problem. DoS achieved the best performance across all key metrics, including Best, Mean, Std and Success, fully demonstrating its superior optimization ability and convergence stability. Although algorithms such as AOO, PSA and FFA performed closely in terms of the Best value, the Mean and Std results show that DoS exhibited higher consistency and robustness over 25 independent runs.

In addition, DoS achieved a 100% success rate, indicating its strong adaptability in handling complex constrained problems. In contrast, although FFA obtained a Best value close to that of DoS, its success rate was only 0.08, suggesting significant shortcomings in its constraint handling strategy. This limits its ability to effectively explore feasible regions in engineering problems.

From the perspective of statistical significance, the Wilcoxon rank-sum test indicates that DoS significantly outperformed all competing algorithms. In the Friedman test, DoS further widened the gap with the second-best AOO by a margin of 2.44, reaffirming its overall performance advantage in this constrained optimization problem.

5.4. Pressure Vessel Design

Pressure vessel design aims to minimize the manufacturing cost of a pressure vessel while satisfying constraints related to structural strength and operational safety. This problem involves four decision variables, representing the inner radius of the cylindrical shell, head thickness, shell thickness and length of the vessel, denoted as: $\mathbf{x} = (x_1, x_2, x_3, x_4)$. The problem includes four inequality constraints. The detailed mathematical formulation is given in Equation 34.

Minimize:

$$f(\mathbf{x}) = 1.7781z_2x_3^2 + 0.6224z_1x_3x_4 + 3.1661z_1^2x_4 + 19.84z_1^2x_3 \quad (34)$$

Subject to:

$$g_1(\mathbf{x}) = 0.00954x_3 - z_2 \leq 0$$

$$g_2(\mathbf{x}) = 0.0193x_3 - z_1 \leq 0$$

$$g_3(\mathbf{x}) = x_4 - 240 \leq 0$$

$$g_4(\mathbf{x}) = -\pi x_3^2 \cdot x_4 - \frac{4}{3}\pi x_3^3 + 1296000 \leq 0$$

Where:

$$z_1 = 0.0625x_1$$

$$z_2 = 0.0625x_2$$

With bounds:

$$x_1, x_2 \in \{1, 2, \dots, 99\}, \quad 10 \leq x_3, x_4 \leq 200$$

Tables 29 and 30 present the experimental results of DoS and competitors on this problem. The statistical results show that DoS achieved the best performance in three key indicators: Best, Mean and Std and reached a 100% success rate across 25 independent runs, demonstrating its excellent optimization performance and convergence stability.

In terms of statistical significance analysis, the Wilcoxon rank-sum test (WSRT) indicates that DoS shows a statistically significant advantage over all competitors. In the Friedman test, DoS ranks first among all algorithms, outperforming the second-best algorithm AOO by 1.2, further validating its overall performance advantage and robustness in this type of engineering optimization problem.

Table 29

The best results for the Pressure vessel design.

	DoS	AOO	PSA	FFA	AVOA	ETO	SGA	WAA
x_1	12.7927137	12.8923688	13.018652	13.4194694	13.0437498	12.7584516	13.3917073	15.7473509
x_2	7.31679176	7.22512106	6.88413741	7.17723922	7.10333375	6.78178608	6.71662934	8.40498716
x_3	42.0984456	42.0982098	42.0984456	42.0721363	42.0984456	42.0512357	42.0984135	51.8132818
x_4	176.636596	176.639524	176.636596	176.963169	176.636596	177.425062	176.636993	84.5827817
Best	6059.7143	6059.74319	6059.71434	6062.92769	6059.71434	6070.20351	6059.71824	6410.20622

Table 30

Statistical results for the Pressure vessel design.

	DoS	AOO	PSA	FFA	AVOA	ETO	SGA	WAA
Mean	6067.5069	6349.98002	6399.20768	6539.31568	6744.7382	6471.54327	6495.56359	6808.79589
Std	14.273598	498.958892	221.108314	264.377381	532.303828	424.078767	385.542707	161.908079
Success	1	1	1	1	1	0.96	1	1
WSRT		1.3E-05(+)	4.5E-09(+)	7.1E-10(+)	9.2E-09(+)	5.7E-09(+)	1.8E-08(+)	5.5E-10(+)
FMR	1.32	3.52	4.16	5.08	5.44	5.16	4.48	6.84
F-Rank	1	2	3	5	7	6	4	8

5.5. Side Impact Design of Automobiles

The Side impact design of automobiles aims to minimize the overall vehicle weight by optimizing the structural parameters of the car body, under the premise of satisfying safety and structural constraints. This problem involves 11 decision variables, each representing the structural thickness of key body components, denoted as: $\mathbf{x} = (x_1, x_2, \dots, x_{11})$. The constraints cover occupant injury indices, structural intrusion and overall vehicle mass, making this a typical constrained single objective optimization problem. The formulation is given in Equation 35.

Minimize:

$$f(\mathbf{x}) = 1.98 + 4.9x_1 + 6.67x_2 + 6.98x_3 + 4.01x_4 + 1.78x_5 + 2.73x_7 \quad (35)$$

Subject to:

$$g_1(\mathbf{x}) = 1.16 - 0.3717x_2 \cdot x_4 - 0.00931x_2 \cdot x_{10} - 0.484x_3 \cdot x_9 + 0.01343x_6 \cdot x_{10} - 1 \leq 0$$

$$g_2(\mathbf{x}) = 46.36 - 9.9x_2 - 12.9x_1 \cdot x_2 + 0.1107x_3 \cdot x_{10} - 32 \leq 0$$

$$g_3(\mathbf{x}) = 33.86 + 2.95x_3 + 0.1792x_3 - 5.057x_1 \cdot x_2 - 11x_2 \cdot x_8 - 0.0215x_5 \cdot x_{10} - 9.98x_7 \cdot x_8 + 22x_8 \cdot x_9 - 32 \leq 0$$

$$g_4(\mathbf{x}) = 28.98 + 3.818x_3 - 4.2x_1 \cdot x_2 + 0.0207x_5 \cdot x_{10} + 6.63x_6 \cdot x_9 - 7.7x_7 \cdot x_8 + 0.32x_9 \cdot x_{10} - 32 \leq 0$$

$$g_5(\mathbf{x}) = 0.261 - 0.0159x_1 \cdot x_2 - 0.188x_1 \cdot x_8 - 0.019x_2 \cdot x_7 + 0.0144x_3 \cdot x_5 + 0.0008757x_5 \cdot x_{10} + 0.08045x_6 \cdot x_9 + 0.00139x_8 \cdot x_{11} + 0.00001575x_{10} \cdot x_{11} - 0.32 \leq 0$$

$$g_6(\mathbf{x}) = 0.214 + 0.00817x_5 - 0.131x_1 \cdot x_8 - 0.0704x_1 \cdot x_9 + 0.03099x_2 \cdot x_6 - 0.018x_2 \cdot x_7 + 0.0208x_3 \cdot x_8 + 0.121x_3 \cdot x_9 - 0.00364x_5 \cdot x_6 + 0.0007715x_5 \cdot x_{10} - 0.0005354x_6 \cdot x_{10} + 0.00121x_8 \cdot x_{11} + 0.00184x_9 \cdot x_{10} - 0.02x_2^2 - 0.32 \leq 0$$

$$g_7(\mathbf{x}) = 0.74 - 0.61x_2 - 0.163x_3 \cdot x_8 + 0.001232x_3 \cdot x_{10} - 0.166x_7 \cdot x_9 + 0.227x_2^2 - 0.32 \leq 0$$

$$g_8(\mathbf{x}) = 4.72 - 0.5x_4 - 0.19x_2 \cdot x_3 - 0.0122x_4 \cdot x_{10} + 0.009325x_6 \cdot x_{10} + 0.000191x_{11}^2 - 4 \leq 0$$

$$g_9(\mathbf{x}) = 10.58 - 0.674x_1 \cdot x_2 - 1.95x_2 \cdot x_8 + 0.02054x_3 \cdot x_{10} - 0.0198x_4 \cdot x_{10} + 0.028x_6 \cdot x_{10} - 9.9 \leq 0$$

$$g_{10}(\mathbf{x}) = 16.45 - 0.489x_3x_7 - 0.843x_5x_6 + 0.0432x_9x_{10} - 0.0556x_9x_{11} - 0.000786x_{11}^2 - 15.7 \leq 0$$

With bounds:

$$0.5 \leq x_1, x_2, x_3, x_4, x_5, x_6, x_7 \leq 1.5,$$

$$x_8, x_9 \in \{0.192, 0.345\}, \quad -30 \leq x_{10}, x_{11} \leq 30$$

Tables 31 and 32 present the best solutions and statistical indicators of each algorithm for the side impact design problem. The results show that all algorithms except FFA successfully converged to feasible solutions in all 25 independent runs, achieving a success rate of 1. In contrast, FFA failed to obtain any feasible solution, indicating that its search strategy lacks adaptability to this problem.

Table 31

The best results for the Side impact design of automobiles.

	DoS	AOO	PSA	FFA	AVOA	ETO	SGA	WAA
x_1	0.5	0.50263548	0.62281348	NaN	0.5	0.5	0.51948093	0.5
x_2	0.97984709	0.97778074	0.88730099	NaN	0.96383745	0.92325516	0.96325679	0.94018371
x_3	0.5	0.50000005	0.5	NaN	0.5	0.5	0.5	0.5
x_4	1.00244987	1.0056303	1.02435596	NaN	1.04103104	1.14925255	1.00876643	1.12618121
x_5	0.5	0.50004965	0.5	NaN	0.50000002	0.5	0.5	0.5
x_6	0.5	0.50854536	0.5	NaN	0.5000684	0.51201813	0.50000657	0.52275068
x_7	0.5	0.50012063	0.5	NaN	0.5	0.5	0.5	0.5
x_8	0.99702629	0.91019198	1	NaN	0.78736634	0.53490886	0.72674984	0.58931079
x_9	5.9061E-15	0.0014404	0.56869178	NaN	0.17163354	0.63277634	0.08640629	0.3080347
x_{10}	30	29.9901901	28.0599228	NaN	25.270859	12.5572851	29.4727881	18.283222
x_{11}	23.0333313	-23.043959	22.4554294	NaN	22.3247219	17.3388072	23.0176274	22.1871779
Best	20.730404	20.7427069	20.8027511	NaN	20.7783303	20.9416146	20.7405328	20.962012

Table 32

Statistical results for the Side impact design of automobiles.

	DoS	AOO	PSA	FFA	AVOA	ETO	SGA	WAA
Mean	20.850749	21.0935379	21.093146	NaN	21.0122346	21.1392367	21.1213781	21.2455305
Std	0.1790251	0.1333431	0.17630027	NaN	0.36347931	0.16308521	0.39526243	0.20830952
Success	1	1	1	0	1	1	1	1
WSRT		4.0E-08(+)	5.3E-06(+)	NaN	4.1E-04(+)	2.2E-07(+)	4.5E-05(+)	4.0E-08(+)
FMR	1.76	3.92	3.72	NaN	3.92	5	3.72	5.96
F-Rank	1	4	2	8	5	6	3	7

In terms of optimization performance, DoS achieved the best results in both Best and Mean indicators, demonstrating excellent optimization capability. Although DoS ranked slightly lower than AOO in the Std indicator, indicating slightly lower stability, the significant advantage in Mean shows that DoS is more consistently able to approach the global optimal solution across most runs. In contrast, AOO, although occasionally producing better results in individual runs, is more prone to getting trapped in local optima, reflecting weaker global search capability.

The Wilcoxon rank-sum test further confirms that DoS shows statistically significant performance advantages over all competitors. In the Friedman test, DoS consistently ranks first, fully demonstrating its superior performance, robustness and practical value in this complex constrained optimization problem.

5.6. Optimal Design of Industrial Refrigeration System

Optimal design of industrial refrigeration system aims to minimize the total energy consumption and investment cost of the equipment while ensuring thermodynamic performance, energy efficiency ratio and system stability. This problem involves 14 decision variables, covering key design parameters such as compressor power, evaporation temperature and condensation pressure, denoted as: $\mathbf{x} = (x_1, x_2, \dots, x_{14})$. The objective function and 15 inequality constraints form the complete mathematical model, as shown in Equation 36.

Minimize:

$$\begin{aligned}
 f(\mathbf{x}) = & 63098.88x_2 \cdot x_4 \cdot x_{12} + 5441.5x_2^2 \cdot x_{12} + \\
 & 115055.5x_2^{1.664} \cdot x_6 + 6172.27x_2^2 \cdot x_6 + \\
 & 63098.88x_1 \cdot x_3 \cdot x_{11} + 5441.5x_1^2 \cdot x_{11} + \\
 & 115055.5x_1^{1.664} \cdot x_5 + 6172.27x_1^2 \cdot x_5 + \\
 & 140.53x_1 \cdot x_{11} + 281.29x_3 \cdot x_{11} + \\
 & 70.26x_1^2 + 281.29x_1 \cdot x_3 + 281.29x_3^2 + \\
 & 14437x_8^{1.8812} \cdot x_{12}^{0.3424} \cdot x_{10}^{-1} \cdot x_1^2 \cdot x_7 \cdot x_9^{-1} + \\
 & 20470.2x_7^{2.893} \cdot x_{11}^{0.316} \cdot x_1^2
 \end{aligned} \quad (36)$$

Subject to:

$$\begin{aligned}
 g_1(\mathbf{x}) &= 1.524x_7^{-1} \leq 1 \\
 g_2(\mathbf{x}) &= 1.524x_8^{-1} \leq 1 \\
 g_3(\mathbf{x}) &= 0.07789x_1 - 2x_7^{-1} \cdot x_9 - 1 \leq 0 \\
 g_4(\mathbf{x}) &= 7.05305x_9^{-1} \cdot x_1^2 \cdot x_{10} \cdot x_8^{-1} \cdot x_2^{-1} \cdot x_{14}^{-1} - \\
 & 1 \leq 0 \\
 g_5(\mathbf{x}) &= 0.0833x_{13}^{-1} \cdot x_{14} - 1 \leq 0 \\
 g_6(\mathbf{x}) &= 47.136x_2^{0.333} \cdot x_{10}^{-1} \cdot x_{12} - 1.333x_8 \cdot x_{13}^{2.1195} + \\
 & 62.08x_{13}^{2.1195} \cdot x_{12}^{-1} \cdot x_8^{0.2} \cdot x_{10}^{-1} - 1 \leq 0 \\
 g_7(\mathbf{x}) &= 0.04771x_{10} \cdot x_8^{1.8812} \cdot x_{12}^{0.3424} - 1 \leq 0
 \end{aligned}$$

Table 33

The best results for the Optimal design of industrial refrigeration system.

	DoS	AOO	PSA	FFA	AVOA	ETO	SGA	WAA
x_1	0.001	0.001	0.001	0.001	0.001	0.00100193	0.001	0.001
x_2	0.001	0.00100134	0.001	0.001	0.001	0.0012729	0.001	0.001
x_3	0.001	0.00100008	0.001	0.001	0.001	0.00130519	0.001	0.0010957
x_4	0.001	0.01079786	0.001	0.001	0.00100005	0.00153374	0.001571	0.01001128
x_5	0.001	0.00100067	0.001	0.001	0.0010001	0.001	0.001	0.00659281
x_6	0.001	0.00100002	0.001	0.001	0.001	0.001	0.00105786	0.00191787
x_7	1.524	1.52435993	1.524	1.5240264	1.524	1.56881568	1.52403173	1.65669373
x_8	1.524	1.53740159	1.524	1.52400052	1.524	1.55532936	1.52404964	1.5253391
x_9	5	4.98194606	5	4.99999918	4.99999988	4.92988068	4.99998572	2.91251926
x_{10}	2	2.03389883	2.00059666	2.00604538	2.00000143	2.09761448	2.12228525	3.77780929
x_{11}	0.001	0.00100011	0.00100028	0.00100441	0.00100012	0.00161822	0.00100005	0.17997694
x_{12}	0.001	0.001	0.00100028	0.0010044	0.001	0.0015924	0.001	0.08448447
x_{13}	0.0072934	0.00731364	0.00729538	0.00731893	0.00729342	0.00897963	0.0075009	0.03468082
x_{14}	0.08755583	0.08772952	0.08757953	0.08786226	0.08755602	0.10752741	0.0900468	0.39091399
Best	0.032213	0.03358755	0.03221638	0.03224857	0.03221349	0.03770509	0.03298267	0.28539794

Table 34

Statistical results for the Optimal design of industrial refrigeration system.

	DoS	AOO	PSA	FFA	AVOA	ETO	SGA	WAA
Mean	0.032213	0.04270679	0.0651192	0.11484867	0.0403492	0.05902045	0.05023075	1.34361959
Std	1.018E-07	0.01463627	0.02767783	0.05306657	0.01459214	0.02002695	0.01265639	1.2266915
Success	0.64	1	0.72	1	0.68	0.88	1	0.84
WSRT		1.3E-09(+)	1.3E-09(+)	1.3E-09(+)	1.2E-09(+)	1.3E-09(+)	1.3E-09(+)	1.2E-09(+)
FMR	1	3.12	5.2	6.52	3.08	4.92	4.16	8
F-Rank	1	3	6	7	2	5	4	8

$$g_8(\mathbf{x}) = 0.0488x_9 \cdot x_7^{1.893} \cdot x_{11}^{0.316} - 1 \leq 0$$

$$g_9(\mathbf{x}) = 0.0099x_1 \cdot x_3^{-1} - 1 \leq 0$$

$$g_{10}(\mathbf{x}) = 0.0193x_2 \cdot x_4^{-1} - 1 \leq 0$$

$$g_{11}(\mathbf{x}) = 0.0298x_1 \cdot x_5^{-1} - 1 \leq 0$$

$$g_{12}(\mathbf{x}) = 0.056x_2 \cdot x_6^{-1} - 1 \leq 0$$

$$g_{13}(\mathbf{x}) = 2x_9^{-1} - 1 \leq 0$$

$$g_{14}(\mathbf{x}) = 2x_{10}^{-1} - 1 \leq 0$$

$$g_{15}(\mathbf{x}) = x_{12} \cdot x_{11}^{-1} - 1 \leq 0$$

With bounds:

$$0.001 \leq x_i \leq 5, \quad i = 1, 2, \dots, 14$$

Tables 33 and 34 summarize the experimental results of DoS and the competing algorithms on this problem. The results show that DoS achieved the best performance across all three key metrics Best, Mean and Std demonstrating excellent optimization accuracy and convergence stability. Specifically, the Mean value obtained by DoS is significantly better than that of AOO and AVOA and the Std is as low as 1.018E-07, indicating extremely low variance and highly stable convergence on feasible solutions.

Although DoS has a slightly lower success rate than some competitors on this problem, in successful experiments, DoS has higher optimization accuracy than its competitors in other metrics, indicating that DoS still has good applicability to this problem.

From a statistical significance perspective, the Wilcoxon rank-sum test indicates that DoS outperforms all competitors significantly. The Friedman test further confirms that DoS ranks first overall, with a margin of 2.08 over the second ranked AVOA, validating its global search capability and overall optimization effectiveness in solving this complex engineering problem.

In summary, despite a slightly lower feasible solution rate, DoS exhibits outstanding performance in terms of optimization precision, stability and statistical superiority, clearly demonstrating its adaptability and engineering applicability in high-dimensional, constrained engineering optimization problems.

5.7. Step-Cone Pulley

Step-cone pulley is a typical mechanical structural optimization problem, aiming to minimize the total volume or weight of the pulley while satisfying multiple constraints such as transmission ratio, profile dimensions and material strength. This problem involves five continuous decision variables, denoted as $\mathbf{x} = (d_1, d_2, d_3, d_4, \omega)$ and includes 8 inequality constraints and three equality constraints, which

significantly increase the problem's complexity and pose higher demands on the algorithm's constraint handling capability and convergence precision. The complete mathematical formulation is provided in Equation 37.

Considering that equality constraints typically impose stricter requirements on both convergence speed and solution accuracy, the evaluation budget specified in the original Equation 30 is insufficient to ensure effective optimization. Therefore, a uniform evaluation budget of 100,000 is used in this experiment.

Minimize:

$$f(\mathbf{x}) = \rho \cdot \omega \left\{ d_1^2 \left[11 + \left(\frac{N_1}{N} \right)^2 \right] + d_2^2 \left[1 + \left(\frac{N_2}{N} \right)^2 \right] + d_3^2 \left[1 + \left(\frac{N_3}{N} \right)^2 \right] + d_4^2 \left[1 + \left(\frac{N_4}{N} \right)^2 \right] \right\} \quad (37)$$

Subject to:

$$h_1(\mathbf{x}) = C_1 - C_2 = 0$$

$$h_2(\mathbf{x}) = C_1 - C_3 = 0$$

$$h_3(\mathbf{x}) = C_1 - C_4 = 0$$

$$g_i(\mathbf{x}) = -R_i - 2 \leq 0, \quad i = 1, 2, 3, 4$$

$$g_i(\mathbf{x}) = 0.75 \times 745.6998 - P_i \leq 0, \quad i = 5, 6, 7, 8$$

Where:

$$C_i = \frac{\pi \cdot d_i}{2} \left(1 + \frac{N_i}{N} \right) + \frac{[(N_i/N) - 1]^2}{4a} + 2a, \quad i = 1, 2, 3, 4$$

$$R_i = \exp \left\{ -2\mu \cdot \sin^{-1} \left[\left(\frac{N_i}{N} - 1 \right) \frac{d_i}{2a} \right] + \pi \cdot \mu \right\}, \quad i = 1, 2, 3, 4$$

$$P_i = s \cdot t \cdot \omega(1 - R_i) \frac{\pi \cdot d_i \cdot N_i}{60}, \quad i = 1, 2, 3, 4$$

$$t = 8 \text{ mm}, \quad s = 1.75 \text{ MPa}, \quad \mu = 0.35$$

$$\rho = 7200 \text{ kg/m}^3, \quad a = 3 \text{ mm}$$

With bounds:

$$0 \leq d_1, d_2 \leq 60, \quad 0 \leq d_3, d_4, \omega \leq 90$$

Tables 35 and 36 present the optimization results of DoS and other competing algorithms on this problem. The results show that AOO, ETO, SGA and WAA failed to find any feasible solution across all 25 independent runs, indicating their inadequate adaptability in handling equality constrained problems. The success rates of FFA and AVOA

were 0.52 and 0.84, respectively, also reflecting partial failure in achieving constraint satisfaction.

Only DoS and PSA successfully converged to feasible solutions in all 25 runs, demonstrating robust performance. However, in terms of the three key metrics Best, Mean and Std DoS outperformed PSA across the board. Specifically, DoS achieved the best Best value, a lower Mean and an almost zero Std, indicating not only high stability across multiple runs, but also greater search accuracy. Although both algorithms converged to a similar solution domain, DoS yielded higher-quality feasible solutions, showcasing superior practical value.

In the Wilcoxon rank-sum test, the WSRT indicate that DoS exhibited statistically significant performance advantages over all other algorithms. Additionally, the Friedman ranking places DoS at the top position, outperforming the second-best algorithm FFA by a margin of 1.36, further validating its superior performance and stability in tackling complex equality-constrained optimization problems.

5.8. Hydro-Static Thrust Bearing Design

Hydro-static Thrust Bearing Design is a classic problem in mechanical design optimization. The objective is to minimize the oil supply flow or total energy consumption of the bearing, while satisfying constraints related to operational performance, structural dimensions and energy consumption. This problem involves 4 continuous decision variables, which respectively represent the diameter of the supply orifice, the throttling parameter, the working oil film thickness and the bearing surface area, denoted as $\mathbf{x} = (x_1, x_2, x_3, x_4)$. The full model is shown in Equation 38.

Minimize:

$$f(\mathbf{x}) = \frac{x_4 \cdot P_0}{0.7} + E_f \quad (38)$$

Subject to:

$$g_1(\mathbf{x}) = 1000 - P_0 \leq 0$$

$$g_2(\mathbf{x}) = W - 101000 \leq 0$$

$$g_3(\mathbf{x}) = 5000 - \frac{W}{\pi(x_1^2 - x_2^2)} \leq 0$$

$$g_4(\mathbf{x}) = 50 - P_0 \leq 0$$

$$g_5(\mathbf{x}) = 0.001 - \frac{0.0307}{386.4P_0} \left(\frac{x_4}{2\pi \cdot x_1 \cdot h} \right) \leq 0$$

$$g_6(\mathbf{x}) = x_1 - x_2 \leq 0$$

$$g_7(\mathbf{x}) = h - 0.001 \leq 0$$

Where:

$$W = \frac{\pi \cdot P_0}{2} \cdot \frac{x_1^2 - x_2^2}{\ln \left(\frac{x_1}{x_2} \right)}$$

$$P_0 = \frac{6x_3 \cdot x_4}{\pi \cdot h^3} \cdot \ln \left(\frac{x_1}{x_2} \right)$$

Table 35

The best results for the Step-cone pulley.

	DoS	AOO	PSA	FFA	AVOA	ETO	SGA	WAA
d_1	38.4139618	NaN	38.4415703	38.4160269	39.6685254	NaN	NaN	NaN
d_2	52.8586378	NaN	52.8966562	52.8614815	54.5862806	NaN	NaN	NaN
d_3	70.4726957	NaN	70.523379	70.4764868	72.775855	NaN	NaN	NaN
d_4	84.4957161	NaN	84.5564332	84.5002576	87.2547612	NaN	NaN	NaN
ω	90	NaN	89.9351938	89.9951493	87.2375442	NaN	NaN	NaN
Best	16.090273	NaN	16.1018141	16.0911367	16.6320727	NaN	NaN	NaN

Table 36

Statistical results for the Step-cone pulley.

	DoS	AOO	PSA	FFA	AVOA	ETO	SGA	WAA
Mean	16.090273	NaN	16.6411059	16.4156844	17.2273553	NaN	NaN	NaN
Std	6.405E-15	NaN	0.35976121	0.3277681	0.47618814	NaN	NaN	NaN
Success	1	0	1	0.52	0.84	0	0	0
WSRT		NaN	4.7E-10(+)	3.5E-10(+)	4.7E-10(+)	NaN	NaN	NaN
FMR	1	NaN	2.84	2.36	3.8	NaN	NaN	NaN
F-Rank	1	5	3	2	4	6	7	8

$$E_f = 9336x_4 \times 0.0307 \times 0.5\Delta T$$

$$\Delta T = 2(10^P - 559.7)$$

$$P = \frac{\lg[\lg(8.122 \times 10^6 x_3 + 0.8)] + 3.55}{10.04}$$

$$h = \left(\frac{2\pi \times 750}{60}\right)^2 \cdot \frac{2\pi \cdot x_3}{E_f} \cdot \left(\frac{x_1^4}{4} - \frac{x_2^4}{4}\right)$$

With bounds:

$$1 \leq x_1, x_2, x_4 \leq 16, \quad 10^{-6} \leq x_3 \leq 1.6 \times 10^7$$

Tables 37 and 38 summarize the experimental results of DoS and the competing algorithms on this problem. As shown, DoS outperforms all competitors across all performance indicators, demonstrating exceptional optimization capability and robustness. In terms of Best, DoS achieved the best solution of 1616.1204 for the entire game, with a significant gap of 203 in objective value compared to the second-best result by ETO. Regarding the Mean indicator, DoS also leads all competitors with an absolute advantage of 506. As for the Std, DoS achieves a remarkably low standard deviation of 57.051917, much lower than that of other competitors, indicating not only its ability to locate superior solution regions but also its stable convergence performance across multiple independent runs.

Moreover, DoS achieves a Success rate of 1, meaning that all 25 independent experiments successfully converged to feasible solutions, further verifying its strong adaptability to the complex constraints of this problem. Although algorithms such as AOO, PSA, FFA and AVOA show a certain level of feasibility, their Mean values are generally higher and Std values fluctuate significantly, suggesting that these algorithms are still inferior to DoS in terms of stability and convergence quality.

Wilcoxon rank-sum test results show that DoS's optimization performance on this problem is significantly better than its competitors. In the Friedman test, DoS once again ranks first and leads the second place algorithm ETO by a margin of 2.36, further demonstrating its stability and practical advantage in this type of mechanical design constrained optimization problem.

5.9. Four-Stage Gear Box

Four-stage gear box is a high-dimensional mechanical system optimization problem. The objective is to minimize the overall weight or cost of the gearbox under constraints such as transmission ratio, material strength and spatial dimensions. This problem involves 22 decision variables, covering parameters such as the radius and module of each gear stage. It is a typical high-dimensional constrained optimization problem and its mathematical model is detailed in Equation 39.

Minimize:

$$f(\mathbf{x}) = \frac{\pi}{1000} \left[\sum_{i=1}^4 \frac{b_i \cdot c_i^2 (N_{pi}^2 + N_{gi}^2)}{(N_{pi} + N_{gi})^2} \right] \quad (39)$$

Subject to:

$$g_1(\mathbf{x}) = \frac{366000}{\pi \cdot \omega_1} \left[\frac{(N_{p1} + N_{g1})^2}{4b_1 \cdot c_1^2 \cdot N_{p1}} \right] + \frac{2c_1 \cdot N_{p1}}{N_{p1} + N_{g1}} \left[\frac{(N_{p1} + N_{g1})^2}{4b_1 \cdot c_1^2 \cdot N_{p1}} \right] - \frac{\sigma_N \cdot J_R}{0.0167W \cdot K_o \cdot K_m} \leq 0$$

Table 37

The best results for the Hydro-static thrust bearing design.

	DoS	AOO	PSA	FFA	AVOA	ETO	SGA	WAA
x_1	5.95551185	5.98000801	6.4667959	6.26446032	6.0918833	6.16587283	7.20625039	6.37381799
x_2	5.38871638	5.41558346	5.94891526	5.70944689	5.53900748	5.55478777	5.68618996	5.76494585
x_3	5.3587E-06	6.4328E-06	8.2294E-06	5.9139E-06	6.6888E-06	5.5526E-06	7.5162E-06	7.9497E-06
x_4	2.25664104	3.26750791	7.65466293	3.01829092	3.68679675	2.69046358	10.3889963	7.00843564
Best	1616.1204	1744.98267	2193.90348	1836.03564	1813.66823	1819.17843	3761.60047	2283.20929

Table 38

Statistical results for the Hydro-static thrust bearing design.

	DoS	AOO	PSA	FFA	AVOA	ETO	SGA	WAA
Mean	1650.2441	2284.54068	2728.81527	2206.51479	2170.76997	2156.02939	5601.09312	5118.3029
Std	57.051917	369.796558	478.199976	290.012353	276.19162	314.054991	2556.66797	2376.17662
Success	1	0.96	1	1	0.96	1	0.2	0.44
WSRT		7.4E-09(+)	1.4E-09(+)	1.6E-09(+)	2.3E-09(+)	2.3E-09(+)	3.9E-10(+)	9.3E-10(+)
FMR	1	4.12	5.36	3.72	3.52	3.36	7.72	7.2
F-Rank	1	5	6	4	3	2	8	7

$$g_2(\mathbf{x}) = \frac{366000N_{g1}}{\pi \cdot \omega_1 \cdot N_{p1}} \left[\frac{(N_{p2} + N_{g2})^2}{4b_2 \cdot c_2^2 \cdot N_{p2}} \right] +$$

$$\frac{2c_2 \cdot N_{p2}}{N_{p2} + N_{g2}} \left[\frac{(N_{p2} + N_{g2})^2}{4b_2 \cdot c_2^2 \cdot N_{p2}} \right] -$$

$$\frac{\sigma_N \cdot J_R}{0.0167W \cdot K_o \cdot K_m} \leq 0$$

$$g_3(\mathbf{x}) = \frac{366000N_{g1} \cdot N_{g2}}{\pi \cdot \omega_1 \cdot N_{p1} \cdot N_{p2}} \left[\frac{(N_{p3} + N_{g3})^2}{4b_3 \cdot c_3^2 \cdot N_{p3}} \right] +$$

$$\frac{2c_3 \cdot N_{p3}}{N_{p3} + N_{g3}} \left[\frac{(N_{p3} + N_{g3})^2}{4b_3 \cdot c_3^2 \cdot N_{p3}} \right] -$$

$$\frac{\sigma_N \cdot J_R}{0.0167W \cdot K_o \cdot K_m} \leq 0$$

$$g_4(\mathbf{x}) = \frac{366000N_{g1} \cdot N_{g2} \cdot N_{g3}}{\pi \cdot \omega_1 \cdot N_{p1} \cdot N_{p2} \cdot N_{p3}} \left[\frac{(N_{p4} + N_{g4})^2}{4b_4 \cdot c_4^2 \cdot N_{p4}} \right] +$$

$$\frac{2c_4 \cdot N_{p4}}{N_{p4} + N_{g4}} \left[\frac{(N_{p4} + N_{g4})^2}{4b_4 \cdot c_4^2 \cdot N_{p4}} \right] -$$

$$\frac{\sigma_N \cdot J_R}{0.0167W \cdot K_o \cdot K_m} \leq 0$$

$$g_5(\mathbf{x}) = \frac{366000}{\pi \cdot \omega_1} \left[\frac{(N_{p1} + N_{g1})^3}{4b_1 \cdot c_1^2 \cdot N_{g1} \cdot N_{p1}^2} \right] +$$

$$\frac{2c_1 \cdot N_{p1}}{N_{p1} + N_{g1}} \left[\frac{(N_{p1} + N_{g1})^3}{4b_1 \cdot c_1^2 \cdot N_{g1} \cdot N_{p1}^2} \right] -$$

$$\left(\frac{\sigma_H}{C_p} \right)^2 \left[\frac{\sin(\phi) \cdot \cos(\phi)}{0.0334W \cdot K_o \cdot K_m} \right] \leq 0$$

$$g_6(\mathbf{x}) = \frac{366000N_{g1}}{\pi \cdot \omega_1 \cdot N_{p1}} \left[\frac{(N_{p2} + N_{g2})^3}{4b_2 \cdot c_2^2 \cdot N_{g2} \cdot N_{p2}^2} \right] +$$

$$\frac{2c_2 \cdot N_{p2}}{N_{p2} + N_{g2}} \left[\frac{(N_{p2} + N_{g2})^3}{4b_2 \cdot c_2^2 \cdot N_{g2} \cdot N_{p2}^2} \right] -$$

$$\left(\frac{\sigma_H}{C_p} \right)^2 \left[\frac{\sin(\phi) \cdot \cos(\phi)}{0.0334W \cdot K_o \cdot K_m} \right] \leq 0$$

$$g_7(\mathbf{x}) = \frac{366000N_{g1} \cdot N_{g2}}{\pi \cdot \omega_1 \cdot N_{p1} \cdot N_{p2}} \left[\frac{(N_{p3} + N_{g3})^3}{4b_3 \cdot c_3^2 \cdot N_{g3} \cdot N_{p3}^2} \right] +$$

$$\frac{2c_3 \cdot N_{p3}}{N_{p3} + N_{g3}} \left[\frac{(N_{p3} + N_{g3})^3}{4b_3 \cdot c_3^2 \cdot N_{g3} \cdot N_{p3}^2} \right] -$$

$$\left(\frac{\sigma_H}{C_p} \right)^2 \left[\frac{\sin(\phi) \cdot \cos(\phi)}{0.0334W \cdot K_o \cdot K_m} \right] \leq 0$$

$$g_8(\mathbf{x}) = \left(\frac{366000N_{g1} \cdot N_{g2} \cdot N_{g3}}{\pi \cdot \omega_1 \cdot N_{p1} \cdot N_{p2} \cdot N_{p3}} + \frac{2c_4 \cdot N_{p4}}{N_{p4} + N_{g4}} \right) \cdot \left[\frac{(N_{p4} + N_{g4})^3}{4b_4 \cdot c_4^2 \cdot N_{g4} \cdot N_{p4}^2} \right] - \left(\frac{\sigma_H}{C_p} \right)^2 \left[\frac{\sin(\phi) \cdot \cos(\phi)}{0.0334W \cdot K_o \cdot K_m} \right] \leq 0$$

$$g_{9-12}(\mathbf{x}) = N_{gi} \sqrt{\frac{\sin^2(\phi)}{4} + \frac{1}{N_{gi}} \cdot \left(\frac{1}{N_{gi}} \right)^2} - N_{pi} \sqrt{\frac{\sin^2(\phi)}{4} - \frac{1}{N_{pi}} + \left(\frac{1}{N_{pi}} \right)^2} + \frac{(N_{pi} + N_{gi}) \sin(\phi)}{2} + CR_{min} \cdot \pi \cdot \cos(\phi) \leq 0, \quad i = 1, 2, 3, 4$$

$$g_{13-16}(\mathbf{x}) = d_{min} - \frac{2c_i \cdot N_{pi}}{N_{pi} + N_{gi}} \leq 0, \quad i = 1, 2, 3, 4$$

$$g_{17-20}(\mathbf{x}) = d_{min} - \frac{2c_i \cdot N_{gi}}{N_{pi} + N_{gi}} \leq 0, \quad i = 1, 2, 3, 4$$

$$g_{21}(\mathbf{x}) = x_{p1} + \frac{(N_{p1} + 2)c_1}{N_{p1} + N_{g1}} - L_{max} \leq 0$$

$$g_{22-24}(\mathbf{x}) = \frac{(N_{pi} + 2)c_i}{N_{gi} + N_{pi}} - L_{max} + x_{g(i-1)} \leq 0, \quad i = 2, 3, 4$$

$$g_{25}(\mathbf{x}) = \frac{(N_{p1} + 2)c_1}{N_{p1} + N_{g1}} - x_{p1} \leq 0$$

$$g_{26-28}(\mathbf{x}) = \frac{(N_{pi} + 2)c_i}{N_{pi} + N_{gi}} - x_{g(i-1)} \leq 0, \quad i = 2, 3, 4$$

$$g_{29}(\mathbf{x}) = y_{p1} + \frac{(N_{p1} + 2)c_1}{N_{p1} + N_{g1}} - L_{max} \leq 0$$

$$g_{30-32}(\mathbf{x}) = \frac{(2 + N_{pi})c_i}{N_{pi} + N_{gi}} - L_{max} + y_{g(i-1)} \leq 0, \quad i = 2, 3, 4$$

$$g_{33}(\mathbf{x}) = \frac{(2 + N_{p1})c_1}{N_{p1} + N_{g1}} - y_{p1} \leq 0$$

$$g_{34-36}(\mathbf{x}) = \frac{(2 + N_{pi})c_i}{N_{pi} + N_{gi}} - y_{g(i-1)} \leq 0, \quad i = 2, 3, 4$$

$$g_{37-40}(\mathbf{x}) = \frac{(2 + N_{gi})c_i}{N_{pi} + N_{gi}} - L_{max} + x_{gi} \leq 0, \quad i = 1, 2, 3, 4$$

$$g_{41-44}(\mathbf{x}) = \frac{(N_{gi} + 2)c_i}{N_{pi} + N_{gi}} - x_{gi} \leq 0, \quad i = 1, 2, 3, 4$$

$$g_{45-48}(\mathbf{x}) = \frac{(N_{gi} + 2)c_i}{N_{pi} + N_{gi}} - L_{max} + y_{gi} \leq 0, \quad i = 1, 2, 3, 4$$

$$g_{49-52}(\mathbf{x}) = \frac{(N_{gi} + 2)c_i}{N_{pi} + N_{gi}} - y_{gi} \leq 0, \quad i = 1, 2, 3, 4$$

$$g_{53-56}(\mathbf{x}) = (N_{pi} + N_{gi})(b_i - 8.255) \cdot (b_i - 5.715)(b_i - 12.7) - 0.945c_i \cdot (b_i - 8.255)(b_i - 5.715) \cdot (b_i - 12.7) \leq 0, \quad i = 1, 2, 3, 4$$

$$g_{57-60}(\mathbf{x}) = (-N_{pi} - N_{gi})(b_i - 8.255) \cdot (b_i - 3.175)(b_i - 12.7) + 0.646c_i \cdot (b_i - 8.255)(b_i - 3.175) \cdot (b_i - 12.7) \leq 0, \quad i = 1, 2, 3, 4$$

$$g_{61-64}(\mathbf{x}) = (-N_{pi} - N_{gi})(b_i - 5.715) \cdot (b_i - 3.175)(b_i - 12.7) + 0.504c_i \cdot (b_i - 5.715)(b_i - 3.175) \cdot (b_i - 12.7) \leq 0, \quad i = 1, 2, 3, 4$$

$$g_{65-68}(\mathbf{x}) = (-N_{gi} - N_{pi})(b_i - 5.715) \cdot (b_i - 3.175)(b_i - 8.255) \leq 0, \quad i = 1, 2, 3, 4$$

$$g_{69-72}(\mathbf{x}) = (-N_{gi} - N_{pi})(b_i - 8.255) \cdot (b_i - 5.715)(b_i - 12.7) + 1.812c_i \cdot (b_i - 8.255)(b_i - 5.715) \cdot (b_i - 12.7) \leq 0, \quad i = 1, 2, 3, 4$$

$$g_{73-76}(\mathbf{x}) = (N_{pi} + N_{gi})(b_i - 8.255) \cdot (b_i - 3.175)(b_i - 12.7) - 0.945c_i \cdot (b_i - 8.255)(b_i - 3.175) \cdot (b_i - 12.7) \leq 0, \quad i = 1, 2, 3, 4$$

$$g_{77-80}(\mathbf{x}) = (-N_{pi} - N_{gi})(b_i - 5.715) \cdot (b_i - 3.175)(b_i - 12.7) + 0.646c_i \cdot (b_i - 5.715)(b_i - 3.175) \cdot (b_i - 12.7) \leq 0, \quad i = 1, 2, 3, 4$$

$$g_{81-84}(\mathbf{x}) = (N_{pi} + N_{gi})(b_i - 5.715) \cdot (b_i - 3.175)(b_i - 8.255) - 0.504c_i \cdot (b_i - 5.715)(b_i - 3.175) \cdot (b_i - 8.255) \leq 0, \quad i = 1, 2, 3, 4$$

$$g_{85}(\mathbf{x}) = \omega_{min} - \frac{\omega_1 \cdot N_{p1} \cdot N_{p2} \cdot N_{p3} \cdot N_{p4}}{N_{g1} \cdot N_{g2} \cdot N_{g3} \cdot N_{g4}} \leq 0$$

$$g_{86}(\mathbf{x}) = \frac{\omega_1 \cdot N_{p1} \cdot N_{p2} \cdot N_{p3} \cdot N_{p4}}{N_{g1} \cdot N_{g2} \cdot N_{g3} \cdot N_{g4}} - \omega_{max} \leq 0$$

Where:

$$c_i = \sqrt{(y_{gi} - y_{pi})^2 + (x_{gi} - x_{pi})^2}$$

Table 39

The best results for the Four-stage gear box.

	DoS	AOO	PSA	FFA	AVOA	ETO	SGA	WAA
N_{p1}	21.5320385	14.4365735	16.3522535	27.6467997	14.2885826	28.4713456	14.541271	24.1665764
N_{g1}	46.6205336	31.0391991	38.1855094	40.6005345	28.4852633	40.2217087	45.1645854	63.3848144
N_{p2}	21.0587073	18.453822	21.4922182	23.1810638	17.9460929	14.009929	15.2618438	14.2695344
N_{g2}	42.4589623	40.109072	38.4061982	49.1868321	41.1803625	35.8717594	19.7370829	31.0863413
N_{p3}	21.4872325	21.2135998	10.7031089	18.2407005	18.6306136	21.4574928	15.2525391	16.5003483
N_{g3}	45.3812778	42.3807148	23.4193648	46.304301	40.6289769	40.5799586	30.8480731	41.069902
N_{p4}	20.9287857	13.5623083	21.2845599	18.1278907	19.0777106	16.1181924	17.013716	22.2135821
N_{g4}	45.4514195	28.1343203	46.3987004	45.1736973	38.2164589	44.1485892	40.6262691	31.1860917
b_1	0.69418949	1.38169063	0.9020677	0.69946145	0.91685304	0.94970777	1.25089483	0.71725398
b_2	0.87511381	1.24663426	1.08084847	1.07914246	0.6267313	1.07177167	2.32819288	0.64327457
b_3	0.75252488	1.44831389	1.70107568	0.61402979	0.93292115	1.36342825	1.10315959	0.51
b_4	1.40641289	0.74910218	0.5587868	1.22326827	0.77502445	1.04994095	1.06786147	0.76960197
x_{p1}	1.71829571	3.05314121	2.59790079	2.81997842	3.57116076	2.38254436	6.2343942	4.44054981
x_{g1}	4.81044719	4.8875494	6.48071995	5.82510208	3.59341973	1.91232332	5.51931233	3.94956775
x_{g2}	4.89132384	4.53238538	5.15785114	6.45530085	5.5288688	3.53161928	5.51279197	5.71913391
x_{g3}	3.17502923	6.42118539	4.33422852	4.60217008	5.31358539	4.77717887	4.99913312	4.15664445
x_{g4}	4.93962556	5.57983126	2.52752637	5.6855937	3.62376827	5.56627464	3.79873123	5.92031571
y_{p1}	5.96903726	2.62620248	2.87021188	2.81976882	7.02282306	5.87311718	2.39255506	8.46009973
y_{g1}	5.47950026	5.98449881	4.95026566	4.5288527	4.45671595	2.853717	5.62743707	4.13487523
y_{g2}	5.63879698	6.22093695	5.18254811	3.55437704	4.36812185	2.72434446	5.31190738	5.19498598
y_{g3}	3.27357283	2.84150747	6.27275755	5.60450977	4.34024296	3.79176373	4.86560138	3.87938439
y_{g4}	5.48673809	2.84181107	6.80551646	4.55627422	4.01089936	5.029828	5.40524818	6.37188674
Best	35.359232	39.9992606	50.1074146	44.7579233	37.2597421	48.144882	50.6500247	49.1011141

Table 40

Statistical results for the Four-stage gear box.

	DoS	AOO	PSA	FFA	AVOA	ETO	SGA	WAA
Mean	42.973019	62.8111705	45.9896535	60.0108344	47.3720259	75.0605268	93.1821241	51.349004
Std	7.65659425	20.7589046	0	13.570429	5.49153005	0	0	8.21682197
Success	0.84	0.4	0.04	0.92	0.2	0.04	0.04	0.24
WSRT		2.6E-08(+)	1.1E-05(+)	4.5E-07(+)	6.0E-05(+)	9.6E-11(+)	9.6E-11(+)	5.3E-06(+)
FMR	1.56	5.36	2.08	5.04	3.16	6.76	7.92	4.12
F-Rank	1	6	2	5	3	7	8	4

$$K_0 = 1.5, \quad d_{min} = 25, \quad J_R = 0.2, \quad \phi = 120^\circ$$

$$W = 55.9, \quad K_M = 1.6, \quad CR_{min} = 1.4$$

$$L_{max} = 127C_p = 464, \quad \sigma_H = 3290, \quad \omega_{max} = 255$$

$$\omega_1 = 5000, \quad \sigma_N = 2090, \quad \omega_{min} = 245$$

With bounds:

$$b_i \in \{3.175, 12.7, 8.255, 5.715\},$$

$$N_{gi}, N_{pi} \in \{7, 8, \dots, 76\},$$

$$x_{p1}, y_{p1}, x_{gi}, y_{gi} \in \{12.7, 38.1, 25.4, 50.8, 76.2, 63.5, 88.9, 114.3, 101.6\}$$

Tables 39 and 40 summarize the experimental results of DoS and the competing algorithms on this problem. The problem includes 86 inequality constraints, imposing high demands on the algorithm's feasibility maintaining ability and convergence accuracy. As shown by the Success indicator, none of the algorithms achieved a 100% success rate.

Among them, PSA, ETO and SGA each obtained only one feasible solution out of 25 runs, indicating poor stability and adaptability. Although FFA achieved a 92% success rate, slightly higher than the 84% of DoS, DoS still outperformed all competitors in both Best and Mean metrics, demonstrating that it not only finds more feasible solutions but also produces higher quality solutions.

In terms of result dispersion, the Std of DoS was slightly higher than that of AVOA, but significantly lower than the other algorithms, indicating that DoS possesses strong local exploitation capability around feasible regions. The Wilcoxon rank-sum test further confirms that the performance advantages of DoS on this problem are statistically significant. Finally, DoS ranked first in the Friedman test, highlighting its optimization performance and practical value in high dimensional, single objective constrained optimization problems.

5.10. Wind Farm Layout

Wind farm layout is a renewable energy optimization problem characterized by spatial coupling. The objective is to maximize the total power output of the wind farm or minimize the levelized cost of energy, under environmental constraints such as geographical layout and wind speed distribution. The problem involves 30 decision variables, representing the positions and spacing design of wind turbines, denoted as $\mathbf{x} = (x_1, \dots, x_{15}, y_1, \dots, y_{15})$. It includes 91 inequality constraints, making it a typical high dimensional, complex constrained optimization problem. The mathematical model is defined in Equation 40.

Minimize:

$$f(\mathbf{x}) = \sum_{i=1}^N E(P_i) \quad (40)$$

Subject to:

$$g_{\frac{(28-i)(i-1)}{2}+(j-i)}(\mathbf{x}) = \sqrt{(x_i - x_j)^2 + (y_i - y_j)^2} \geq 5R, \\ i = 1, 2, \dots, 15, \quad i < j < 14$$

Where:

$$E(P_i) = \sum_{n=1}^h \xi_n \cdot P_r \left(e^{-\left\{ \frac{v_r}{c_i^{[(\theta_{n-1} + \theta_n)/2]}} \right\}^{k_i(\theta_{n-1} + \theta_n)/2}} - e^{-\left\{ \frac{v_{co}}{c_i^{[(\theta_{n-1} + \theta_n)/2]}} \right\}^{k_i(\theta_{n-1} + \theta_n)/2}} \right) + \sum_{n=1}^h \xi_n \cdot \left\{ \sum_{j=1}^s \left[\left(e^{-\left\{ \frac{v_{j-1}}{c_i^{[(\theta_{n-1} + \theta_n)/2]}} \right\}^{k_i(\theta_{n-1} + \theta_n)/2}} - e^{-\left\{ \frac{v_j}{c_i^{[(\theta_{n-1} + \theta_n)/2]}} \right\}^{k_i(\theta_{n-1} + \theta_n)/2}} \right) \cdot \frac{e^{(v_{j-1} + v_j)/2}}{\alpha + \beta \cdot e^{(v_{j-1} + v_j)/2}} \right] \right\}$$

With bounds:

$$40 \leq x_i \leq 1960, \quad 40 \leq y_i \leq 1960, \quad i, j = 1, 2, \dots, 15$$

Tables 41 and 42 present the experimental results of DoS and its competitors on this problem. Except for ETO, which failed to converge to any feasible solution in all 25 independent runs, the success rates of the other algorithms are relatively high. However, in terms of the Best and Mean indicators, DoS achieves the best performance, indicating stronger search capabilities and a higher likelihood of approaching the global optimal solution. DoS also significantly outperforms competitors in terms of the Std indicator, demonstrating high convergence accuracy and good stability.

The results of the Wilcoxon rank-sum test show that DoS is statistically significantly better than all other competitors.

In the Friedman test, DoS also ranks first. In summary, DoS demonstrates outstanding performance and practical value in high dimensional constrained optimization problems and Power System related tasks.

6. Application to Mountainous Terrain Path Planning

In unmanned aerial vehicle (UAV) power inspection tasks, the planning of flight paths is directly related to the operational safety of transmission lines. Therefore, developing a scientifically sound and reasonable flight path for UAVs (Hrabar, 2008; Ergezer and Leblebicioğlu, 2014; Yang et al., 2014) is key to ensuring task safety and operational efficiency. This problem involves multiple complex discontinuous constraints [73], making it highly significant in engineering applications. To verify the adaptability of DoS in real-world engineering problems, this study uses this problem as a representative case for evaluation.

Section 6.1 presents the mathematical model of the mountainous terrain path planning problem. In Section 6.2, DoS and advanced competitors are evaluated through 25 independent experiments under typical mountainous terrain. The performance of DoS on this problem is comprehensively analyzed using statistical indicators, including the best value (Best), average value (Mean), standard deviation (Std), success rate (Success), Wilcoxon rank-sum test (WSRT) at a 5% significance level, Friedman mean rank (FMR) and overall rank (F-Rank).

6.1. Mathematical Model

This problem aims to plan a safe and efficient flight path for UAVs based on mountainous terrain, starting point and destination. In the mathematical model, the flight path is discretized into 7 nodes and the variations in the X-axis, Y-axis and relative terrain height between adjacent nodes are defined as the optimization decision variables. Accordingly, the coordinates of the i-th node are expressed as:

$$x_i = \text{round} \left(0.5 + x_s + \sum_{j=1}^i \Delta x_j \right), \\ y_i = \text{round} \left(0.5 + y_s + \sum_{j=1}^i \Delta y_j \right), \\ z_i = H_i + \Delta z_i \quad (41)$$

where Δx_j and Δy_j denote the variations in the X-axis and Y-axis directions of the j-th node relative to its previous node and Δz_i is the relative change in terrain height. H_i represents the terrain elevation at coordinates (x_i, y_i) . Thus, the decision variables can be represented as: $\mathbf{x} = (\Delta x_1, \Delta y_1, \Delta x_2, \dots, \Delta x_7, \Delta y_7, \Delta z_7)$.

Considering that using only seven nodes is insufficient to generate a smooth trajectory in complex terrain, a cubic spline interpolation is applied to smooth the flight path after determining all node coordinates. Let the number of

Table 41
The best results for the Wind farm layout.

	DoS	AOO	PSA	FFA	AVOA	ETO	SGA	WAA
x_1	1462.63623	686.727895	40.0266304	40	1144.00883	NaN	1077.02246	569.828992
x_2	788.942125	522.561888	1959.9987	40	1392.90003	NaN	1704.95946	1377.66413
x_3	1547.23036	945.95155	1841.77117	1959.68289	147.650041	NaN	1555.44313	1859.44004
x_4	1960	1329.53655	40.000101	46.0147221	230.504712	NaN	86.8739308	1954.81841
x_5	272.001925	1922.48364	40.0000206	300.774847	40.0000368	NaN	316.67443	1018.64235
x_6	842.392038	1324.08245	40.0576999	490.453593	41.1868254	NaN	634.290145	1727.97915
x_7	1390.37725	1908.0378	884.311937	1340.8296	863.90748	NaN	1802.51133	161.93923
x_8	1206.13361	776.749987	1959.99999	1050.91353	1049.11352	NaN	549.996432	1833.87805
x_9	204.925464	40.0010407	1854.60593	1482.3778	263.304927	NaN	40.0002408	700.456074
x_{10}	1166.54878	47.0173447	940.869654	1667.20654	432.259573	NaN	40.0000978	277.850598
x_{11}	1880.12588	1959.94023	61.1963451	1032.63369	871.317476	NaN	40	1172.18597
x_{12}	40	1773.72515	312.665753	41.2434693	40.0002229	NaN	1028.90997	1953.05298
x_{13}	1450.03348	1018.67944	80.1754666	548.781031	40	NaN	1935.82257	1959.5862
x_{14}	1568.89917	51.7275145	1530.50398	833.668985	835.664244	NaN	1493.48728	766.354613
x_{15}	767.013635	77.4062641	1477.98049	174.166882	1960	NaN	1960	79.9992837
x_{16}	1960	1352.85886	1619.74265	1959.51005	1960	NaN	40.227523	890.87749
x_{17}	40	1282.64443	1938.97	48.2132852	40.3312575	NaN	1075.44001	1271.45673
x_{18}	40	1956.8046	1417.09561	1332.7715	1051.02581	NaN	1960	1177.37466
x_{19}	75.1699377	1908.16395	1004.07086	1261.23706	1054.3472	NaN	1959.9974	144.458628
x_{20}	1960	991.344764	40.0013151	1318.91042	1959.38814	NaN	1698.13098	1348.60015
x_{21}	1831.25155	1812.41881	1030.56244	49.9481137	1960	NaN	42.6953317	441.650516
x_{22}	386.167552	516.356072	921.338735	1005.27441	1404.10714	NaN	1960	395.806647
x_{23}	88.6507558	101.379005	1876.83318	1101.3501	40.0000698	NaN	1960	670.118121
x_{24}	1554.62265	1903.4665	414.691574	1958.34857	1395.69065	NaN	1960	833.40477
x_{25}	710.239709	1750.42917	98.5915384	257.201323	1959.99999	NaN	40.3455457	624.67494
x_{26}	40	57.5901493	888.69544	1623.99716	52.7654481	NaN	417.095965	1872.00174
x_{27}	123.208964	130.895825	1960	1931.81424	210.534434	NaN	1960	920.743972
x_{28}	377.04397	876.670144	1959.99963	1960	1960	NaN	393.128088	91.6274283
x_{29}	40	1956.62571	61.786189	1346.83705	1960	NaN	1960	368.043789
x_{30}	40	1955.55095	528.352934	773.437113	1960	NaN	1960	661.56747
Best	-6262.972	-5986.9772	-6084.7437	-5815.6126	-6043.438	NaN	-5903.1683	-5247.7343

Table 42
Statistical results for the Wind farm layout.

	DoS	AOO	PSA	FFA	AVOA	ETO	SGA	WAA
Mean	-6205.214	-5806.3767	-5913.9266	-5496.6945	-5747.3537	NaN	-5546.75	-4913.6592
Std	30.581606	125.853091	86.1246327	76.656197	135.130191	NaN	193.119997	239.132835
Success	1	1	1	1	1	0	0.88	1
WSRT		1.4E-09(+)	1.4E-09(+)	1.4E-09(+)	1.4E-09(+)	NaN	1.4E-09(+)	1.4E-09(+)
FMR	1	3.16	2.4	5.4	3.92	NaN	5.16	6.96
F-Rank	1	3	2	6	4	8	5	7

interpolated trajectory points be m , with coordinates denoted as X_1, X_2, \dots, X_m , where each $X_i = (\tilde{x}_i, \tilde{y}_i, \tilde{z}_i)$.

The optimization objectives for the UAV flight path primarily include path length minimization and altitude smoothness, which are formulated as follows:

$$F_1(\mathbf{x}) = \sum_{i=1}^{m-1} \|X_{i+1} - X_i\| \quad (42)$$

$$F_2(\mathbf{x}) = \sqrt{\frac{1}{m} \sum_{i=1}^m (\tilde{z}_i - z_{mean})^2} \quad (43)$$

where z_{mean} represents the average flight altitude of all trajectory points. In addition, the mountainous terrain path planning problem involves four types of constraints:

Turning angle constraint: Limits the angle between adjacent trajectory segments from being smaller than a critical value ψ , in order to avoid sharp turns:

$$G_1(\mathbf{x}) = \arccos\left(\frac{A_i \cdot B_i}{\|A_i\| \|B_i\|}\right) - \psi \leq 0, \quad i = 2, 3, \dots, m-1 \quad (44)$$

where A_i and B_i represent the direction vectors formed between the i -th trajectory point and the $(i-1)$ -th and $(i+1)$ -th trajectory points, respectively. The flight turning angle can be calculated by combining the cosine law with the inverse trigonometric function.

$$A_i = X_i - X_{i-1}, \quad B_i = X_{i+1} - X_i$$

Collision avoidance constraint: Trajectory points must maintain sufficient clearance above the terrain:

$$G_2(\mathbf{x}) = \tilde{z}_{(\tilde{x}_i, \tilde{y}_i)} + \Delta h_{\min} - \tilde{z}_i \leq 0, \quad (45)$$

$$i = 1, 2, \dots, m$$

where $\tilde{z}_{(\tilde{x}_i, \tilde{y}_i)}$ denotes the interpolated terrain height at point $(\tilde{x}_i, \tilde{y}_i)$ based on the terrain results and Δh_{\min} represents the minimum safety distance required to avoid terrain collision.

Since the trajectory points are generated via interpolation from the discrete nodes, there is a possibility that some points may fall outside the boundary. To address this, the following boundary constraint is established:

$$G_3(\mathbf{x}) = \begin{cases} M_L - \tilde{x}_i \leq 0 \\ \tilde{x}_i - M_U \leq 0 \\ M_L - \tilde{y}_i \leq 0 \\ \tilde{y}_i - M_U \leq 0 \end{cases}, \quad i = 1, 2, \dots, m \quad (46)$$

where M_L and M_U represent the lower and upper bounds of the ground area respectively.

Since the UAV's flight altitude is also a critical factor affecting safety, the following altitude constraint is introduced in the mathematical model:

$$G_4(\mathbf{x}) = \tilde{z}_i - h_{\max} \leq 0, \quad i = 1, 2, \dots, m \quad (47)$$

where h_{\max} denotes the maximum allowable flight altitude for the UAV.

Since optimizing a single objective before verifying constraints significantly reduces the extraction rate of feasible solutions, we also use the penalty function method to handle constraints in this problem. That is, for solutions that violate constraints, their objective function values are adjusted by adding penalty terms. The corresponding auxiliary function is defined as follows:

$$Q(G_s(\mathbf{x})) = \begin{cases} 0, & G_s(\mathbf{x}) \leq 0 \\ 10000, & G_s(\mathbf{x}) > 0 \end{cases}, \quad s = 1, 2, 3, 4 \quad (48)$$

Finally, the optimization objective of the mountainous terrain path planning problem is formulated as:

$$F = F_1 + F_2 + Q[G_1(\mathbf{x})] + Q[G_2(\mathbf{x})] + Q[G_3(\mathbf{x})] + Q[G_4(\mathbf{x})] \quad (49)$$

6.2. Performance Analysis

Based on multiple preliminary experiments, the evaluation budget for each algorithm in this section is set to 10,000 function evaluations and 25 independent runs are conducted

to assess algorithm performance. The best solution results of each algorithm are shown in Table 43 and the statistical indicators are presented in Table 44.

As shown in Table 43, DoS achieved the best Best value in 25 independent runs, indicating its strong local exploitation ability on this problem. Further, Table 44 reveals that DoS outperforms all competitors in terms of Mean, demonstrating its more stable and reliable overall performance. Although its Std is slightly higher than that of WAA, it remains close to zero, reflecting good stability.

In the Wilcoxon rank-sum test, DoS exhibits comparable performance to WAA and AVOA, while significantly outperforming other competitors. In the Friedman test, DoS ranks first, ahead of WAA, further validating its advantage in this problem. In summary, DoS demonstrates high convergence accuracy and stability in mountainous terrain path planning tasks, showing strong engineering adaptability.

To help readers intuitively understand the performance differences among algorithms, Fig. 14 provides a visualization of the mountainous terrain and the corresponding flight paths obtained during the experiments.

6.3. Mountainous Terrain Path Planning with No Fly Zones

As verified in Section 6.2, the performance of DoS in mountainous terrain path planning under standard terrain conditions has been demonstrated. To further evaluate its effectiveness in discontinuous terrains, this section introduces five no-fly zone cylinders on the original mountainous terrain. The UAV is required to minimize the path length without intersecting any of these no-fly zones. The center coordinates (x_c, y_c) , radius (r_c) and height (h_c) of each no-fly zone are detailed in Table 45.

To account for the no fly zone restrictions, a fifth constraint is added to the mathematical model from Section 6.1, as shown in Equation 50.

$$G_5(\mathbf{x}) = \sqrt{(\tilde{x}_i - x_c^j)^2 + (\tilde{y}_i - y_c^j)^2} > r_c^j \quad \text{and} \quad (50)$$

$$\tilde{z}_i > h_c^j, \quad i = 1, \dots, m, \quad j = 1, \dots, 5$$

where x_c^j, y_c^j, h_c^j and r_c^j denote the center coordinates, height and radius of the j -th no fly zone, respectively. Accordingly, the original objective function (Equation 50) is updated to Equation 51.

$$F = F_1 + F_2 + Q[G_1(\mathbf{x})] + Q[G_2(\mathbf{x})] + Q[G_3(\mathbf{x})] + Q[G_4(\mathbf{x})] + Q[G_5(\mathbf{x})] \quad (51)$$

Based on Equation 51, 25 independent experiments were conducted for DoS and the advanced competitors under 10,000 evaluations. The best solutions are listed in Table 46 and the statistical results are shown in Table 47.

As shown in Tables 46 and 47, DoS ranks first in five key performance metrics demonstrating the best overall performance. With the addition of no fly zones, only DoS maintains a 100% success rate, further validating its adaptability to no-fly zone constraints.

Table 43

The best results for mountainous terrain path planning.

	DoS	AOO	PSA	FFA	AVOA	ETO	SGA	WAA
x_1	12.9888909	13.3089578	14.3835712	NaN	10.3624115	6.10146067	2.2170757	9.90246732
x_2	13.8690372	13.7325103	14.8694544	NaN	8.77075093	4.52803833	2.05372255	10.4415022
x_3	2.50699876	2.40820912	2.59246594	NaN	2.77900294	2.72990543	2.21872515	3.07949599
x_4	6.48131699	9.37718037	10.5927012	NaN	7.25823212	0.72235314	4.2335812	5.81442362
x_5	6.33422166	11.6377417	12.3866256	NaN	9.5216832	2.72726476	1.46826182	5.2906585
x_6	3.95329554	3.40000558	2.39321317	NaN	3.78592371	2.54084754	3.9254009	4.17795437
x_7	8.18867199	2.12047252	2.21619303	NaN	9.30716946	1.46474564	6.19247403	9.41297312
x_8	9.49747645	1.45326478	2.03145342	NaN	10.8418392	1.99592892	8.26377253	10.4078648
x_9	1.56757028	2.99775567	1.76327833	NaN	1.77738873	1.50679381	3.35051702	2.87116885
x_{10}	10.8948181	6.96976651	10.7605182	NaN	10.6614498	1.02559479	9.15197199	10.2419927
x_{11}	11.3355857	7.10015945	10.4132149	NaN	10.9663482	-0.0027454	12.6743471	9.52118694
x_{12}	3.19192349	1.81821068	3.07970717	NaN	2.65054604	1.91553843	4.36618523	2.32941245
x_{13}	9.11686592	11.9292805	9.67542029	NaN	11.8307123	4.89502925	16.8599053	8.73907293
x_{14}	9.51696602	11.6578647	12.7824881	NaN	12.9130449	4.04181626	15.5477379	10.5080317
x_{15}	1.71999706	2.13675858	2.13118587	NaN	2.81417943	3.02497411	4.61624824	2.50188693
x_{16}	5.63803607	7.83496928	6.6648707	NaN	10.5297882	2.33637529	13.7479204	6.94191714
x_{17}	5.96924972	8.92472529	6.92384978	NaN	11.531419	3.27194708	13.2380064	9.03256409
x_{18}	2.48864298	2.90505994	1.53419283	NaN	2.39877312	3.88518424	3.15550806	2.83347527
x_{19}	7.97981168	10.7482806	7.28957934	NaN	10.2280648	17.9821989	10.243686	7.45934563
x_{20}	8.1123124	10.6989156	6.77729394	NaN	8.7034067	23.4440988	11.5825813	7.35780639
x_{21}	2.30288825	2.65683761	2.63959671	NaN	2.72170739	2.06283091	2.85644707	1.5002853
Best	115.457868	115.613739	115.525492	NaN	115.786401	117.535791	117.470719	115.66231

Table 44

Statistical results for mountainous terrain path planning.

	DoS	AOO	PSA	FFA	AVOA	ETO	SGA	WAA
Mean	115.70175	116.664178	117.451852	NaN	116.386235	126.408888	124.175462	115.897928
Std	0.15175712	1.12785545	2.36536695	NaN	1.37315754	4.90373033	8.51917331	0.1045847
Success	1	0.96	0.92	0	1	1	1	1
WSRT		2.4E-06(+)	2.2E-07(+)	NaN	5.5E-03(+)	1.4E-09(+)	1.4E-09(+)	3.3E-07(+)
FMR	1.52	3.84	4.12	NaN	2.96	6.52	6.2	2.84
F-Rank	1	4	5	8	3	7	6	2

Table 45

Information of no fly zones.

	No fly zone 1	No fly zone 2	No fly zone 3	No fly zone 4	No fly zone 5
x_c	56.7157	32.6590	13.1987	65.9033	64.0290
y_c	18.5965	39.5000	45.5621	70.4151	44.1858
r_c	5.0676	4.7530	10.5505	4.9743	8.7564
h_c	6.4409	8.2620	3.8032	8.5927	9.5035

In terms of optimization accuracy, DoS outperforms other algorithms in both Best and Mean values and has the smallest Std, indicating stronger exploitation capability and better stability in this problem. The WSRT results show that, except for AVOA and WAA, all other algorithms are statistically significantly inferior to DoS. In the Friedman test, DoS again ranks first, further verifying its practicality in complex mountainous terrain path planning problems.

Fig. 15 visualizes the flight paths obtained by each algorithm over terrain with no fly zones, enabling a more intuitive comparison of their performances in this scenario.

7. Discussion

Based on the experimental results of DoS in Sections 4 to 6, covering CEC2017 and CEC2022 benchmark test functions, 10 engineering optimization problems, and the mountainous terrain path planning application, this subsection will discuss the key distinctions between DoS and traditional metaheuristic algorithms, and analyze the fundamental reasons behind its performance advantages.

7.1. Advantages of DoS

As shown in Fig. 7, the exploration and exploitation rate curves of DoS vary significantly across different functions, indicating that DoS exhibits strong adaptability when solving various types of optimization problems. Furthermore, the information in Fig. 8 demonstrates that DoS achieves

Dogfight Search

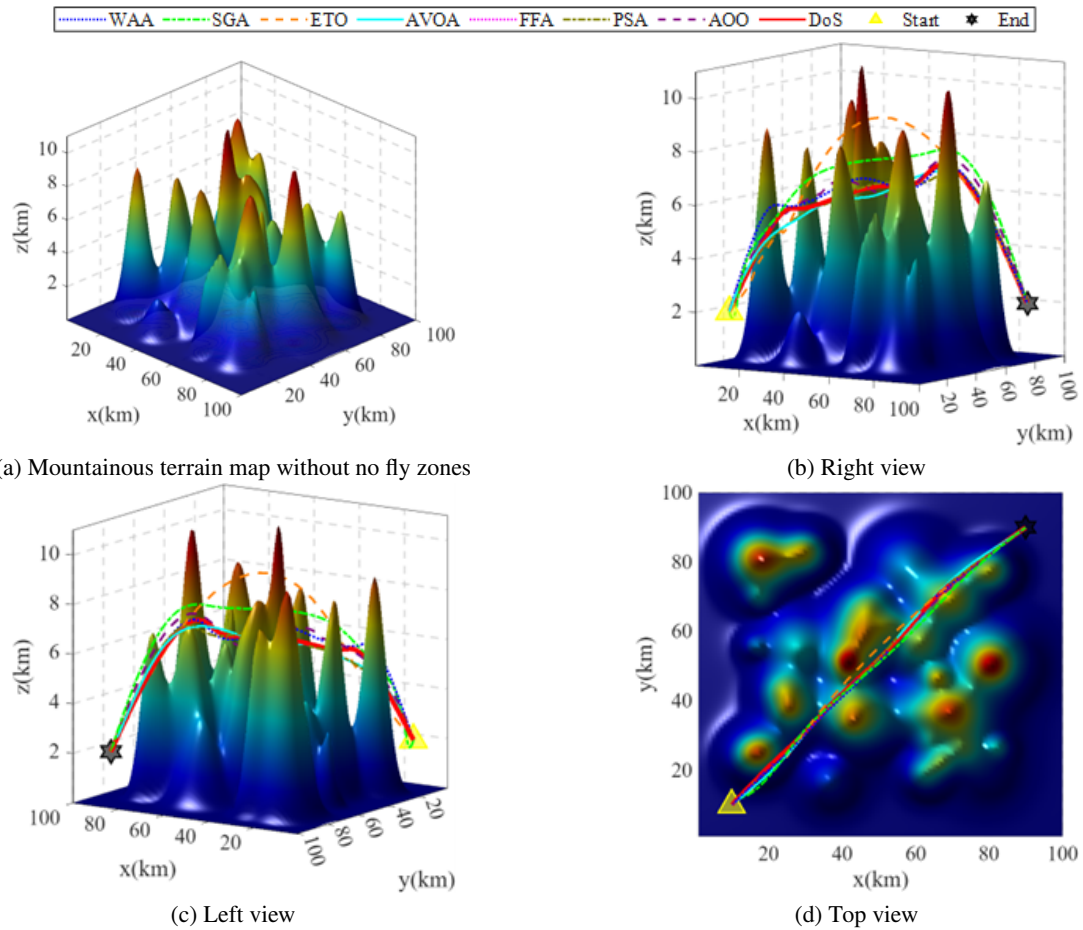


Figure 14: Visualization of mountainous terrain path planning.

Table 46

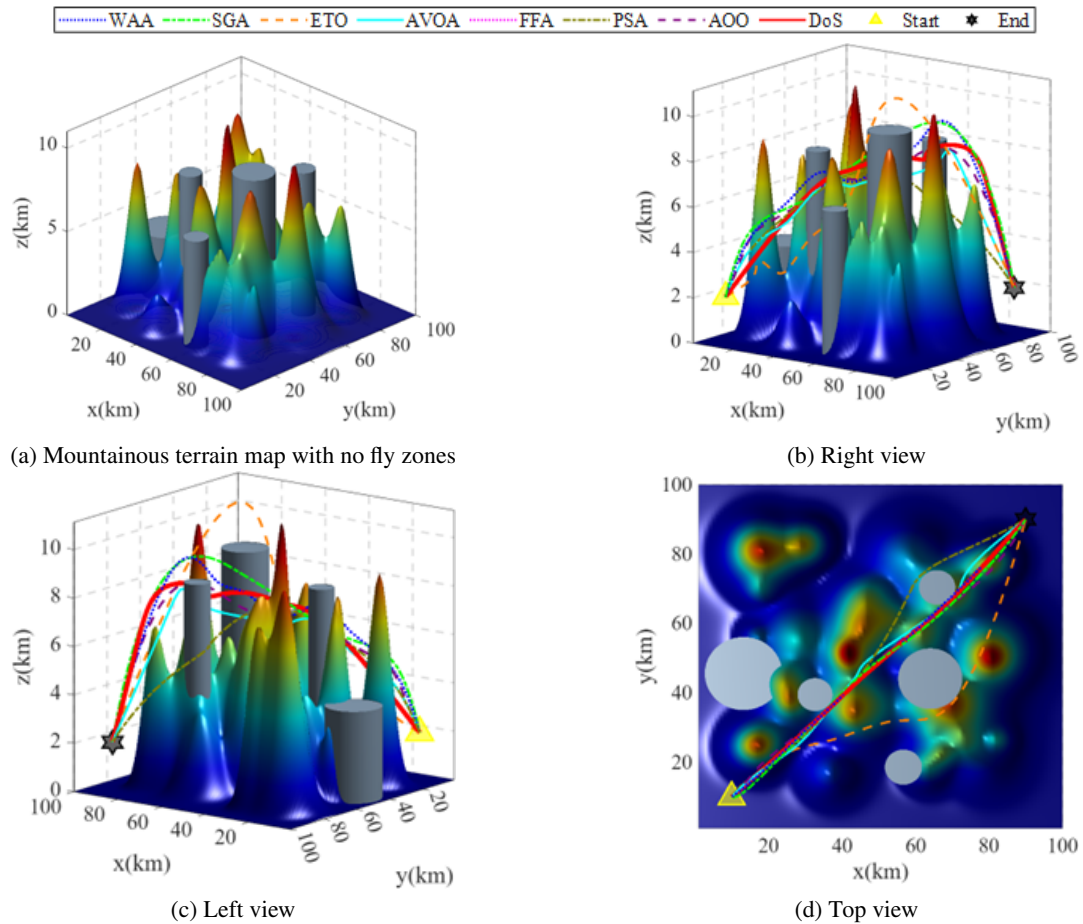
The best results of mountainous terrain path planning with no fly zones.

	DoS	AOO	PSA	FFA	AVOA	ETO	SGA	WAA
x_1	24.6151727	6.19575074	5.83758569	NaN	9.653058	8.35983887	1.35877043	9.10803916
x_2	24.3137897	7.18586063	6.44106836	NaN	9.27005726	7.07298245	-0.1705658	8.19400313
x_3	3.69506866	3.39562003	3.25904729	NaN	2.69756453	1.91506739	2.38150614	3.55724855
x_4	10.4177494	5.70624126	11.9844314	NaN	9.03563824	0.33891949	2.50262731	9.27551588
x_5	9.43944082	6.02840097	9.26556372	NaN	6.61331424	0.62194985	1.69667884	8.90176369
x_6	3.02437287	1.75030092	4.31175872	NaN	4.22084634	1.96825997	3.71290435	4.76670039
x_7	12.1206834	13.2568275	19.3167965	NaN	7.87895285	2.11268223	6.58050107	8.50796062
x_8	11.1233053	10.5697383	21.9059203	NaN	10.2328007	2.07845911	6.36037763	8.8398287
x_9	3.64572418	3.45413548	3.73734884	NaN	2.41774344	1.36523701	4.10445474	3.06226768
x_{10}	8.72585555	4.00668196	10.7922801	NaN	7.75352486	7.34281971	11.1271871	9.43526576
x_{11}	8.2382542	4.29188002	20.5549274	NaN	8.75100226	3.84754704	12.7144057	9.46919635
x_{12}	3.22731975	1.56173136	3.8820003	NaN	1.93019374	2.07339549	4.42039303	3.05984284
x_{13}	2.24884308	5.31807437	1.73387989	NaN	4.1888267	10.5138342	13.9973874	9.46240553
x_{14}	1.82812146	5.02473278	3.63358891	NaN	6.31302907	2.91577219	15.7358933	8.4837311
x_{15}	2.89644401	2.07465456	2.44401085	NaN	3.53826108	3	3.83985846	4.31680178
x_{16}	8.68999588	12.9995088	4.7233468	NaN	19.1727522	16.6093988	13.3722614	8.56006039
x_{17}	9.5890141	13.2086192	4.53099461	NaN	13.7208065	5.67094357	9.69266408	8.43153517
x_{18}	3.16433811	2.76574832	1.91770311	NaN	2.11226421	4.45068555	3.39367589	3.70199248
x_{19}	6.30480295	16.9155338	10.9790725	NaN	4.93688188	14.4558711	15.8873627	9.00155613
x_{20}	7.52608428	12.4222365	5.64191406	NaN	8.56534178	4.5718354	14.7960556	8.65555913
x_{21}	3.96077692	3.14030899	2.32702171	NaN	2.91844852	2.2050623	4.59898876	3.66490752
Best	116.451419	116.884378	118.018618	NaN	117.230664	129.290161	118.430385	116.845406

Table 47

Statistical results of mountainous terrain path planning with no fly zones.

	DoS	AOO	PSA	FFA	AVOA	ETO	SGA	WAA
Mean	118.36611	122.097895	129.442151	NaN	120.574604	138.719413	133.276447	119.678824
Std	1.2245701	8.08930431	8.54127858	NaN	7.3629909	7.81870547	12.0252177	7.52920892
Success	1	0.44	0.6	0	0.96	0.88	0.96	0.56
WSRT		3.8E-05(+)	1.8E-07(+)	NaN	9.4E-01(\approx)	1.4E-09(+)	1.2E-08(+)	6.8E-01(\approx)
FMR	2.2	3.88	5.08	NaN	2.6	6.48	5.32	2.44
F-Rank	1	4	5	8	3	7	6	2

**Figure 15:** Visualization of mountainous terrain path planning with no fly zones.

faster convergence speed and higher solution accuracy compared to advanced competitors across diverse functions. This fully demonstrates that under the same computational cost, DoS can achieve better optimization results.

The results in Fig. 9 and 11 show that for 92.7% of the CEC2017 and CEC2022 benchmark test functions, the performance of DoS is not significantly affected by increasing dimensionality. Moreover, on F28, C11 and C12, the performance of DoS improves with increasing dimension, further verifying that DoS possesses good scalability across various types of optimization problems. In addition, the results in Fig. 10 and 12 indicate that DoS consistently ranks first in Friedman ranking across five different dimensions of benchmark test functions, significantly outperforming

advanced competitors. Furthermore, in comparison with SOTA algorithms, DoS demonstrates superior performance, validating its outstanding optimization capability and great potential across various problem types.

In the engineering problem experiments of Section 5, DoS was evaluated on low-dimensional and high-dimensional problems (up to 30-dimensions), with both few and many constraints (up to 91 inequality constraints). The experimental results consistently show that DoS achieves higher success rates and better optimization results than advanced competitors, demonstrating its strong competitiveness in solving constrained optimization problems.

In the mountainous terrain path planning application experiments, DoS also demonstrates strong competitiveness.

According to the results in Tables 42 to 45, DoS outperforms advanced competitors in terms of higher success rates and superior optimization outcomes, fully highlighting its advantage in mountainous terrain path planning tasks.

7.2. Disadvantages of DoS

Although DoS demonstrates strong optimization capabilities, its performance remains suboptimal on F28 (30-dimensions) and on C11 and C12 (10-dimensions). Moreover, the proposed DoS is currently limited to single objective optimization problems and its extension to multi objective versions has not yet been explored. Compared with metaheuristic algorithms such as PSA and SGA, which feature simpler designs, DoS does not hold an advantage in computational cost.

8. Conclusions

Inspired by the dogfighting behavior of fighter jets, this paper proposes a metaphor-free metaheuristic algorithm named DoS, aiming to introduce more effective solution methods for optimization problems. Its performance is first evaluated on CEC2017 (30D, 50D, 100D) and CEC2022 (10D, 20D) benchmark test functions. We analyze DoS's design advantages and characteristics from the perspectives of exploration and exploitation rates, convergence, scalability, behavioral characteristics, and computational cost. Subsequently, we validated DoS's performance on 10 constrained engineering optimization problems and analyzed its applicability. Finally, we applied DoS to mountainous terrain path planning task, further demonstrating its advantages in this domain.

Based on comparisons with advanced competitors and SOTA algorithms, the main conclusions of this study can be summarized as follows:

- (1) The design of DoS alleviates the dependency of swarm-based algorithms on the current best solution by integrating multiple search strategies and a dynamic selection mechanism, thus achieving a better balance between exploration and exploitation;
- (2) In experiments on the CEC2017 and CEC2022 benchmark test functions, DoS significantly outperforms advanced competitors and shows strong competitiveness compared to SOTA algorithms;
- (3) On 10 constrained engineering problems, DoS achieves higher success rates and better optimization results than its competitors, demonstrating clear performance advantages;
- (4) In the practical application of mountainous terrain path planning, DoS consistently outperforms its competitors in both the absence and presence of no fly zones, with higher success rates and superior optimization results.

Given DoS's promising design, performance, and applicability, future work may consider the following directions:

- (1) Developing a multi objective version of DoS;

- (2) Extending the dynamic selection mechanism of DoS to other metaheuristic algorithms to improve the balance between exploitation and exploration;
- (3) Applying DoS to more challenging and high complexity engineering problems to further validate its practical value;
- (4) Expanding the application scope of DoS, such as solving numerical differential equations.

9. Declaration of Generative AI in Scientific Writing

After drafting the manuscript, the authors used ChatGPT for language editing. The content was subsequently reviewed and revised as necessary by the authors, who take full responsibility for the final publication.

CRediT authorship contribution statement

Yujing Sun: Conceptualization, Methodology, Writing - Original Draft, Software, Validation. **Jie Cai:** Validation, Formal analysis, Investigation, Visualization. **Xingguo Xu:** Writing - Review & Editing, Supervision. **Yuansheng Gao:** Writing - Review & Editing, Supervision, Project administration. **Lei Zhang:** Investigation. **Kaichen Ouyang:** Writing - Review & Editing. **Zhanyu Liu:** Visualization.

References

- Abdollahzadeh, B., Gharehchopogh, F. S., and Mirjalili, S. (2021). African vultures optimization algorithm: A new nature-inspired metaheuristic algorithm for global optimization problems. *Computers & Industrial Engineering*, 158:107408.
- Abualigah, L., Al-qaness, M. A., Abd Elaziz, M., Ewees, A. A., Oliva, D., and Cuong-Le, T. (2024). The non-monopolize search (no): A novel single-based local search optimization algorithm. *Neural Computing and Applications*, 36(10):5305–5332.
- Ahrari, A., Elsayed, S., Sarker, R., Essam, D., and Coello, C. A. C. (2022). Problem definition and evaluation criteria for the cec'2022 competition on dynamic multimodal optimization. In *Proceedings of the IEEE World Congress on Computational Intelligence (IEEE WCCI 2022)*, Padua, Italy, pages 18–23.
- Arani, B. O., Mirzabeygi, P., and Panahi, M. S. (2013). An improved pso algorithm with a territorial diversity-preserving scheme and enhanced exploration–exploitation balance. *Swarm and Evolutionary Computation*, 11:1–15.
- Ashraf, M. W., Sultani, W., and Shah, M. (2021). Dogfight: Detecting drones from drones videos. In *Proceedings of the IEEE/CVF Conference on Computer Vision and Pattern Recognition*, pages 7067–7076.
- Camacho-Villalón, C. L., Dorigo, M., and Stützle, T. (2023). Exposing the grey wolf, moth-flame, whale, firefly, bat, and antlion algorithms: six misleading optimization techniques inspired by bestial metaphors. *International Transactions in Operational Research*, 30(6):2945–2971.
- Cheng, J. and De Waele, W. (2024). Weighted average algorithm: A novel meta-heuristic optimization algorithm based on the weighted average position concept. *Knowledge-Based Systems*, 305:112564.
- Chu, D., Ma, W., Yang, Z., Li, J., Deng, Y., and Cheong, K. H. (2021). A physarum-inspired algorithm for logistics optimization: From the perspective of effective distance. *Swarm and Evolutionary Computation*, 64:100890.
- Deb, K., Pratap, A., Agarwal, S., and Meyarivan, T. (2002). A fast and elitist multiobjective genetic algorithm: Nsga-ii. *IEEE transactions on evolutionary computation*, 6(2):182–197.

- Dhiman, G. and Kumar, V. (2019). Seagull optimization algorithm: Theory and its applications for large-scale industrial engineering problems. *Knowledge-based systems*, 165:169–196.
- Dorigo, M. (1991). Ant colony optimization—new optimization techniques in engineering. by Onwubolu, GC, and BV Babu, Springer-Verlag Berlin Heidelberg, pages 101–117.
- Dye, C.-Y. (2012). A finite horizon deteriorating inventory model with two-phase pricing and time-varying demand and cost under trade credit financing using particle swarm optimization. *Swarm and Evolutionary Computation*, 5:37–53.
- Ergezer, H. and Leblebicioğlu, K. (2014). 3d path planning for multiple uavs for maximum information collection. *Journal of Intelligent & Robotic Systems*, 73(1):737–762.
- Ezugwu, A. E., Shukla, A. K., Nath, R., Akinyelu, A. A., Agushaka, J. O., Chiroma, H., and Muhuri, P. K. (2021). Metaheuristics: a comprehensive overview and classification along with bibliometric analysis. *Artificial Intelligence Review*, 54(6):4237–4316.
- Gao, Y. (2023). Pid-based search algorithm: A novel metaheuristic algorithm based on pid algorithm. *Expert Systems with Applications*, 232:120886.
- Gao, Y., Wang, J., and Li, C. (2025a). Escape after love: Philoponella prominens optimizer and its application to 3d path planning. *Cluster Computing*, 28(2):81.
- Gao, Y., Wang, J., Qin, L., Zhang, J., and Wang, Y. (2025b). Freedom from inspiration! achieving efficient metaheuristic optimization with delta plus. *Cluster Computing*, 28(7):424.
- Gao, Y., Zhang, J., Wang, Y., Wang, J., and Qin, L. (2024). Love evolution algorithm: A stimulus–value–role theory-inspired evolutionary algorithm for global optimization. *The Journal of Supercomputing*, 80(9):12346–12407.
- Gholizadeh, S., Danesh, M., and Gheytratmand, C. (2020). A new newton metaheuristic algorithm for discrete performance-based design optimization of steel moment frames. *Computers & Structures*, 234:106250.
- Gong, W., Cai, Z., and Ling, C. X. (2010). De/bbo: a hybrid differential evolution with biogeography-based optimization for global numerical optimization. *Soft Computing*, 15(4):645–665.
- Greenwood, N. (1992). A differential game in three dimensions: The aerial dogfight scenario. *Dynamics and Control*, 2(2):161–200.
- Hao, R., Hu, Z., Xiong, W., and Jiang, S. (2025). A composite particle swarm optimization algorithm with future information inspired by non-equidistant grey predictive evolution for global optimization problems and engineering problems. *Advances in Engineering Software*, 202:103868.
- Holland, J. H. (1992). Genetic algorithms. *Scientific american*, 267(1):66–73.
- Hosseinali, F. (2024). Accelerated gradient descent using improved selective backpropagation. *Expert Systems with Applications*, 255:124426.
- Houssein, E. H., Hossam Abdel Gafar, M., Fawzy, N., and Sayed, A. Y. (2025). Recent metaheuristic algorithms for solving some civil engineering optimization problems. *Scientific Reports*, 15(1):7929.
- Hrabar, S. (2008). 3d path planning and stereo-based obstacle avoidance for rotorcraft uavs. In *2008 IEEE/RSJ International Conference on Intelligent Robots and Systems*, pages 807–814. IEEE.
- Hussain, K., Salleh, M. N. M., Cheng, S., and Shi, Y. (2019). On the exploration and exploitation in popular swarm-based metaheuristic algorithms. *Neural Computing and Applications*, 31(11):7665–7683.
- Keivani, F. and Chiong, R. (2022). A novel hybrid fuzzy–metaheuristic approach for multimodal single and multi-objective optimization problems. *Expert Systems with Applications*, 195:116199.
- Kennedy, J. and Eberhart, R. (1995). Particle swarm optimization. In *Proceedings of ICNN'95-international conference on neural networks*, volume 4, pages 1942–1948. IEEE.
- Kirkpatrick, S., Gelatt Jr, C. D., and Vecchi, M. P. (1983). Optimization by simulated annealing. *science*, 220(4598):671–680.
- Koza, J. R. (1994). Genetic programming as a means for programming computers by natural selection. *Statistics and computing*, 4(2):87–112.
- Kumar, A., Wu, G., Ali, M. Z., Mallipeddi, R., Suganthan, P. N., and Das, S. (2020). A test-suite of non-convex constrained optimization problems from the real-world and some baseline results. *Swarm and evolutionary computation*, 56:100693.
- Kuo, P.-H., Yang, W.-C., Lin, Y.-S., and Peng, C.-C. (2025). Artificial rabbits optimization-based motion balance system for the impact recovery of a bipedal robot. *Advanced Engineering Informatics*, 63:102965.
- Li, Y., Han, T., Zhou, H., Tang, S., and Zhao, H. (2022). A novel adaptive l-shade algorithm and its application in uav swarm resource configuration problem. *Information Sciences*, 606:350–367.
- Lu, F., Wang, K., Wang, J., Wang, Z., and Ma, Y. (2025). Research on optimization and regulation of air volume in mine ventilation network based on multi-strategy beetle swarm optimization. *Advanced Engineering Informatics*, 68:103654.
- Luan, T. M., Khatir, S., Tran, M. T., De Baets, B., and Cuong-Le, T. (2024). Exponential-trigonometric optimization algorithm for solving complicated engineering problems. *Computer Methods in Applied Mechanics and Engineering*, 432:117411.
- McKight, P. E. and Najab, J. (2010). Kruskal-wallis test. *The corsini encyclopedia of psychology*, pages 1–1.
- Mirjalili, S. (2016). Sca: a sine cosine algorithm for solving optimization problems. *Knowledge-based systems*, 96:120–133.
- Mirjalili, S., Mirjalili, S. M., and Hatamlou, A. (2016). Multi-verse optimizer: a nature-inspired algorithm for global optimization. *Neural computing and applications*, 27(2):495–513.
- Mirjalili, S., Mirjalili, S. M., and Lewis, A. (2014). Grey wolf optimizer. *Advances in engineering software*, 69:46–61.
- Mohamed, A. W., Hadi, A. A., Fattouh, A. M., and Jambi, K. M. (2017). Lshade with semi-parameter adaptation hybrid with cma-es for solving cec 2017 benchmark problems. In *2017 IEEE Congress on evolutionary computation (CEC)*, pages 145–152. IEEE.
- Myers, P. L. and Spencer, D. B. (2016). Application of a multi-objective evolutionary algorithm to the spacecraft stationkeeping problem. *Acta Astronautica*, 127:76–86.
- Olser, G. and Breakwell, J. (1974). Role determination in an aerial dogfight. *International Journal of Game Theory*, 3(1):47–66.
- Osaba, E., Yang, X.-S., Fister Jr, I., Del Ser, J., Lopez-Garcia, P., and Vazquez-Pardavila, A. J. (2019). A discrete and improved bat algorithm for solving a medical goods distribution problem with pharmacological waste collection. *Swarm and evolutionary computation*, 44:273–286.
- Ouyang, K., Fu, S., Chen, Y., Cai, Q., Heidari, A. A., and Chen, H. (2024). Escape: an optimization method based on crowd evacuation behaviors. *Artificial Intelligence Review*, 58(1):19.
- Ouyang, K., Wei, D., Sha, X., Yu, J., Zhao, Y., Qiu, M., Fu, S., Heidari, A. A., and Chen, H. (2025). Beaver behavior optimizer: A novel metaheuristic algorithm for solar pv parameter identification and engineering problems. *Journal of Advanced Research*.
- Prajapati, V. K., Jain, M., and Chouhan, L. (2020). Tabu search algorithm (tsa): A comprehensive survey. In *2020 3rd International Conference on Emerging Technologies in Computer Engineering: Machine Learning and Internet of Things (ICETCE)*, pages 1–8. IEEE.
- Rashedi, E., Nezamabadi-Pour, H., and Saryzdi, S. (2009). Gsa: a gravitational search algorithm. *Information sciences*, 179(13):2232–2248.
- Shayanfar, H. and Gharehchopogh, F. S. (2018). Farmland fertility: A new metaheuristic algorithm for solving continuous optimization problems. *Applied Soft Computing*, 71:728–746.
- Sörensen, K. (2015). Metaheuristics—the metaphor exposed. *International Transactions in Operational Research*, 22(1):3–18.
- Storn, R. and Price, K. (1997). Differential evolution—a simple and efficient heuristic for global optimization over continuous spaces. *Journal of global optimization*, 11(4):341–359.
- Su, C.-L., Yang, S.-M., and Huang, W. (2011). A two-stage algorithm integrating genetic algorithm and modified newton method for neural network training in engineering systems. *Expert Systems with Applications*, 38(10):12189–12194.
- Sudholt, D. (2019). The benefits of population diversity in evolutionary algorithms: a survey of rigorous runtime analyses. *Theory of evolutionary computation: Recent developments in discrete optimization*, pages 359–404.

- Tanabe, R. and Fukunaga, A. S. (2014). Improving the search performance of shade using linear population size reduction. In 2014 IEEE congress on evolutionary computation (CEC), pages 1658–1665. IEEE.
- Thomas H, C., Charles, E., Ronald L, R., Clifford, S., et al. (2009). Introduction to algorithms third edition.
- Tian, A.-Q., Liu, F.-F., and Lv, H.-X. (2024). Snow geese algorithm: A novel migration-inspired meta-heuristic algorithm for constrained engineering optimization problems. Applied Mathematical Modelling, 126:327–347.
- Wang, J., Gao, Y., Qin, L., and Li, Y. (2025a). Logistic-gauss circle optimizer: Theory and applications. Applied Mathematical Modelling, 143:116052.
- Wang, J. and Shang, Z. (2025). Traffic jam optimizer: A novel swarm-based metaheuristic algorithm for solving global optimization problems. Applied Mathematical Modelling, page 116410.
- Wang, J., Wang, W.-c., Hu, X.-x., Qiu, L., and Zang, H.-f. (2024). Black-winged kite algorithm: a nature-inspired meta-heuristic for solving benchmark functions and engineering problems. Artificial Intelligence Review, 57(4):98.
- Wang, M., Wang, J., and Gao, W. (2025b). Towards large-scale cotton blending optimization: dual-pheromone crossover ant colony algorithm with expert heuristic cognition. Advanced Engineering Informatics, 68:103657.
- Wang, R.-B., Hu, R.-B., Geng, F.-D., Xu, L., Chu, S.-C., Pan, J.-S., Meng, Z.-Y., and Mirjalili, S. (2025c). The animated oat optimization algorithm: A nature-inspired metaheuristic for engineering optimization and a case study on wireless sensor networks. Knowledge-Based Systems, page 113589.
- Wangying, X. and Naiming, X. (2025). Scheduling and route planning for forests rescue: Applications with a novel ant colony optimization algorithm. Engineering Applications of Artificial Intelligence, 155:111042.
- Wilcoxon, F. (1992). Individual comparisons by ranking methods. In Breakthroughs in statistics: Methodology and distribution, pages 196–202. Springer.
- Winder, R. O. (1966). Partitions of n-space by hyperplanes. SIAM Journal on Applied Mathematics, 14(4):811–818.
- Wolpert, D. H. and Macready, W. G. (2002). No free lunch theorems for optimization. IEEE transactions on evolutionary computation, 1(1):67–82.
- Wu, G., Mallipeddi, R., and Suganthan, P. N. (2017). Problem definitions and evaluation criteria for the cec 2017 competition on constrained real-parameter optimization. National University of Defense Technology, Changsha, Hunan, PR China and Kyungpook National University, Daegu, South Korea and Nanyang Technological University, Singapore, Technical Report, 9:2017.
- Wu, R., Tian, Z., Li, X., Wu, C., Tang, H., and Li, Y. (2025). Improved discrete particle swarm optimization algorithm for solving fuzzy flexible job shop machines and automated guided vehicles fusion scheduling problem. Engineering Applications of Artificial Intelligence, 160:111951.
- Yang, L., Qi, J., Xiao, J., and Yong, X. (2014). A literature review of uav 3d path planning. In Proceeding of the 11th world congress on intelligent control and automation, pages 2376–2381. IEEE.
- Zabinsky, Z. B. et al. (2009). Random search algorithms. Department of Industrial and Systems Engineering, University of Washington, USA, pages 1–16.
- Zhang, J. and Sanderson, A. C. (2009). Jade: adaptive differential evolution with optional external archive. IEEE Transactions on evolutionary computation, 13(5):945–958.
- Zhao, W., Wang, L., and Zhang, Z. (2019). Atom search optimization and its application to solve a hydrogeologic parameter estimation problem. Knowledge-Based Systems, 163:283–304.
- Zohar, I., Ailon, A., and Rabinovici, R. (2011). Mobile robot characterized by dynamic and kinematic equations and actuator dynamics: Trajectory tracking and related application. Robotics and autonomous systems, 59(6):343–353.